FIELD APPLICATION OF AN ARC-SPRAYED TITANIUM ANODE FOR CATHODIC PROTECTION OF REINFORCING STEEL IN CONCRETE

Interim Report

State Planning and Research Project Number 5265

by

Galen E. McGill, P.E.
Bridge Engineering Section

and

Stephen D. Cramer, Sophie J. Bullard,
Bernard S. Covino, Jr., and Gordon R. Holcomb
Albany Research Center
U.S. Department of Energy

Prepared for

Oregon Department of Transportation
Research Unit
Salem, OR 97310
and
Federal Highway Administration
Washington, D.C. 20560

October 1996

Technical Report Documentation Page

1. Report No. FHWA-OR-RD-97-01	2. Government Accession No.	3. Recipient's Catalog No.
4. Title and Subtitle Field Application Of An Arc-Sprayed Titanium Anode For Cathodic Protection Of Reinforcing Steel In Concrete Interim Report		5. Report Date October 1996 6. Performing Organization Code
7. Author(s) Galen E. McGill, P.E. Stephen D. Cramer, Sophie J. Bullard, Bernard S. Covino, Jr., and Gordon R. Holcomb		8. Performing Organization Report No.
9. Performing Organization Name and Address Oregon Department of Transportation Bridge Unit 329 Transporation Building Salem, Oregon 97310		10. Work Unit No. (TRAIS) 11. Contract or Grant No. SPR 5265m
12. Sponsoring Agency Name and Address Department of Transportation Federal Highway Administration Washington, D.C. 20560 and Oregon Department of Transportation Research Unit 2950 State Streete Salem, Oregon 97310		13. Type of Report and Period Covered Interim Report (July 1994 - June 1996) 14. Sponsoring Agency Code
15. Supplementary Notes		

16. Abstract

This study provided the first field trial of a catalyzed, arc-sprayed titanium anode for cathodic protection of steel reinforced concrete structures. Catalyzed titanium as an anode material offers the advantage of long life due to the inherent non-corrosive nature of the metal in atmospheric exposure. To continue to serve as an anode, the titanium will require a periodic and easily accomplished re-application of the catalyst rather than re-application of the metal. The purpose of this study was to evaluate the installation and operation of the catalyzed titanium anode and to evaluate the economics of the titanium anode system compared to arc-sprayed zinc.

The initial phase of the study included modification of the spray equipment for spraying titanium wire and determination of the optimal spray parameters for applying the titanium anode to the bridge. Coating resistivity was found to be the best measure for evaluating the effectiveness of the coating. Decreasing spray distance, increasing current, and using nitrogen as the atomizing gas (propellant) all decrease coating resistivity. A multiple regression equation developed from the collected data showed that, for the data collected in this study, spray gun travel speed and atomizing gas pressure have an insignificant effect on coating resistivity

Coating analysis showed that the arc-sprayed titanium is a non-homogeneous coating due to reactions with atmospheric gases. The coating contains, on average, 88 weight percent titanium. The principal coating constituents are α-Ti containing interstitial nitrogen, interstitial oxygen, and γ-TiO with the possibility of some TiN. The coating consists of alternating layers of α-Ti rich and γ-TiO rich material. The use of nitrogen as the atomizing gas results in a coating with less cracking, more uniform chemistry, and therefore, lower coating resistivity than is produced using air atomization.

The field trial resulted in installation of 280 m^2 (3015 ft^2) of catalyzed, arc-sprayed titanium on the Depoe Bay Bridge. Several lessons were learned during the field trial. Although use of a grade 1, annealed titanium wire for spraying was found to reduce equipment wear, frequent equipment maintenance caused by rapid wear of the copper spray tips had a significant impact on operator productivity. The switchmode power supply furnished with the spray equipment was unable to provide the stable arc needed for smooth operation of the spray equipment. Current distribution plates embedded flush in a concrete patch material proved to be the best method for providing a low resistance connection between the anode and the power supply.

Although some difficulty was experienced during the field trial, the costs for performing this work exceeded the bid costs for installing arc-sprayed zinc on this same structure by just 18 percent. If the long-term performance of the catalyzed titanium anode system is proven, the arc-sprayed titanium system will provide a life cycle cost advantage over the arc-sprayed zinc system.

17. Key Words CATHODIC PROTECTION, ARC-SPRAYED, TITANIUM ANODE	18. Distribution Statement No restrictions.		
19. Security Classif. (of this report) Unclassified	20. Security Classif. (of this page) Unclassified	21. No. of Pages 124	22. Price

SI* (MODERN METRIC) CONVERSION FACTORS

APPROXIMATE CONVERSIONS TO SI UNITS

Symbol	When You Know	Multiply By	To Find	Symbol
		LENGTH		
in	inches	25.4	millimeters	mm
ft	feet	0.305	meters	m
yd	yards	0.914	meters	m
mi	miles	1.61	kilometers	km
		AREA		
in^2	square inches	645.2	millimeters squared	mm^2
ft^2	square feet	0.093	meters squared	m^2
yd^2	square yards	0.836	meters squared	m^2
ac	acres	0.405	hectares	ha
mi^2	square miles	2.59	kilometers squared	km^2
		VOLUME		
fl oz	fluid ounces	29.57	milliliters	mL
gal	gallons	3.785	liters	L
ft^3	cubic feet	0.028	meters cubed	m^3
yd^3	cubic yards	0.765	meters cubed	m^3
NOTE: Volumes greater than 1000 L shall be shown in m^3.				
		MASS		
oz	ounces	28.35	grams	g
lb	pounds	0.454	kilograms	kg
T	short tons (2000 lb)	0.907	megagrams	Mg
		TEMPERATURE (exact)		
°F	Fahrenheit temperature	5(F-32)/9	Celsius temperature	°C

APPROXIMATE CONVERSIONS FROM SI UNITS

Symbol	When You Know	Multiply By	To Find	Symbol
		LENGTH		
mm	millimeters	0.039	inches	in
m	meters	3.28	feet	ft
m	meters	1.09	yards	yd
km	kilometers	0.621	miles	mi
		AREA		
mm^2	millimeters squared	0.0016	square inches	in^2
m^2	meters squared	10.764	square feet	ft^2
ha	hectares	2.47	acres	ac
km^2	kilometers squared	0.386	square miles	mi^2
		VOLUME		
mL	milliliters	0.034	fluid ounces	fl oz
L	liters	0.264	gallons	gal
m^3	meters cubed	35.315	cubic feet	ft^3
m^3	meters cubed	1.308	cubic yards	yd^3
		MASS		
g	grams	0.035	ounces	oz
kg	kilograms	2.205	pounds	lb
Mg	megagrams	1.102	short tons (2000 lb)	T
		TEMPERATURE (exact)		
°C	Celsius temperature	1.8 + 32	Fahrenheit	°F

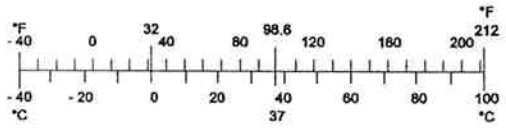

* SI is the symbol for the International System of Measurement

(4-7-94 jbp)

ACKNOWLEDGMENTS

The authors wish to thank Jack Bennett, formerly of Eltech Research Corporation, for his many contributions to this project. The authors also wish to thank Frank Rogers, of Thermion, Inc., for assistance with adaptation of the spray equipment. The authors also gratefully acknowledge Marty Laylor and the rest of the technical advisory committee for their direction and review of this work.

DISCLAIMER

FIELD APPLICATION OF AN ARC-SPRAYED TITANIUM ANODE FOR CATHODIC PROTECTION OF REINFORCING STEEL IN CONCRETE

TABLE OF CONTENTS

APPENDICES

LIST OF TABLES

LIST OF FIGURES

1.0 INTRODUCTION

1.1 BACKGROUND

Oregon is graced with a rugged and majestic coastline. The ruggedness of the coastline along US 101 combined with the remoteness of many of the coastal areas in the 1920s and 1930s make the bridge engineering accomplishments of Conde B. McCullough impressive. McCullough was the internationally recognized designer of most of the major structures which link the Oregon Coast Highway. McCullough combined a keen sense of aesthetics with engineering innovation to create a magnificent sequence of structures spanning the rivers and estuaries of the coast. His arched-bridge theme extends the length of Oregon's Coast Highway and provides Oregon with a significant number of bridges which are listed on the National Historic Register.

McCullough probably did not envision the damage his bridges would suffer from the effects of corrosion in the coastal environment. Today, however, the effects of the coastal environment are apparent. Chloride-induced corrosion of reinforcing steel is the primary contributor to the deterioration of Oregon's coastal bridges.

1.2 PROBLEM DEFINITION

Techniques to arrest the corrosion of concrete-embedded reinforcing steel began development in the 1970's through the work of Dick Stratfull of the California Department of Transportation (Caltrans) (*Stratfull, 1974*). The early development of cathodic protection systems focused on systems to protect decks from corrosion resulting from de-icing salt. None of these techniques, however, were applicable to the marine corrosion problem which occurs on the underdeck and substructure components of a bridge. Not only must it be possible to apply cathodic protection to the vertical and overhead surfaces of the substructure, it must also conform to the complex, decorative shapes typical on historic structures.

An early solution to this problem was a high-carbon content conductive paint material. Because the installed coating is black, it requires an overcoat to maintain the appearance of the bridge. While this coating can be successfully installed, there is a high probability of electrical short circuits between the coating and the rebar, and the coating has poor conductivity. Further, durability problems in freeze-thaw conditions, and in areas of surface wetting, such as splash zones, have been documented (*Swiat and Rog, 1987*).

Building on work performed by Caltrans (*Carello, et al, 1989*), the Oregon Department of Transportation (ODOT) selected arc-sprayed zinc as the anode material for use in cathodic protection systems for coastal bridges and have applied 33,630 square meters (362,000 square feet) of arc-sprayed zinc to coastal structures.

The arc-sprayed zinc coatings meet the desired properties for installation on a bridge substructure — high conductivity, preservation of architectural shapes and details, good bond strength, and a color that matches concrete. Zinc can even initially serve as a galvanic anode, but its galvanic function as an active metal is also its major disadvantage as the coatings require periodic replacement of the zinc. The Oregon Department of Transportation (ODOT) currently uses a life estimate of 12 to 15 years for a 0.508 mm (20 mil) zinc coating. Caltrans recently increased their system life estimate to 20 years for the first thermal-sprayed zinc system installed on the San Rafael Bridge in May 1983 (*McGovern, 1994*).

Although the system life estimates for zinc are not entirely certain at this time, it is certain that the zinc will eventually require replacement. Along with this replacement come the high costs associated with gaining access to the underside of the bridge, removing and reapplying the zinc, and containing the waste by-products of this process. The cost for obtaining access and containing wastes on recent ODOT cathodic protection contracts have been as high as 44% of the total contract cost, or $\$252.95/m^2$ ($\$23.50/ft^2$) of anode surface area.

1.3 THERMAL-SPRAYED TITANIUM ANODE

The primary advantage to using titanium is that, unlike zinc, it is very corrosion resistant. In seawater the corrosion rate is reported as 0.0008 mm/yr. (*Uhlig, 1985*). Titanium is an active-passive metal. The pure metal will actively corrode with the electrode potential equal to -1.63 v (standard hydrogen electrode potential at 25 $^{\circ}$ C) for $Ti^{2+} + 2e^{-} \rightarrow Ti$ compared to the less active potential for the zinc reaction, $Zn^{2+} + 2e^{-} \rightarrow Zn$, of -0.763 v (standard hydrogen electrode potential at 25 $^{\circ}$ C) (*Uhlig and Revie, 1985*). Titanium, however, readily passivates forming a thin, tightly adherent protective oxide film. Titanium then remains passive until a sufficiently high applied potential is reached. At this potential and above the metal resumes active behavior and corrosion will occur.

While the oxide film is beneficial from the perspective of corrosion resistance of the metal, the resistance of the film interferes with titanium's ability to perform as an anode. If titanium is connected to an impressed current system as an anode, the resistive surface film will prevent significant current flow until the breakdown potential is exceeded. Above this potential, corrosion of the titanium will occur. However, a catalyst exists which allows the titanium/catalyst system to serve as an anode without application of a high potential and breakdown of the titanium oxide film (*Bennett, et al, 1995*).

In this titanium/catalyst system, the titanium serves as a conductive medium for distributing the cathodic protection current and as a support structure for the catalyst. The catalyst allows anodic reactions to take place at a lower energy level but is not consumed in the anodic reactions. With time, however, the catalyst may dissipate through migration, leaching, or

reaction with other compounds, but since the titanium is not consumed in the anodic reactions, the catalyst can be reapplied at any time without requiring replacement of the titanium.

The most likely anodic reaction for the catalyzed titanium system has been reported to be:

$$4OH^- \rightarrow 2O_2 + 2H_2O + 4e^- \qquad (1\text{-}1)$$

(*Bennett, 1995*). This reaction will tend to decrease the pH at the anode/concrete interface. However, research with catalyzed titanium mesh anodes has shown that at low current density (less than 108 mA/m^2 [10mA/ft^2]) the pH does not become sufficiently acidic to attack the concrete paste.[1]

1.4 EXPERIMENT OBJECTIVES

This project is based upon initial research performed by Eltech Research Corporation that resulted in the development of a process to catalyze thermal-sprayed titanium coatings. The laboratory testing performed by Eltech showed promising results for the catalyzed thermal-sprayed titanium. Although the results should be viewed with caution, accelerated life testing has indicated an anode lifetime for catalyzed titanium in excess of 40 years (*Bennett, 1995*).

The Eltech research examined three different techniques for applying titanium to the concrete surface: wire flame spray, plasma spray using powdered metal, and wire arc-spray. The wire arc-spray appeared to give the best combination of titanium deposit efficiency and application rate (*Bennett, 1995*). Based on Eltech's results as well as ODOT's own experience with wire arc-spray for zinc application, the focus of this field trial was on the arc-spray process.

The objective of this study was to evaluate the installation and operation of an arc-sprayed, catalyzed, titanium anode on an actual reinforced concrete structure. Included in the study was a determination of the optimal installation parameters and an examination of the economics of the catalyzed titanium anode versus arc-sprayed zinc.

1.5 WORK PLAN SYNOPSIS

The initial phase of this study was a shop investigation of the spray parameters to achieve an optimum coating. Desired coating properties are: low coating resistance, low titanium usage, high production rate, and high bond strength. Also included in this phase was an investigation of health and environmental concerns for the materials being used, and the development and modification of equipment necessary for installation and testing of the titanium.

The initial work was intended to provide the basis for writing specifications for installation of the catalyzed titanium anode to 280 m^2 (3015 ft^2) of the Depoe Bay Bridge. The Depoe Bay Bridge was selected for this work because of an ongoing contract for rehabilitation and cathodic protection of the bridge. This existing contract offered two advantages. With a contractor and work platform/enclosure already on site, the costs for this experimental work were greatly reduced, and since the rest of the substructure and underdeck areas of the bridge will be coated with zinc, this bridge provides an opportunity for a side-by-side comparison of

[1] Jack Bennett, in personal conversation, December 5, 1995.

arc-sprayed, catalyzed titanium and arc-sprayed zinc. In this phase of work, training, based on what was learned in the first phase, was provided to the contractor, and the installation was monitored to identify problems and evaluate the economics of installation.

The final phase of this study is an 18-month evaluation of system operation. Information on system operation will be included in the final report for this project.

2.0 PRELIMINARY INVESTIGATION AND EQUIPMENT DEVELOPMENT

2.1 ENVIRONMENTAL AND HEALTH CONCERNS

The first task accomplished in this project was verification that there are no health or environmental concerns with the titanium or the catalyst material. Titanium is fairly inert in the environment, and there are no known environmental impacts from titanium. The catalyst material is an irritant, but it poses no known serious health effects. The dust or mist of the catalyst can cause respiratory tract irritation if inhaled, so a NIOSH-approved dust mask or breathing apparatus should be worn. Eye and skin protection should also be used during catalyst installation to prevent eye or skin irritation.

2.2 EQUIPMENT TESTING, DEVELOPMENT AND MODIFICATION

2.2.1 TITANIUM RESISTANCE PROBE

Since the titanium in this system serves to distribute current throughout the zone, the resistance of the titanium coating is more important than the thickness. Resistance and thickness are related by the following formula:

$$\mathbf{R} = \frac{\rho \cdot \mathbf{L}}{\mathbf{A}} \qquad \textbf{(2-1)}$$

where:

$\mathbf{R}$ = resistance (Ω)
ρ = resistivity ($\Omega - \text{cm}$)
$\mathbf{L}$ = length of coating (cm)
$\mathbf{A}$ = coating cross-sectional area (cm^2)

Since the cross-sectional area of the coating is equal to the width of the coating being measured (w) multiplied by the coating thickness (T), Equation 2-1 becomes:

$$\mathbf{R} = \frac{\rho \cdot \mathbf{L}}{\mathbf{w} \cdot \mathbf{T}} \qquad \textbf{(3-2)}$$

If the resistance measuring probe is constructed such that the width of coating being measured is equal to the length of the coating being measured, the equation reduces to:

$$\mathbf{R} = \frac{\rho}{\mathbf{T}} \qquad \textbf{(2-3)}$$

This measure, which is independent of length and width as long as width and length are equal, is commonly reported with the units of ohms per square. The significance of this measurement is that, on a coating that is reasonably uniform on a macroscopic scale, the resistance readings will be independent of the size of the square.

The probe constructed for this project consisted of spring-loaded contact pins installed in a 127 mm x 152 mm x 13 mm (5"x6"x0.5") sheet of fiberglass (see Figure2.1 - Resistance probe design). The spring-loaded pins provided 6.35 mm (0.25") of movement and were used to obtain good contact with the rough concrete surface. To eliminate contact resistance, a four-pin measurement technique was used to connect the probe to a Nilsson 400 AC resistance meter. The outer rows of pins are used to pass a constant current through the titanium coating. The inner pins are used to measure the voltage drop through the coating. To obtain uniform current flow through the length of coating being measured, the current distribution pins were spaced closely (9.5 mm; 0.375").

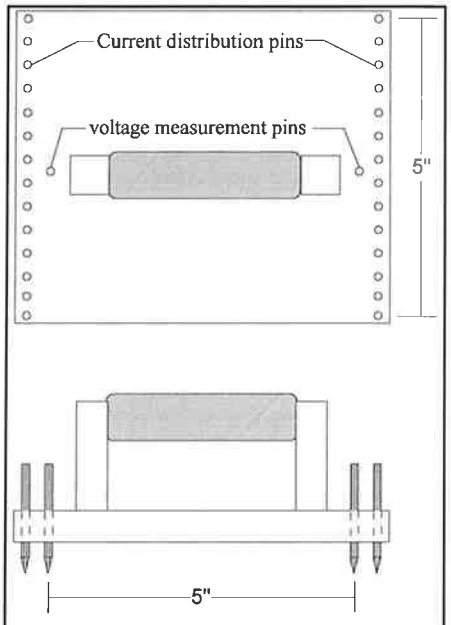

Figure2.1 - Resistance probe design

This probe provides accurate results when the sample being measured is of the same width as the probe. When a sheet of greater width than the probe is measured, errors are introduced as a result of additional current paths outside the outer edge of the probe. The effect of the additional parallel current paths is a reduction in the measured resistance of the sample.

The impact of sheet width was investigated empirically using aluminum foil. Although arc-sprayed titanium was not used for this empirical study, the results should be similar regardless of the material used provided the sheet is thin. Figure 2.2 illustrates that for sheet width greater than two times the probe width, the measured resistance will be about 60% of the true resistance. Eltech performed a similar study using sheets of conductive gel, and their results indicated that as sheet width increased the measured resistance decreased to about 50% of the true resistance. Based on these results, the specifications for the field trial require a measured coating resistance of 0.25 ohms/square (50% of the design value of 0.5 ohms/square).

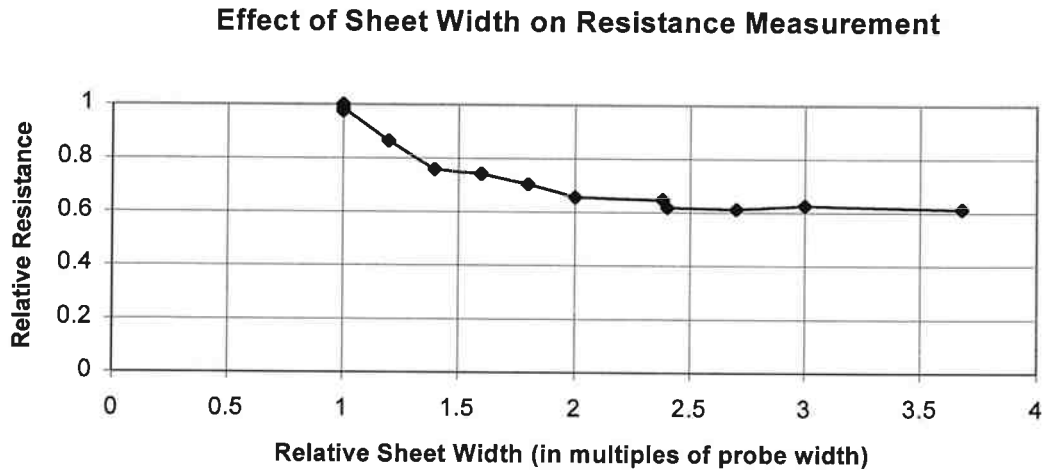

Figure 2.2 Effect of Sheet Width on Coating Resistance Measurement

2.2.2 ARC-SHORTING CONTROL

The spray equipment used for the shop spraying and for the field application was the Thermion Bridgemaster arc-spray system. A significant feature of this equipment is its patented arc-shorting control system which monitors the voltage across the arc gap and stops the wire feed when this voltage becomes too low. A decreasing voltage is an indication that the arc gap is closing; stopping the wire feed allows the arc gap to be re-established before the wires become shorted. When the voltage increases, the wire feed restarts. This process occurs very quickly and is transparent to the equipment user except for the fact that there is little or no problem with shorted feed wires.

A similar arc-shorting control technique was desired for spraying the titanium. The arc-shorting control system included in this model of the Thermion arc-spray equipment was designed for the much lower arc voltages associated with spraying zinc. The titanium is sprayed at an arc voltage of 36 to 41 volts compared to 24 to 26 volts for zinc. for this project, Thermion's arc-shorting control system was modified to provide arc-shorting control at the higher titanium arc voltage.

2.2.3 AUTOMATED SHORT-CIRCUIT DETECTION

Short circuits can occur when undetected surface metal, such as a tie wire, provides contact between the rebar and the arc-sprayed anode. When they occur in highly conductive anodes such as zinc, short circuits provide a local low-resistance path between the anode and the rebar rendering the system ineffective at distributing the protection current throughout the zone. Since the arc-sprayed titanium anode is much less conductive than the zinc, such short circuits are of less consequence. If the short circuit occurs away from the current distribution plate, resistance in the coating can mask the effect of the short circuit. Although the effect of the

short circuit on the system would tend to be more localized, the short circuit would still decrease the effectiveness of the system.

When applying arc-sprayed zinc anodes, an automated short circuit detection system monitors the differential metal corrosion cell voltage occurring between the zinc and steel in contact with the electrolyte within the concrete pores. When this voltage drops too low, indicating a short circuit, the detection system stops the spray equipment to warn the operator of the short circuit condition. A similar system was desired for application of arc-sprayed titanium anodes. However, since passivated titanium is a much less active metal than zinc, the steel-titanium corrosion cell voltage cannot be reliably used for detecting short circuits.

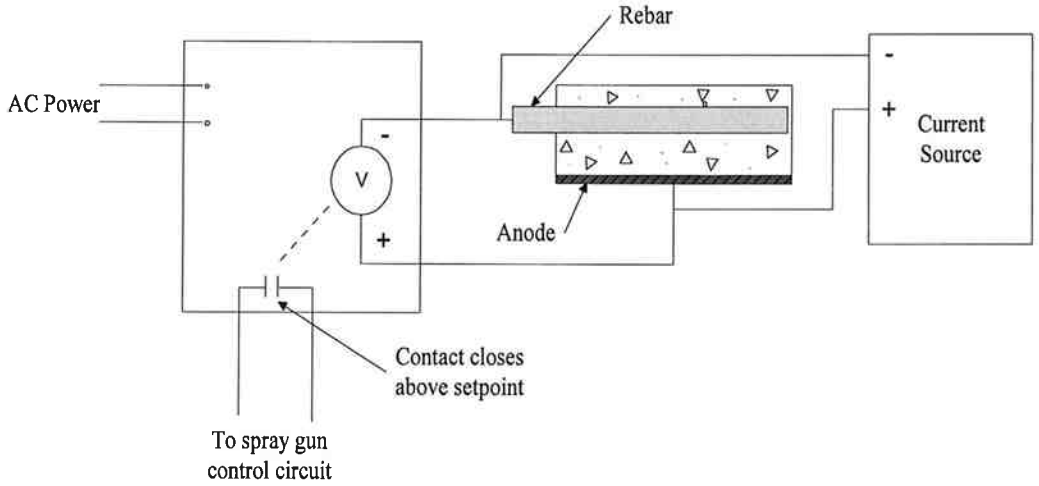

Figure 2.3 Schematic for Automated Short Circuit Detection System

A system was assembled using the same system that is used for spraying zinc with the addition of a constant current supply to achieve a reliable voltage difference between the rebar and the titanium. A constant current supply was selected because this type of supply is tolerant to short circuiting. The short detection system consists of an alarm voltmeter with a programmable setpoint and a relay. The meter used for this purpose was model number Q2005AVR2-SPC as manufactured by Newport Electronics. The setpoint for the meter was set to 0.150 volts, so a voltage difference of 0.15 volts or less between the titanium and the rebar would stop the spray equipment.

The system functioned, and one short circuit was detected during spraying. There were, however, several features of the system which caused less than optimal performance. Because a constant current source was used, the voltage decreased as the area sprayed increased. Increasing area decreases the equivalent resistance of the circuit because additional parallel resistive paths are added to the circuit, and the relationship between equivalent resistance and parallel resistive paths is:

$$R_{Eq} = \frac{1}{\left(\frac{1}{R_1} + \frac{1}{R_2} + \cdots + \frac{1}{R_n}\right)} \qquad (2\text{-}4)$$

This fact required periodic adjustments to the amount of current delivered to compensate for the change in surface area. At the same time, polarization of the system caused the voltage of the system to increase. Also, because of the resistance in the titanium coating, current delivery to the titanium must occur near the area being sprayed to minimize voltage drop in the coating. If this is not done, voltage drop in the coating could mask a short circuit. To eliminate this possible problem, temporary connections to the sprayed titanium were made by taping the current source lead to the titanium with duct tape near the area being sprayed.

These three problems made the voltage measurement displayed on the short circuit detection system difficult to interpret. Before large scale field application, further work is needed on this system to create amore infallible system.

2.2.4 SPRAY PERFORMANCE TEST

Initial testing was performed to determine the range of possible operating parameters for arc-spraying titanium with the thermion Bridgemaster system, and to determine the effect of the high arc temperature on the equipment. The first step in this process was to determine whether 1/8-inch titanium wire could be effectively sprayed. If not, the plan was to proceed using 3/32-inch titanium wire which had been successfully sprayed previously. The larger diameter wire was tried because a higher application rate is possible with larger diameter wire. Two 4.55 kg (10lb) spools of annealed, grade 2 titanium were purchased for this test.

The test spraying of 1/8-inch wire was successful, and there were no heat-related problems in an approximately 10-minute spray test. During this test, smooth arc operation was achieved between 250 and 350 amps resulting in arc voltages between 36 and 41 volts. Air pressure was varied from 586 to 724 kPa (85 to 105 psi).

3.0 SHOP TESTING

3.1 SPRAY PARAMETER OPTIMIZATION

3.1.1 EXPERIMENT DESIGN

This portion of the experiment was intended to determine the spray parameters which result in the optimum deposit efficiency and minimum coating resistance. The following spray parameters were investigated:

Table 3.1: Spray Parameters

Variable	Test Settings	
Current	250, 290, 350 A	
Propellant Pressure	586, 655, 724 kPa	85, 95, 105 psi
Spray Distance	102, 178, 254 mm	4, 7, 10 inches
Propellant Gas	Compressed Air, Nitrogen	
Gun Speed	0.3, 0.46, 0.6 m/s	12, 18, 24 in/s

To obtain constant spray distance and gun speed, samples were sprayed using a custom-designed and fabricated X-Y traversing system. The system used two stepper motors, one each for the X and Y directions, and a programmable indexer to control the spray pattern, gun acceleration, and gun speed. Spray distance was set using height adjustments in the support frame legs.

The samples sprayed during this phase were 127 mm x 152 mm x 13 mm (5" x 6" x 1/2") concrete blocks. Since the size of the concrete block was small, the weight of the uncoated samples was in the range of 500 to 600 grams. This allowed the weight gain of the samples, which is required to determine deposit efficiency, to be measured directly on a 2 kg balance. Samples were weighed prior to spraying and immediately after each pass. A minimum of four spray passes were applied to each sample, and additional passes were added as required to achieve a coating resistance of less than 0.5 ohms/square.

An encoder on the wire feed roll shaft was used to measure the length of wire fed through the spray machine. The amount of time that the spray head is over the sample can be calculated from the gun speed and spray pattern. Since the total spray time was also measured, the amount of titanium used over the sample can be calculated. Using the weight gain of the sample and the weight of titanium used, the deposit efficiency of each pass was calculated.

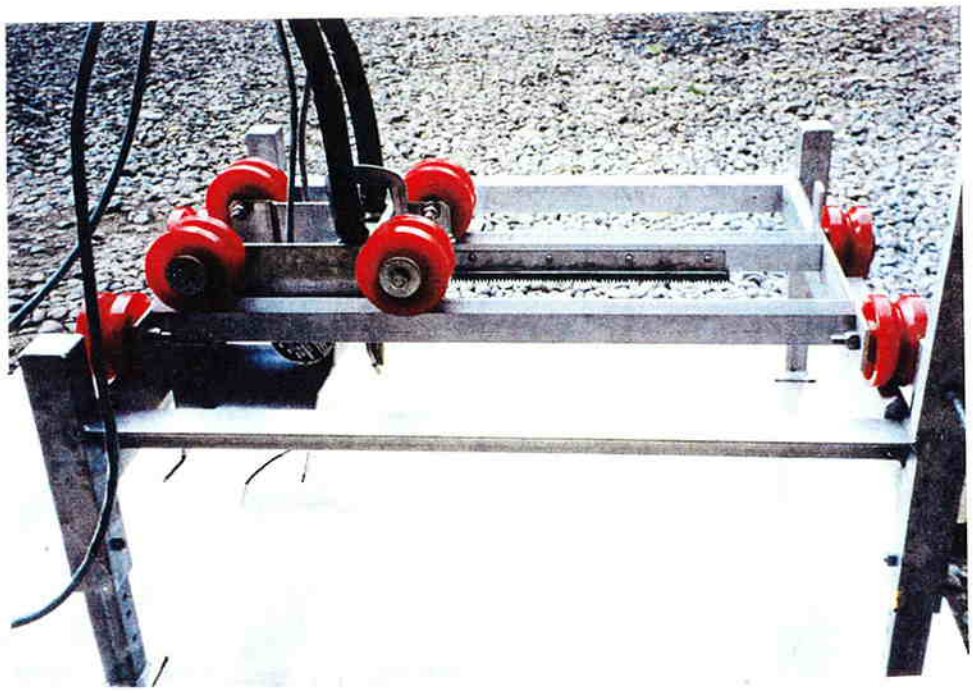

Figure 3.1 X-Y traversing system for spray parameter optimization work

3.1.2 DEPOSIT EFFICIENCY MEASUREMENTS

Previous studies have utilized steel plates for spray parameter studies (*Berndt, et al, 1995*). Measurement of deposit efficiency on concrete samples showed that the initial deposit efficiency of arc-sprayed titanium on concrete is much different than the deposit efficiency of sprayed titanium on steel. Deposit efficiency measurements on steel tend to show relatively uniform deposit efficiencies per pass while measurements on concrete show deposit efficiencies that increase significantly over the first three to four passes.

There are several mechanisms that can explain the low initial deposit efficiency observed on concrete samples. Although the samples were dry from two months of storage in an office environment, the heat from the spray process may evaporate some remaining water from the sample. The effect would be to decrease the weight of the sample which would decrease the measured weight gain of the sample and cause an apparent decrease in deposit efficiency.

This effect was observed while preheating a sample prior to spraying it for bond strength testing. The sample was weighed, heated, sprayed, and weighed once again, and the sample was observed to lose 3.3 g. This is an extreme example, however, since this sample received extended heat input with a torch. The heat input to a sample during spraying is of much shorter duration, so the weight loss from water evaporation in the sample is likely to depress the deposit efficiency measurement by only a small amount.

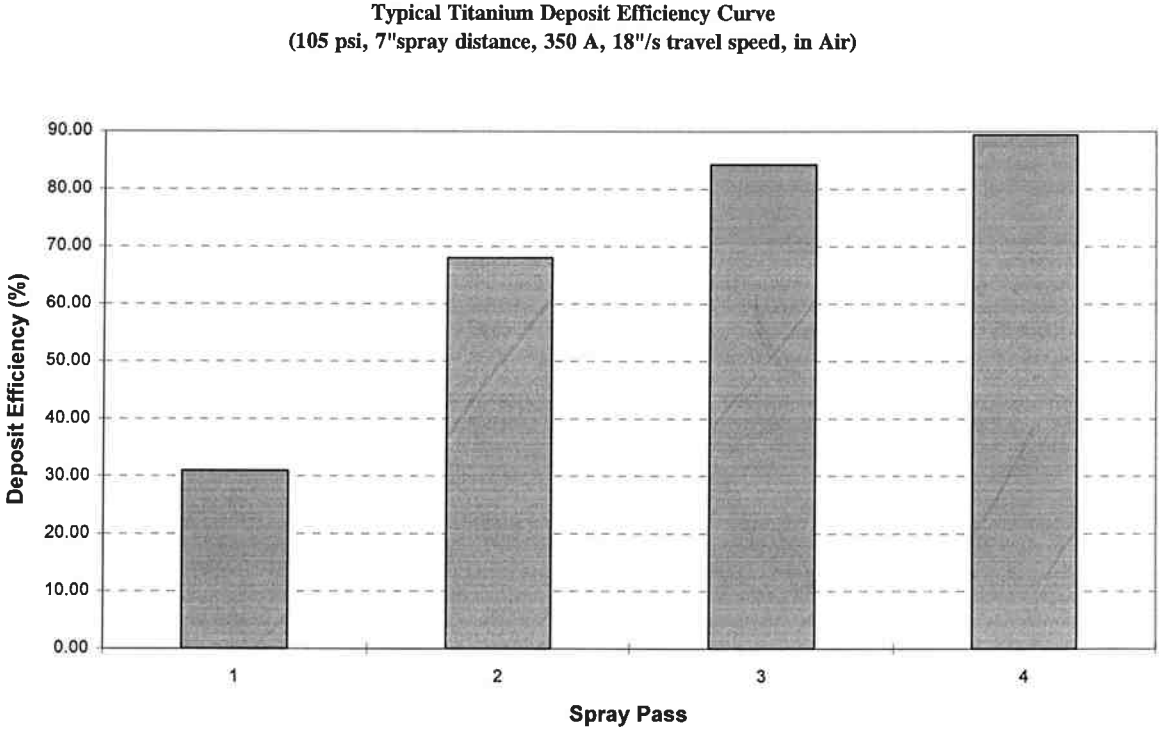

Figure 3.2 Typical titanium deposit efficiency per spray pass

The effect of water evaporation on the deposit efficiency measurement could be determined by oven drying a sample prior to spraying to remove the moisture content. The drying should take place at a low temperature to avoid damaging the concrete. This test, however, was not performed during this study.

A possibly more significant contributor to the low deposit efficiency of the initial pass is the abrading effect of the particle stream from the spray gun. Although not as severe as abrasive blasting, the molten metal droplets impinging on the concrete surface perform a similar function. Visual observations after the first spray pass showed areas where small aggregate had been removed from the substrate. As the particles abrade the substrate, not only is there an apparent decrease in deposit efficiency due to a decrease in the weight of the sample, but there is also a real loss in deposit efficiency as the particles that rebound from and break away with the substrate decrease the amount of titanium remaining on the surface.

An additional difficulty with deposit efficiency measurements is that titanium, at high temperatures, readily absorbs and reacts with nitrogen and oxygen, so the sample weight gain measurements include weight gain from these elements. What this means is that the calculated deposit efficiency is higher than the true deposit efficiency due to the weight gain from these elements which are present interstitially and as titanium compounds. The coating analysis work described in Chapter 4 revealed that titanium accounts for an average of 87 weight percent using air atomization and 88 weight percent using nitrogen atomization.

3.1.3 PARAMETER STUDY

The initial plan for this phase of the project was to collect deposit efficiency measurements for various spray parameters. The collected data would then be analyzed using multiple regression techniques to yield a mathematical relationship that could account for interactive effects between variables to determine the optimum spray parameters in terms of titanium usage. It was thought that the spray parameters which yielded the highest deposit efficiency would be the parameters which should be used for field spraying since these parameters minimized the use of titanium wire. During this data collection phase, coating resistance data was also collected since the possibility that deposit efficiency wouldn't provide a complete picture was recognized.

The attempt to construct a multiple regression equation for the relationship between deposit efficiency and the spray parameters was unsuccessful. The best fits to the data yielded R^2 values around 40% leaving 60% of the variability in the data unexplained. An attempt to develop a relationship between coating resistance and the spray parameters provided only a slight improvement in the regression results generating an R^2 value of about 50%. This was not very surprising since reasonably good correlation was expected between coating resistance and deposit efficiency. However, when a simple regression equation was constructed for the relationship between coating resistance and deposit efficiency, the R^2 value was less than 20% indicating very little relationship between these two dependent variables.

During the shop spraying portion of this study, two samples had been sprayed on glass plates to allow an investigation of the coating thickness at the specified coating resistance. Each sample had been sprayed at different spray parameters, so an investigation of the effect of changing parameters on coating properties was possible. The glass plate provided a uniform substrate that allowed determination of an average coating thickness. The coating was uniform, varying by about $\pm$ 0.013 mm (0.0005") across the sample. Thickness measurements were made by measuring the thickness of the glass plate with a micrometer at specific points on the plate prior to spraying and again after spraying. The calculated results are shown in Table 3.2.

Both samples were sprayed at a gun travel speed of 0.457 m/s (18 in/s). From these results, it is apparent that changes in spray parameters can have a large impact on the structure of the coating. These two sets of parameters led to large differences in the coating density which resulted in a 2:1 difference in coating resistivity, and the electrical characteristics of the

Table 3.2: Coating Properties

Parameters	Avg. Thickness	Wt. Gain	Coating Resistance	Coating Density	Coating Resistivity
Air, 724 kPa, 300A, 178 mm (Air, 105 psi, 300A, 7")	0.19 mm (0.007")	7.17 g (0.25 oz)	0.375 ohms	1.95×10^{-3} g/mm^3	6.99×10^{-3} ohm-cm
N, 793 kPa, 275 A, 152 mm (N, 115 psi, 275 A, 6")	0.13 mm (0.005")	6.53 g (0.23 oz)	0.27 ohms	2.6×10^{-3} g/mm^3	3.43×10^{-3} ohm-cm

coating are the characteristics that determine how well the coating will perform its intended purpose of distributing current throughout the zone. These results indicate that, for arc-sprayed titanium anodes, deposit efficiency should not be the primary dependent variable for optimization of spray parameters.

Another multiple regression relationship was attempted using the sample resistance multiplied by the sample weight gain as the dependent variable. This product accounts for the interaction between these two variables and provides a measure of effectiveness of the deposited titanium for conducting current. To gain a better understanding of this product (r x w), it is useful to study Equation 2-3. Although the relationship between thickness and weight gain is imperfect due to variation in coating density and difficulty in measuring weight gain as discussed in Section 3.1.2, weight gain is expected to have a fairly high correlation with coating thickness. This means that the product of coating resistance (in ohms/square) and weight gain yields a quantity that is highly correlated to coating resistivity.

The log of the product was taken to account for non-linearity in the relationship between the dependent variable and the independent variables. The resulting equation provided a good fit to the data with an R^2 value of 81%. The best fit relationship is as follows:

$$\mathbf{Ln(r \times w) = 0.633 - 6.75 \times 10^{-6}\left(c \times d^2\right) + 3.33 \times 10^{-3} d^2 - 0.366p} \qquad \mathbf{(3.1)}$$

where: **r** = coating resistance in ohms/square
w = sample weight gain in grams
d = spray distance in cm
c = current in amps
p = propellant (0 = air, 1 = nitrogen)

For the data collected during this study, the pressure of the propellant and the gun travel speed did not prove to be significant variables, so they were removed from the resulting equation. These variables, however, have been reported as significant in other work (*Berndt, et al, 1995*).

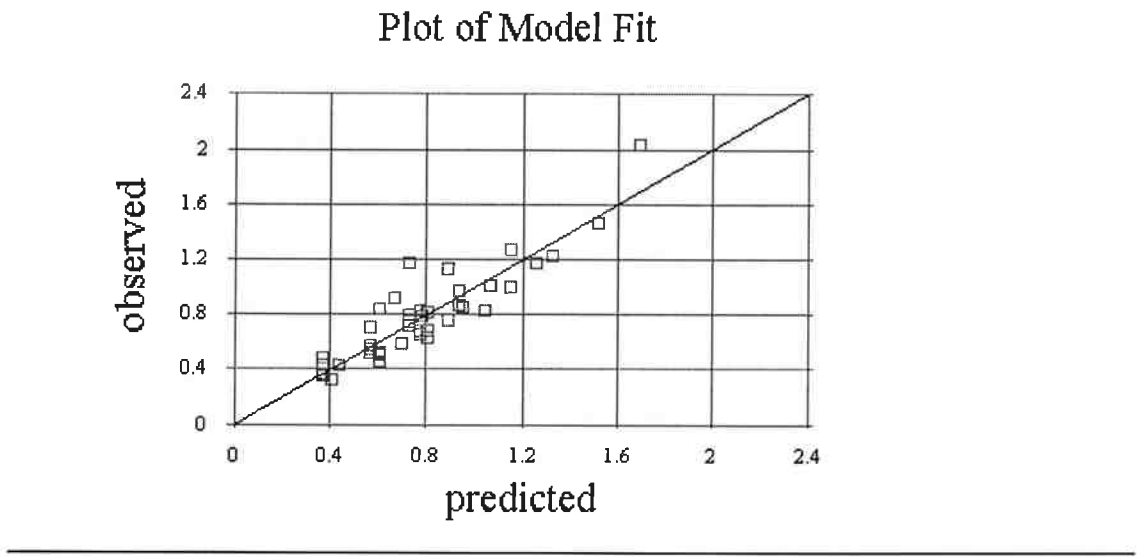

Figure.3.3 Fit of regression equation to empirical data

The most effective coating for distributing current is the coating with the lowest resistivity which is approximated by the product of r and w in the regression analysis. The results of the regression analysis demonstrate that the spray parameters which reduce the coating resistivity: nitrogen propellant, low spray distance, and high current. Figure 3.3 and Table 3.3 present the results of the multiple regression analysis.

Although the regression results indicate that low spray distance, nitrogen propellant, and high current provide a more effective coating, the shop spraying experience indicated that, at 102 mm (4"), 0.3 m/s (12 in/s), and 350 A, the coating tended to burn and blister. Additionally, operating the gun at 350 A produced sufficient heat to caused melt a hole in the arc shield on the gun. Manual application of arc-sprayed titanium, therefore, was specified to take place at around a 150 mm (6") spray distance and 300 A.

It is important to note that spray distance appears in the regression equation as a squared term, so the effect of a change in spray distance is amplified. At the specified spray parameters (300 A, air), the equation predicts that changing from a 100 mm (4 inch) spray distance to 150 mm (6 inches) requires a 17% increase in sample weight gain to achieve the required coating resistance of 0.5 ohms/square. The second term also indicates an interactive effect between current and the square of spray distance. For a given spray distance, higher current tends to produce a more effective coating, but the effect of higher current is greater for larger spray distances.

Table 3.3: Multiple Regression Analysis Results

Dependent variable: Ln(Sample Resistance Sample Wt gain)				
Parameter*	Estimate	Standard Error	T Statistic	P-Value
CONSTANT	0.63	0.045	13.9	0.00
Current*(Dist.)^2	-6.75 10^{-6}	1.65x10^{-6}	-4.1	0.00
(Dist.)^2	0.0033	0.00052	6.4	0.00
Propellant	-0.37	0.046	-8.0	0.00

*Dimensions are in cm; propellant - 0 = air, 1 = N; current is in amps

Analysis of Variance

Source	Sum of Squares	Df	Mean Square	F-Ratio	P-Value
Model	3.77	3	1.26	58.9	0.00
Residual	0.81	38	0.021		
Total (corr.)	4.58	41			

R-squared = 82.3 percent
R-squared (adjusted for d.f.) = 80.9 percent
Standard error of est. = 0.15
Mean absolute error = 0.104

Equation 3-1 provides a mathematical expression that can be used for predicting coating performance for a given set of spray parameters. Its most appropriate use, however, is to provide an understanding of the effect of changes in the independent variables on the dependent variable. Care must be taken when using Equation 3-1 for prediction outside the range of the data used to construct the equation.

Equation 3-1 indicates that the use of nitrogen as a propellant is beneficial. Compressed air, however, was specified for use on Depoe Bay because Depoe Bay is remote from nitrogen supply points. The spray equipment uses a large volume of propellant during spraying, so the extra costs to get nitrogen on site more than offset the savings in titanium usage from improved deposition efficiency

Note that a titanium consumption rate calculated from Equation 3-1 for a set of spray parameters is a minimum consumption rate. The actual titanium usage is expected to be significantly higher due to titanium wire waste, inability to spray the coating to exactly the maximum permitted coating resistance, and variability in spray parameters during manual spraying.

3.2 BOND STRENGTH TESTING

Eight 127 mm x 152 mm (5" x 6") samples were prepared for testing the bond strength of the sprayed titanium coating. All samples except Sample 1 were sprayed using nitrogen as the propellant. The nitrogen samples were sprayed with the same spray parameters [759 kPa (110 psi), 178 mm (7") spray distance, 290 amps]. The sample sprayed in air was sprayed at 724 kPa (105 psi), 100 mm (4") spray distance, and 250 amps. The bond test results are shown in Table 3.4.

Table 3.4: Bond Test Results

Sample	Bond Strength		Resistance $\left(\frac{\text{ohms}}{\text{square}}\right)$	Treatment
	kPa	psi		
1	1028	149	0.23	Sprayed in air
41	1269	184	0.365	Surface temp. = 17.2°C (63°F)
42	924	134	0.34	Surface temp. = 18.9°C (66°F)
43	1414	205	0.37	Surface temp. = 13.3°C (56°F)
44	945	137	0.305	Surface temp. = 104.4°C (220°F)
45	1214	176	0.28	Sample submerged in water for 15 minutes immediately prior to spraying.
46	1221	177	0.37	Surface temp. = 1.1°C (34°F)
47	1428	207	0.385	Surface temp. = 8.3°C (47°F), condensation present on surface prior to spraying.

Although these results cannot be considered an extensive study of the bond strength of titanium to concrete, multiple regression analysis applied to the test data resulted in equation 3-2.

$$\mathbf{B = -3719.9 + 13399.9r + 5.586t} \qquad \textbf{(3-2)}$$

where: **B** = coating bond strength in kPa
r = coating resistance in ohms/square
t = substrate temperature in $^{\circ}$C

The fit was good with an adjusted R^2 of 90%. The large coefficient for coating resistance in Equation 3-2 shows that the effect of coating resistance factors on coating bond strength is much more significant than that of substrate temperature. Since coating resistance is inversely proportional to coating thickness, Equation 3-2 demonstrates that increasing coating thickness decreases bond strength. This result is consistent with studies performed with other thermal-sprayed coatings (*Boyer, et al, 1994: Krepski, 1993*).

Although the fit of the equation to the observed values is good, Equation 3-2 should be used with care outside the resistance range of the data points (0.305 to 0.385 ohms/square). Equation 3-2 predicts a bond strength of zero at a coating resistance of 0.27 ohms/square which contradicts observed bonding at lower coating resistance during the spray parameter optimization portion of this study. The equation's predictive capability is limited, and it should be used simply as an indicator of the effect these variables have on coating bond strength.

The titanium spray appears to be much more tolerant of surface moisture than zinc. Reasonable bond strength was achieved even on the sample that was submerged in water prior to spraying. However, the presence of a high amount of moisture in the concrete appears to effect deposit efficiency since more spray passes were required to achieve the desired coating resistance.

Table 3.5: Regression Results for Equation 3-2

Regression Statistics	
Multiple R	0.97
R^2	0.94
Adjusted R^2	0.90
Standard Error	69.55
Observations	6

ANOVA

	df	*SS*	*MS*	*F*	*Significance F*
Regression	2	229673	114837	23.74	0.014
Residual	3	14510	4837		
Total	5	244183			

	Coefficients	*Stnd. Error*	*t Stat*	*P-value*	*Lower 95%*	*Upper 95%*
Intercept	-3719.91	938.30	-3.96	0.029	-6706.02	-733.81
X Variable 1	13399.92	2504.85	5.35	0.013	5428.36	21371.47
X Variable 2	5.59	1.89	2.96	0.059	-0.41	11.59

Bond strength testing was performed by first affixing a 50 mm aluminum disk to the surface with epoxy and then measuring the force required to pull the disk from the surface with a Proceq Dyna Z-5 adhesion tester. Since the titanium coating is thin, a potential problem was penetration of the epoxy through the coating to the substrate. To minimize this problem, a viscous, quick setting epoxy was used. The epoxy used for this bond strength measurement was Duro Master Mend® TM-81 epoxy. To provide a reference point for the bond strength measurements, a bond test was taken on a bare concrete sample, and the strength of the concrete was 1710 kPa (248 psi). Measurement of the concrete area on the removed aluminum disks indicated that bond failure occurred approximately 30-40% within the concrete and 60-70% at the interface or within the titanium.

3.3 THE APPLICATION OF TITANIUM SPRAY OVER SUBSTRATE CRACKS

The ability of arc-sprayed titanium to span cracks in the concrete substrate was investigated by preparing concrete samples with simulated cracks. The samples were prepared using the 127 mm x 152 mm (5"x 6") concrete samples that were prepared for the spray parameter optimization study. A sample was saw cut in half and glued to an unsawed sample. Shims were placed between the two halves of the cut sample to achieve the desired crack width.

The largest crack which the coating successfully bridged was a crack that measured 0.127 mm (0.005 inches) in width. This crack required eight spray passes to span the crack and achieve the desired coating resistance. The spray settings used for this test would typically achieve the desired resistance on an uncracked sample in four spray passes. Wider cracks require more spray passes creating a thicker coating. As the coating becomes thicker, it can begin to experience bonding problems.

An arc-sprayed titanium coating is not tolerant of cracks in the substrate. Only very narrow cracks can be spanned by the titanium without excess thickness build-up. During the field spraying, this limitation did not appear to create problems. Most cracks on the structure, although wide on the surface, become very narrow with depth. The coating seems to be able to adequately span such cracks by penetrating into the crack and bridging the crack where it becomes narrow. Where wide cracks did exist, there were typically sufficient alternate paths for current flow around the crack to provide current distribution to all areas of the anode. Had any problem cracks been discovered during the field application, titanium strips would have been installed to conduct current across the crack.

3.4 OPERATIONAL SAMPLES

Five operational samples were prepared for accelerated testing. The dimensions for the concrete slabs cast for this experiment are 230 mm x 330 mm x 50 mm (9"x13"x2"). The slabs were cast with a 12.5 mm (0.5 inch), No. 16 expanded metal mesh covering the full dimensions of the bottom of the form. A thin layer of the concrete mixture was spread in the bottom of the form prior to placing the mesh to ensure that there were no voids behind the mesh. The resulting concrete cover over the mesh was 44.5 mm (1.75"). Steel wire was welded to the mesh and extended above the top surface of the form to provide a means to make electrical connections to the mesh.

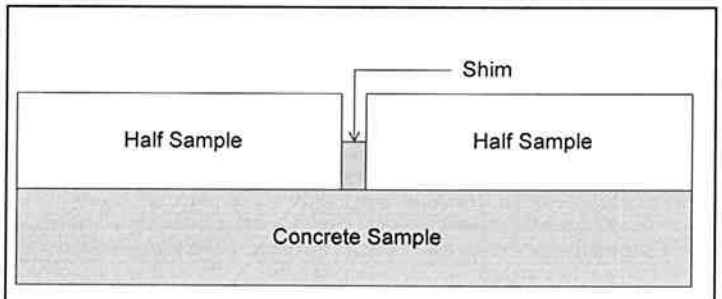

Figure3.4 Crack simulation

The concrete mix design is shown in Table 3-6.

Table 3.6: Concrete Mix Design

Cement	259 kg	570 lbs
Coarse aggregate[a]	704.5 kg[b]	1550 lbs[b]
Sand	738 kg[b]	1624 lbs[b]
Water	125 kg	275 lbs

[a]4.75 mm to 6.35 mm (0.19" to 0.25")
[b]Saturated surface dry basis

The water cement ratio was 0.48 which is similar to but probably slightly less than is typical for ODOT's older coastal structures. A smaller aggregate size was used in the slabs to obtain uniform current distribution, something that is not possible when large aggregate is present. To simulate marine-exposed concrete and to increase the conductivity of the slabs, 99.9% pure, reagent grade sodium chloride was added to the concrete mix at the rate of 3 kg/m^3 (5 lbs. per cubic yard) of concrete.

The samples received the titanium spray and catalysis treatments shown in Table 3.7. The catalyst was brush applied to the titanium coating on the slab surface approximately two months after the slabs were sprayed. The catalyst was applied to each slab (except number 5) with a power supply connected to provide 29 mA of cathodic protection current per square

Table 3.7: Operational Sample Treatments

Slab	Propellant	Pressure	Current	Distance	Notes
5	Air	105	300	152 mm	Uncatalyzed sample, R = 0.2 Ω/square
6	Air	105	300	152 mm	Catalyzed R = 0.2 Ω/square
48	N	115	275	152 mm	Catalyzed R = 0.16 Ω/square
49	N	115	275	152 mm	Catalyzed R = 0.155 Ω/square
50	N	115	275	152 mm	Catalyzed simulated overhead surface R = 0.155 Ω/square

meter of anode surface area. Sample 5 was not catalyzed and serves as a control sample. The catalyst was brush applied to sample 50 with the sample inverted to simulate an overhead surface. The purpose of simulating the overhead surface was to verify that the catalyst could effectively reach the titanium/concrete interface without assistance from gravity. The operating data to date (see Figure 3.5) indicate that overhead surfaces can be effectively post catalyzed.

Current was applied to the slabs for one month before they were transferred to a humidity controlled room at the US Bureau of Mines in Albany, Oregon (now US Department of Energy, Albany Research Center). The slabs will continue to receive cathodic protection current at an accelerated level of approximately 29 mA/m^2 (2.5 mA/ft^2) until the conclusion of this study.

The five slabs are connected in series to a power supply operating in constant current mode. The power supply output current and the output voltage (for five slabs in series) for the first 300 days of operation is shown in Figure 3.6. The smoothing of the output current at day 227 corresponds to replacement of the constant current power supply. The electrical connection to each slab was made by drilling a hole in the center of the sprayed titanium surface. Silicone was inserted into the hole prior to installing a plastic expansion anchor. A steel washer and ring connector were placed over a steel screw, and the screw was inserted into the anchor. Corrosion problems were expected from using steel parts for this anode connection, but properly sized titanium components could not be located.

The expected corrosion was experienced and can be seen in Figure 3.6 as a rapid increase in system voltage beginning on day 131. That corrosion problem was corrected by replacing all slab connections, but a general rise in voltage level and some additional voltage peaks indicate that addition corrosion problems have occurred. Slab connections were replaced once again on day 289.

As is shown in Figure 3.5, the individual slab voltages for the catalyzed samples have remained fairly stable. Individual slab voltages were measured independently of the steel electrical connections to the slabs. Although the voltage of the uncatalyzed slab has not yet increased as expected, its voltage has exhibited large fluctuations with humidity variations. The brief peak at day 289 is related to corrosion of the current contact, but the remaining peaks are related to intermittent failure of the humidifying system which caused the room humidity to fluctuate. Although the catalyzed samples also fluctuated with humidity, the uncatalyzed sample appears much more sensitive to humidity changes.

The voltage of the uncatalyzed sample was expected to climb because the passivating oxide layer that forms on bare titanium is expected to resist current flow until the anodic breakdown potential of titanium is exceeded. Above this potential, titanium is no longer passive and corrosion will occur. The anodic breakdown potential varies with the purity of the titanium, the composition of the electrolyte, and the temperature. As a reference point, the anodic breakdown potential of grade 2 titanium in a solution of 1 N NaCl at 25°C is 11.0 volts versus a Ag/AgCl reference electrode (*Boyer, et al, 1994*).

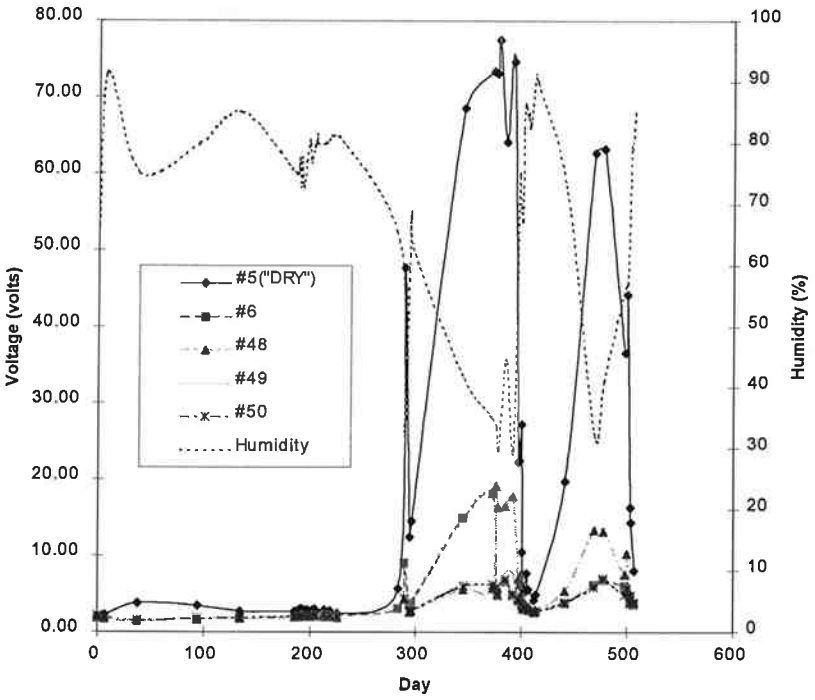

Figure 3.5 Individual slab voltages

Previous work performed by Eltech Research Corporation showed a substantial voltage increase for an uncatalyzed slab beginning at approximately 130 days (*Berndt, et al, 1995*). The current density for the Eltech study was 21.5 mA/m^2 (2 mA/ft^2). The uncatalyzed sample in this study has shown large voltage increases during low humidity, but when the humidity increases, the slab voltage returns to a voltage level similar to the catalyzed samples. The individual slab voltages will continue to be gathered until the conclusion of the study. Further investigation of this humidity related behavior will be completed and included in the final report.

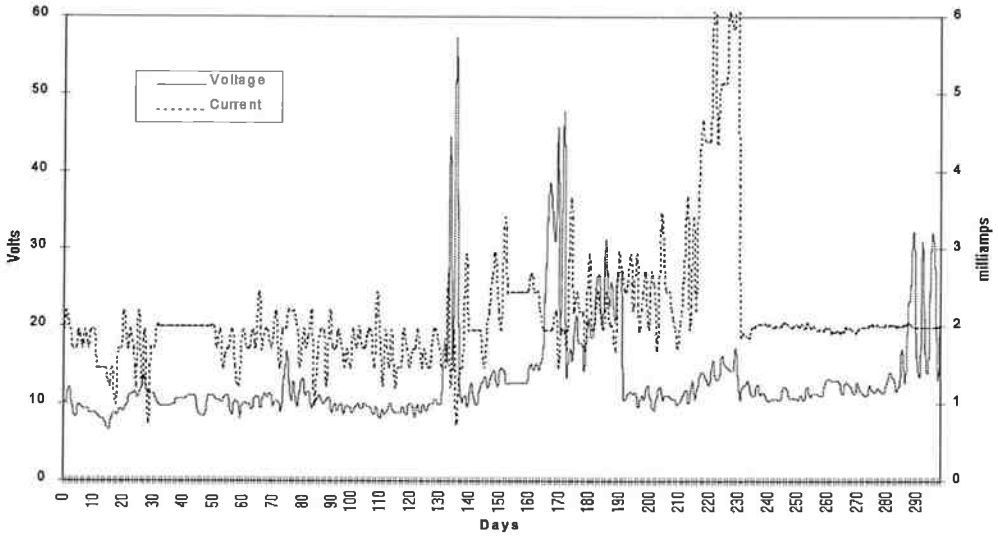

Figure 3.6 Operating slab voltage and current for 5 slabs in series

4.0 COATING CHARACTERIZATION

Thermal-spray coatings of titanium are increasingly being used in industrial applications, particularly to produce corrosion-resistant surfaces for the chemical process industries (*Krepski, 1993*). These coatings are typically applied in an inert atmosphere or a vacuum using shrouds or chambers to prevent or to minimize reactions with the atmosphere (*Krepski, 1993*). Coatings of titanium applied in air or nitrogen, as done in the present study (*Bennett, et al, 1995*), are a novel use of thermal spray technology. An understanding of the properties of these coatings requires an understanding of the significant titanium-atmosphere reactions and their effect on the chemistry of the coating that is produced.

Chemical analyses provide the basis for understanding how reactions with the atmosphere may affect the chemical, electrochemical, and mechanical properties of the Ti anode. Prior to these analyses, the coating would nominally have been described as a thin layer of coalesced titanium metal droplets or "splats" with an oxidized surface, possibly TiO_2. However, there was an appreciation that reaction products formed by the titanium droplets and the atmosphere, and the structures they form, could have a significant effect on the volume resistivity of the coating, the insulating nature of surface layers, electrochemical reactions at the coating surface, the mechanical properties of the coating, and coating internal stresses.

4.1 SELECTED PROPERTIES OF THE TI-O-N SYSTEM

Tabulated below are property data useful for interpreting and understanding the nature and performance of the arc-sprayed Ti coatings. Table 4.1 describes physical properties of possible coatings constituents. Volume ratio is the molecular volume of the compound of interest divided by the atomic volume of the Ti producing the compound.

Table 4.1 Physical Properties of Coating Constituents

Compound/Element	Molecular Weight	Melting Point, °C	Theoretical Density, g/cm^3	Volume Ratio
Ti	47.9	1660	4.50	--
TiO	63.9	1750	4.93 [a]	1.20 [b]
TiO_2	79.9	1840	4.25 [a]	1.73 [c]
TiN	61.9	2930, N_2 liberated	5.44 [c]	1.09 [c]

a. *"Engineering Property Data on Selected Ceramics-Single Oxides", 1981.*
b. *Kubaschewski and Hopkins, 1992.*
c. *"Engineering Property Data on Selected Ceramics-Nitrides", 1976.*

Similarly, Table 4.2 describes transport properties of possible coatings constituents. Electrical resistivity is particularly important because resistance measurements are used by thermal spray applicators to gauge when the Ti coating is sufficiently conductive. Coefficient of linear thermal expansion and thermal conductivity can aid in understanding the highly dynamic mass and heat transfer processes occurring when the molten Ti droplets are in flight and after they "splat" on the structure surface to be incorporated into the developing coating. Conduction classification suggests possible ways, such as alloying the Ti with small amounts of other elements, to alter oxidation processes affecting the coating and to change the coating electrical resistivity.

Table 4.2 Transport Properties of Coatings Constituents

Compound/Element	Conduction Classification	Resistivity, μohm-cm	Coefficient Linear Thermal Expansion, μinch/in-°C	Thermal Conductivity, cal/s-cm-°C
Ti	metallic	50 [a] 42 [c]	8.5 [d]	0.0495 [e]
TiO	metallic [a]	350 [b]	---	---
TiO_2	n-type [a]	$> 3 \times 10^7$ [f]	9.4 [g]	0.0156 [h]
TiN	n-type [a]	15.5 [i] 21.7 [j]	8.0 [g]	0.0579 [k]

a. *Kubaschewski and Hopkins, 1992.*
b. *Gruber and Krautz, 1986.*
c. *Weast, p. F-172, 1980.*
d. *Weast, p. D-189, 1980.*
e. *Weasp, p. E-12 through 17, 1980.*
f. *Campbell and Sherwood, 1967.*
g. *Lackey, et al, 1987.*
h. *Weast, p. d-51 through 60, 1980.*
i. *Munster and Sagel, 1956; Goldsmith, et al, 1961.*
j. *Blocher, 1967.*
k. *"Engineering Property Data on Selected Ceramics-Single Oxides", 1981.*

Table 4.3 Stable Low-pressure Phases in the Ti-O System. [a]

Phase	Composition, wt pct O	Space Group
β-Ti	0 to 3	Im3m
α-Ti	0 to 13.5	$P6_3/mmc$
Ti_3O	~8 to ~13	P3lc
Ti_2O	~10 to 14	P3ml
γ-TiO	15.2 to 29.4	Fm3m
Ti_3O_2	~18	P6/mmm
β-TiO	~24 to 29.4	---
α-TiO	~25.0	A2/m or B*/*
$\beta\text{-}Ti_{1-x}O$	~29.5	I222
$\alpha\text{-}Ti_{1-x}O$	~29.5	I4/m
$\beta\text{-}Ti_2O_3$	33.2 to 33.6	R3c
$\alpha\text{-}Ti_2O_3$	33.2 to 33.6	R3c
$\beta\text{-}Ti_3O_5$	35.8	---
$\alpha\text{-}Ti_3O_5$	35.8	C2/m
$\alpha'\text{-}Ti_3O_5$	35.8	Cc
$\gamma\text{-}Ti_4O_7$	36.9	P1
$\beta\text{-}Ti_4O_7$	36.9	P1
$\alpha\text{-}Ti_4O_7$	36.9	P1
$\gamma\text{-}Ti_5O_9$	37.6	P1
$\beta\text{-}Ti_6O_{11}$	38.0	A1
Ti_7O_{13}	38.3	P1
Ti_8O_{15}	38.5	A1
Ti_9O_{17}	38.7	P1
TiO_2, rutile	40.1	$P4_2/mnm$

a. "Oxygen-Titanium Alloy Phase Diagrams", 1992.

Phase diagrams describe the temperature-composition-structure relationships that exist for alloy systems under thermal and chemical equilibrium conditions. While thermal spray coatings are typically highly non-equilibrium systems, phase diagrams can provide useful guidance on the compositions and structures that the coatings will tend towards. A ternary diagram with sufficient detail was not available for the Ti-O-N system. Shown in Figure 4.1 and 4.2 are the binary phase diagrams for Ti-O and Ti-N respectively. Tables 4.3 and 4.4 contain specific composition and structure data.

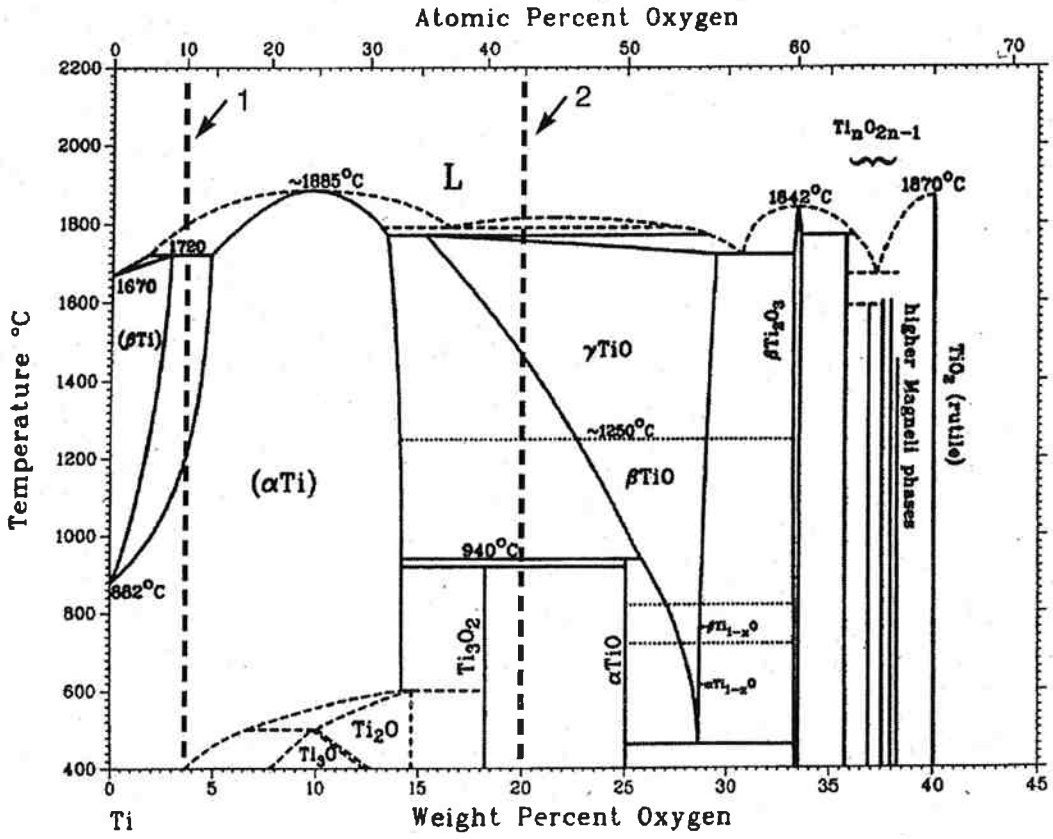

Figure .4.1 Ti-O phase diagram (*"Oxygen-Titanium, Alloy Phase Diagrams", 1992*).
Lines 1 and 2 represent the composition of typical Ti-rich and Ti-poor phases, respectively, in the arc-sprayed Ti coatings

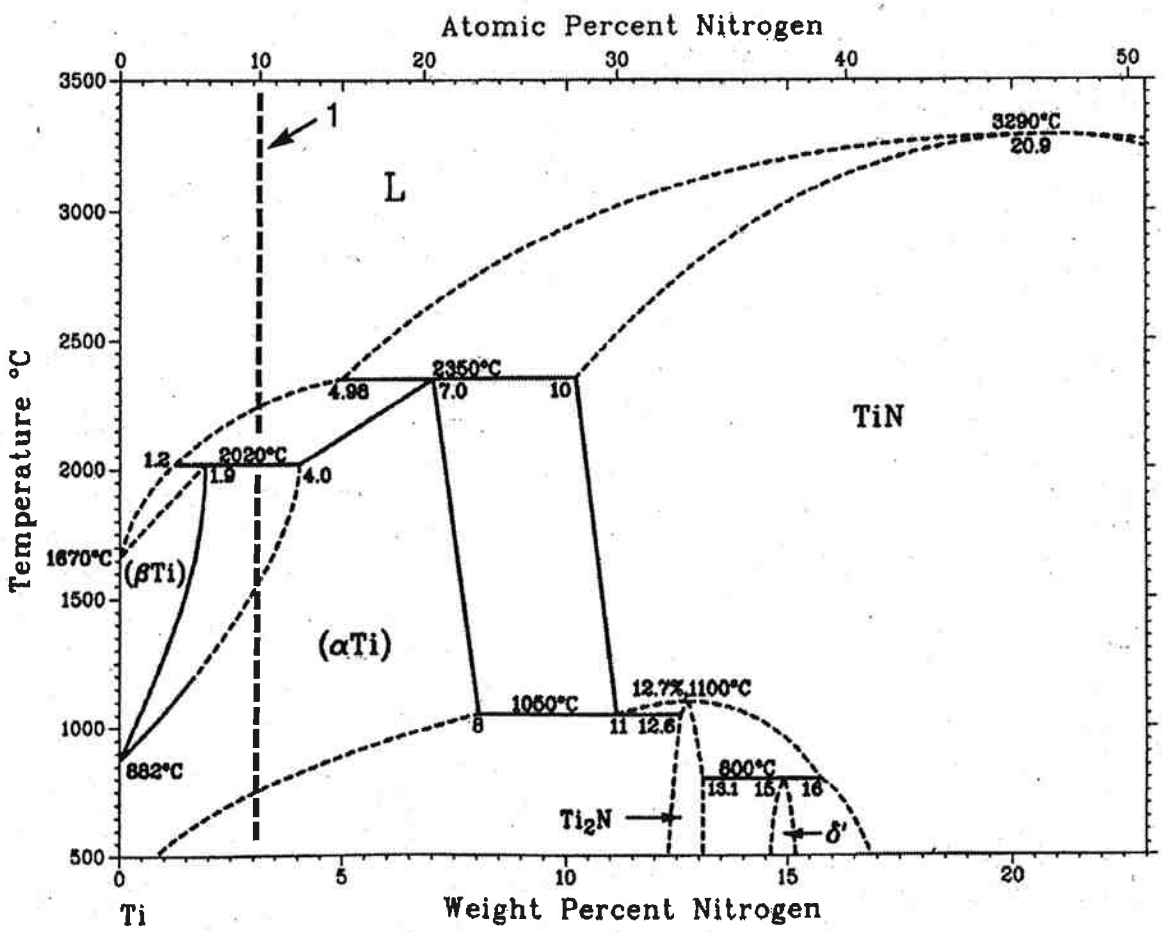

Figure 4.2 Ti-N phase diagram (*"Nitrogen-Titanium, Alloy Phase Diagrams", 1992).*
Line 1 represents the composition of a typical Ti-poor phase in the arc-sprayed Ti coatings.

Table 0-4 Stable Phases in the Ti-N System. [a]

Phase	Composition, wt pct N	Space Group
α-Ti	0 to 8	$P6_3/mmc$
β-Ti	0 to 1.9	Im3m
Ti_2N	~13	$P4_2/mnm$
TiN	10 to >22.6	Fm3m
d'	~15	$I4_1/amd$
w	~0	---

a. "Nitrogen-Titanium, alloy Phase Diagrams", 1992.

4.2 CHARACTERIZATION TECHNIQUES

Specific information sought from the chemical analyses were: (1) an identification of the phases present in the coating, (2) the amount of interstitial oxygen and nitrogen associated with the titanium matrix, and (3) the structure of the coating. No single analytical technique directly gives this information because of the potentially complex nature of the coatings. However,

coatings thermal-sprayed on glass and on concrete were examined by several techniques (X-ray fluorescence and diffraction, gas analysis, electron microprobe (EMP), analytical scanning electron microscopy (SEM), and X-ray photoelectron spectroscopy) to provide a more detailed understanding of the surface and bulk chemistry of the coatings.
samples

Coatings were prepared on glass and concrete substrates using air and nitrogen as the atomizing gas. A Thermion Bridgemaster twin-wire arc-spray unit with a PowCon 630 SMP inverter power supply was operated at or near the optimum parameters for coatings application. Prior to coating, concrete surfaces were sandblasted; glass surfaces were degreased with ethyl alcohol. The feed wire for the arc-spray unit was grade 1 titanium wire, 1/8-inch diameter, specification AWS A5.16-90 ERTI 1, containing (in wt pct) 0.004 N, 0.01 C, 0.0009 H, 0.10 Fe 0.054 O, bal Ti.

The wire was annealed in air at 1300° F (700° C) for one hour, air cooled, then pickled in HNO_3-HF to remove oxides from the surface. Mechanical properties were: tensile strength, 54,500 psi; yield strength (0.2%), 37,200 psi; elongation, 36.6 pct; reduction of area, 72.2 pct (*Gernitsky, 1995*). Hardness values were measured in the laboratory using a Knoop diamond microindentor and a 1000g load. The hardness of cold drawn Ti wire averaged KHN_{1000} 173 (HRB 83) and the annealed wire was KHN_{1000} 122 (HRB 61). The measured hardness of the annealed wire was close to that reported in the literature for annealed grade 1 Ti, HRB 64.7 to 87.1 (*Donachie, 1988*).

Titanium coatings used in the chemical analyses are described in Table 4.5. The coatings were between 2 and 6 mils (50 to 150 mm) in thickness and were formed by multiple passes of the spray head. All samples were sprayed without special shrouding to exclude atmospheric oxygen from contact with the hot titanium. Some were sprayed using air from a compressor as the atomizer gas; others were sprayed using bottled nitrogen (99.9 pct pure) as the atomizer gas. The first four samples (TiCA, TiCN, TiPA, TiPN) were sprayed in a laboratory environment using robotics to control the spray pattern. The fifth sample, TiQA, was applied in the field to quartz glass using air as the atomizing gas and a Miller Model FC-6 constant potential DC welding power supply substituted for the PowCon 630 SMP.

Table 4.5 Arc-sprayed Ti Coating Samples for Chemical Analyses.

Sample Identification	Substrate	Atomizing Gas
TiCA	concrete	air
TiCN	concrete	nitrogen
TiPA	Pyrex glass	air
TiPN	Pyrex glass	nitrogen
TiQA	quartz glass	air

4.2.2 ANALYSES

4.2.2.1 X-Ray Fluorescence

Coating samples were analyzed by energy-dispersive X-ray fluorescence spectrometry to determine if contaminants (other than oxygen and nitrogen) were picked up by the titanium during the arc-spray process. A Philips PV9500 spectrometer system equipped with a Rh X-ray tube and Si-Li semiconductor detector was used. The samples analyzed were TiPA, TiPN, and TiCA. They were degreased and dried before analysis. Coating flakes were stripped from TiPA and TiPN with a razor blade. The flakes were finely ground in an agate mortar and mounted on cellophane tape for analysis. Coatings were also analyzed *in situ* on small samples cut from TiPA, TiPN, and TiCA.

4.2.2.2 Gas Analyses

Coating samples were analyzed for total concentration of oxygen and nitrogen using a LEECO 436 oxygen-nitrogen gas analyzer. The samples analyzed were TiPA and, TiPN. Coating flakes were stripped from the substrates with a razor blade. Coatings on Pyrex glass sprayed using air atomization were more adherent than those using nitrogen atomization.

Samples of the coating flakes were weighed and then sealed in a tin capsule for analysis. The coatings samples gave normal-shaped gas evolution curves with a single peak for oxygen and some tailing of the oxygen peak. The gas analyses results represent the total oxygen and nitrogen present in the coating as Ti compounds plus that contained interstitially within the metallic Ti.

An NBS glass standard was run to determine if adhering glass fragments affected the oxygen analyses. The NBS glass curve was very different from the coatings curve with three distinct gas evolution peaks. A small peak was present in the range where oxygen was evolved from the coatings samples. The two larger peaks appeared later in the determination. The absence of these larger peaks in the determination of oxygen in the coatings samples suggests that the glass fragments did not contribute significant oxygen to the coatings samples analyses.

4.2.2.3 X-Ray Diffraction

Coatings samples were analyzed by X-ray diffraction to identify crystalline phases and to determine if gases were dissolved interstitially in metallic Ti. Phase and lattice parameter analysis was performed using a Philips APD 3720 diffractometer system. The instrument was equipped with an automated goniometer, Cu X-ray tube, variable divergence slit, focusing graphite monochromator and scintillation counter. The samples analyzed were TiPA, TiPN, TiQA, and TiCA. Coating flakes were stripped

from TiPA, TiPN, and TiQA with a razor blade and finely ground in an α-alumina mortar for analysis. In addition, coatings were analyzed *in situ* using small samples cut from TiPA, TiPN, and TiCA.

The measurement error for lattice parameter analyses was ± 0.0001 nm for the powder samples. The error for the *in situ* samples is larger because of sample roughness and the presence of fragments of low-absorption-coefficient glass substrate. Sample TiQA, which contained some glass fragments from mechanically stripping the coating from the substrate, was mixed with NBS "d" value standard and re-measured. The results, after correcting the data, showed that measurement error increased to ± 0.0002 nm due to the glass fragments; the error for *in situ* samples will be larger than this. Since the error in lattice parameter measurement is about the same for both the "a" and "c" axes, the c/a ratio should not be significantly affected by these errors.

4.2.2.4 Electron Microprobe and Scanning Electron Microscopy

Coatings were analyzed with an electron microprobe (EMP) and an analytical scanning electron microscope (SEM) to determine the local composition and physical structure of the coatings. The results should establish the relationship between local chemistry, structure, and properties of the coatings. Samples examined were TiPA, TiPN, TiCA and TiCN. All were analyzed *in situ* by cutting samples from the sprayed substrate. Cross-sectioned samples were mounted on-edge in epoxy and polished to a 1 mm diamond surface finish. Coatings were also examined normal to the plane of the coating. Carbon coating was not required prior to analysis because of good coating conductivity. However, coatings formed using air atomization were less conductive than those using nitrogen atomization.

Images of the coatings were obtained with a Leica Stereoscan S440 scanning electron microscope using secondary and backscattered electrons. Secondary electron images yield primarily topographical detail. Backscattered electron images are sensitive to average atomic number of the analysis volume and accentuate compositional differences. Since voids and cracks are one extreme in the spectrum of atomic number (*i.e.* ~0) the backscattered electron images show these features in stark detail.

Line scans of local composition across the coating cross-section were made using a CAMECA SX-50 electron microprobe equipped with four wavelength-dispersive spectrometers. Selected spots on the coatings were analyzed with the Leica Stereoscan S440 using a wavelength-dispersive spectrometer with four crystals, and an energy-dispersive spectrometer with atmospheric thin window for low atomic number elements. All analytical results were ZAF (atomic number, absorption, and fluorescence) corrected and based on calibration standards.

4.2.2.5 X-Ray Photoelectron Spectroscopy

Coatings were analyzed by X-ray photoelectron spectroscopy to determine the composition of the outer surface of the coating and the chemical state of the reactants. Samples examined were TiPA and TiPN. Samples were analyzed *in situ* by cutting samples from the sprayed substrate. In addition, coating flakes were scraped from TiPA with a razor blade. The Ti-glass interface was examined using flakes from TiPA.

Analyses were performed on a Surface Science Laboratory SSX-100 ESCA spectrometer, using a 600 mm analysis spot size. Argon ion sputter etching, at a rate of 0.00007μm per second (0.07 nm per second) based on SiO_2, was used to incrementally remove material from the sample surface to produce a profile of coating composition as a function of coating depth (*i.e.*, depth-profile). Two survey scans were performed on each sample, one before etching and one after etching for three minutes, to determine the elements present and the binding energies to use for depth profiling. Areas selected for the depth profiles were different from those used for the survey scans. Using the adventitious C peak as a guide, there was no evidence of charging of the sample surfaces during analysis.

4.3 CHARACTERIZATION RESULTS

4.3.1 X-RAY FLUORESCENCE

Samples were examined by optical microscopy before X-ray fluorescence analysis. Many flakes from TiPA and TiPN had a thin layer of glass firmly attached to the substrate side of the coating. The outer surface, in contact with the atmosphere, appeared oxidized and had mixed blue and gold hues. When *in situ* samples on glass, TiPN and TiPA, were backlit by strong illumination, light showed through the coating at many discontinuities, voids and cracks.

X-ray fluorescence spectra from flakes of TiPA and TiPN showed strong peaks for Ti and Si, with lesser amounts of K and Fe present. Si and K are constituents of Pyrex glass and likely present due to the glass fragments attached to the flakes. Spectra collected from *in situ* coatings on glass had smaller Si and Fe peaks. Estimates of the Fe concentration in the *in situ* coatings, using fundamental parameters, indicated less than 0.1 wt pct Fe. This is similar to the concentration of Fe present in the grade 1 Ti feed wire.

4.3.2 GAS ANALYSES

Table 4.1: Results of LEECO Gas Analyses on Coating Samples.

Sample ID	Concentration, atomic fraction				(O+N)/Ti atom
	C	O	N	Ti	
TiPA	0.014	0.294	0.150	0.542	0.82
TiPN	0.012	0.296	0.173	0.519	0.90

The results of the LEECO gas analyses are shown in Table 4.6. Carbon levels were typically around 1 atomic percent (at pct) or less. Oxygen concentrations were of the same magnitude but always greater than nitrogen concentrations. Nitrogen concentrations were slightly higher using nitrogen atomization than air atomization. Based on these measurements, oxygen concentration did not appear to change with the atomization gas. The atomic ratio (O+N)/Ti suggests lower bounds for the fraction of titanium present as metallic Ti. These range from 10 to 20 percent of the total titanium present, and would be higher if some O and N is present interstitially in the metallic Ti.

4.3.3 X-RAY DIFFRACTION

The major phases identified in all of the samples, both flake and *in situ*, were a-Ti having a close-packed hexagonal (hcp) structure, and a phase similar to TiN and/or TiO having a face-centered cubic (fcc) structure. No TiO_2 was detected by X-ray diffraction, nor was there any body-centered cubic b-Ti. The pattern for flakes from TiPA and TiPN also included a peak associated with Ti_5Si_3. This peak was not present in the results for the *in situ* samples. It suggests a reaction between the molten Ti droplets initially contacting the substrate and the glass. It is likely Ti_5Si_3 is the phase responsible for a good bond between the Pyrex glass substrate and the coating. The fcc phase appeared to have a slightly contracted lattice structure (relative to the lattice dimensions for the TiN standard), not unusual considering the non-equilibrium nature of the thermal spray coating.

The a-Ti lattice was greatly expanded for all of the samples. This suggests substantial interstitial oxygen and/or nitrogen dissolved in the metal. For example, published lattice parameters for pure a-Ti are 0.2950 and 0.4682 nm for "a" and "c", respectively, yielding a c/a ratio of 1.587(*Bars, et al, 1983*). However, values from the diffraction pattern for sample TiCA were 0.2973 and 0.4788 nm, indicating the lattice was greatly expanded along the "c" axis. The resulting c/a ratio was 1.610. If this expansion were attributed entirely to interstitial N, the lattice parameters correspond to a N concentration of roughly 22 at pct in the a-Ti lattice(*Bars, et al, 1983*).

The relative amount of each major phase was estimated from the diffraction data and is given in Table 4.7. There was substantially more a-Ti (lower TiN and/or TiO) present in the flake samples than the *in situ* samples. Apparently, this is because the *in situ* results represent the outer surface of the coating, which is more strongly influenced by reactions between the coating and the atmosphere, whereas the flake results represent the average composition of the coating.

Table 4.2: Relative Amounts of Major Phases in Coatings Estimated from XRD Results.

Sample ID	c/a ratio for a-Ti lattice	α-Ti vol pct	TiN and/or TiO, vol pct
TiPA, *in situ*	1.609	0.28	0.72
TiPN, *in situ*	1.612	0.28	0.72
TiPA, flake	1.612	0.44	0.56
TiPN, flake	1.614	0.35	0.65
TiQA, flake	1.610	0.43	0.57

There was no difference in lattice expansion for coatings on Pyrex and on quartz. The c/a ratios for all of the samples suggest the α-Ti matrix contains a substantial amount of interstitial N and/or O.

4.3.4 ELECTRON MICROPROBE AND SCANNING ELECTRON MICROSCOPY

A cross-section of TiPA, typical of coatings applied on glass using air atomization, is shown in Figure 4.3. Figure 4.3(a) is a secondary electron (SE) image and Figure 4.3(b) is a backscattered electron (BE) image of the same area. The BE image shows banding in the coating related to composition differences which is not evident in the SE image. The banding is produced by gradients in composition of the coating. The brighter bands contain higher concentrations of metallic Ti, and the darker bands higher concentrations of TiO and/or TiN, thus alternating layers first rich in α-Ti and then poor in α-Ti (but rich in TiO and/or TiN).

Electron microprobe depth profiles, Figure 4.4, also indicate the presence of gradient bands by the "saw-tooth" pattern of the Ti curve. Seven bands are suggested by the depth profile data and can be matched visually with seven distinct gradient bands in Figure 4.3(b). The depth profile data show the brighter bands contain 70-80 at pct Ti while the darker bands contain 60-65 at pct Ti. The balance is N and O in similar amounts varying between 10 and 20 at pct.

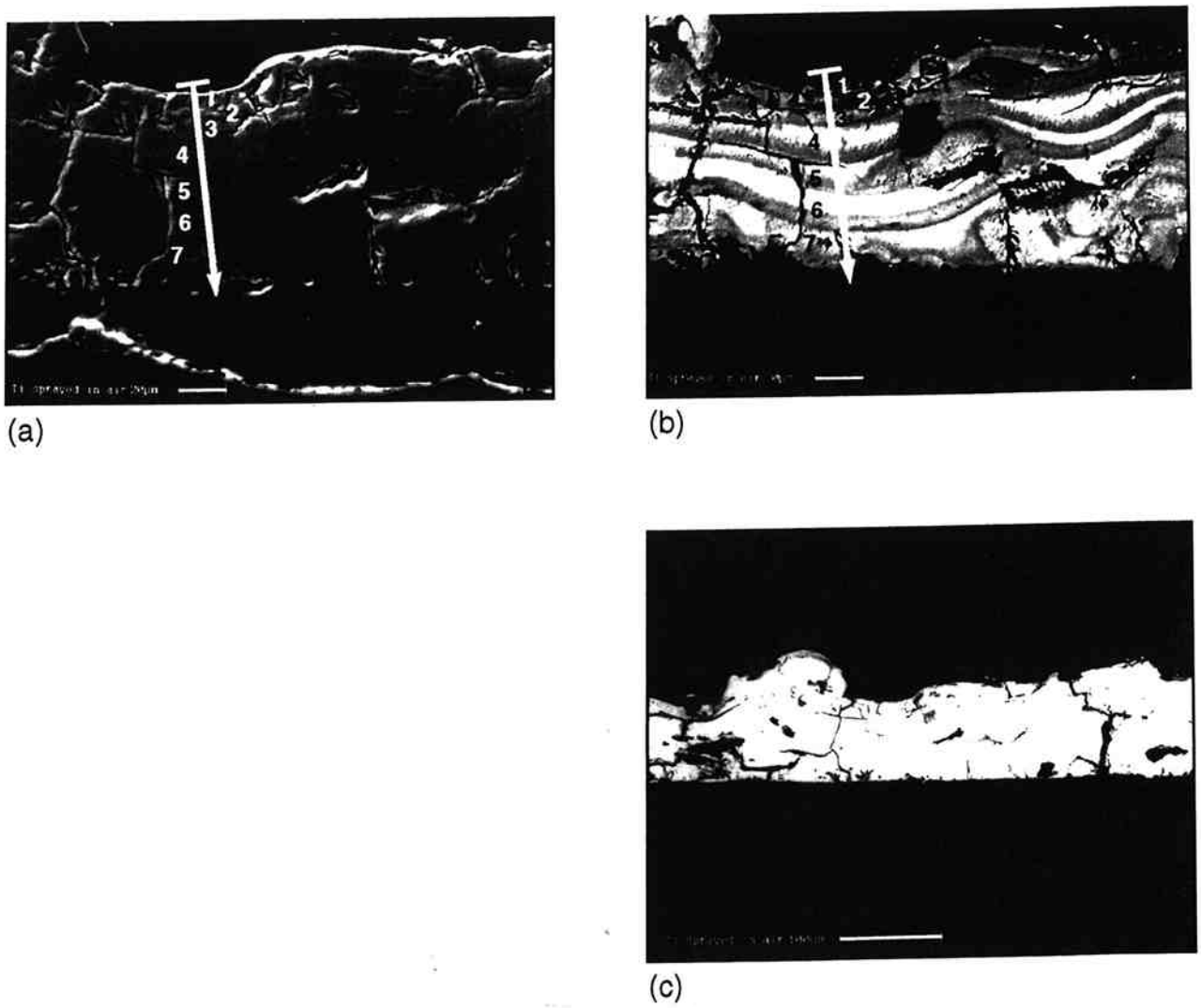

Figure 4.1 SEM photomicrographs of TiPA cross-section:
(a) SE image, 350X; (b) BE image, 350X; (c) BE image, 140X.
Arrow shows path of EMP traverse and the location of seven Ti gradient bands in the coating.

Typically the dark portion of a gradient band is characterized by a sharp interface with a light band on the side towards the substrate, and by a diffuse interface on the side away from the substrate. The sharp interface appears to be the outer surface of the oxidized skin formed on the molten droplet while it was in flight to the substrate. Upon striking the substrate, the oxidized skin splits and unfolds, probably in fragments, with the outer surface welded to the preceding splat. The denser Ti-rich core is crushed against this debris and spreads out to cover it leaving an α-Ti rich layer over an oxidized layer. The diffuse interface appears to be the boundary between the Ti-rich core and the oxidized layer. It is diffused because it is the inner reaction front for oxygen and nitrogen diffusing into the droplet and reacting with the Ti

and because some convective mixing may occur along the front on impact of the droplet with the substrate. The concentration gradient is substantially higher at the sharp interface than the diffuse interface. Consequently, the gradient of other properties related to coating chemistry will also be higher at the sharp interface.

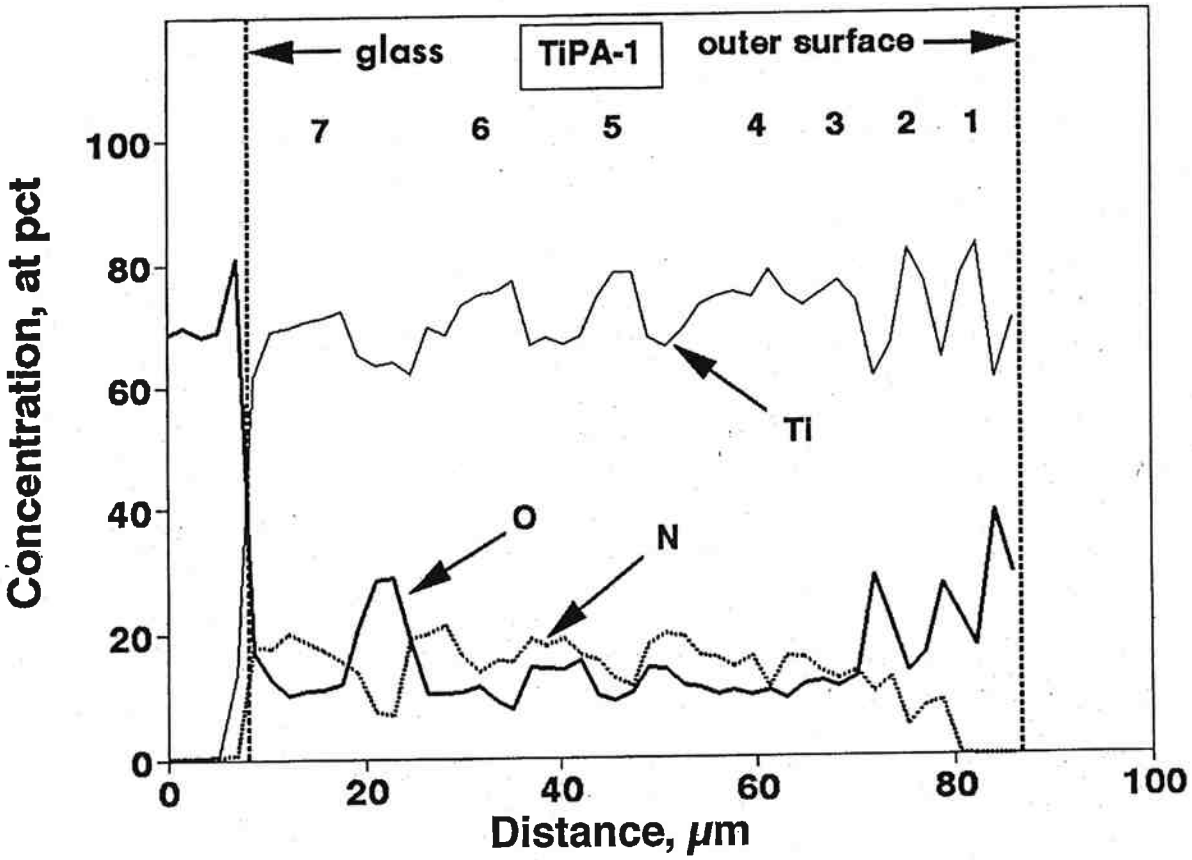

Figure 4.2 EMP composition depth profile for TiPA cross-section shown in Figure 4.3. Glass-coating interface and outer surface of coating are shown with seven Ti gradient bands.

Figures 4.3(a) and (b) show substantial cracking of the coating both parallel and normal to the coating/glass interface. Cracks parallel to the coating/glass interface tend to form in the dark bands where the concentration of nonmetallic constituents is highest and the coating is most brittle. The cracks tend to propagate along the sharp interface as opposed to other locations within the dark band. This, of course, is the region with the highest concentration gradient and highest gradient of other material properties.

The normal or transverse cracks suggest the build-up of substantial internal tensile stress within the coating as it cools and contracts. The transverse cracks are typically linked by parallel cracks radiating along the dark bands. The transverse cracks may cross multiple gradient bands, indicating cracking was delayed until the coating was at least substantially formed.

Figure 4.3(c) shows no separation of the coating from the glass substrate. Instead cracks within the coating are shown to cross the coating substrate interface and link into a network of cracks in the substrate, caused perhaps by thermal shock of the glass. For this to occur, the bond between the coating and substrate must be fairly strong to prevent parting at this interface. The XRD results show that the Ti reacts with the glass substrate to form Ti_5Si_3, which probably accounts for the strong bond of the coating to glass.

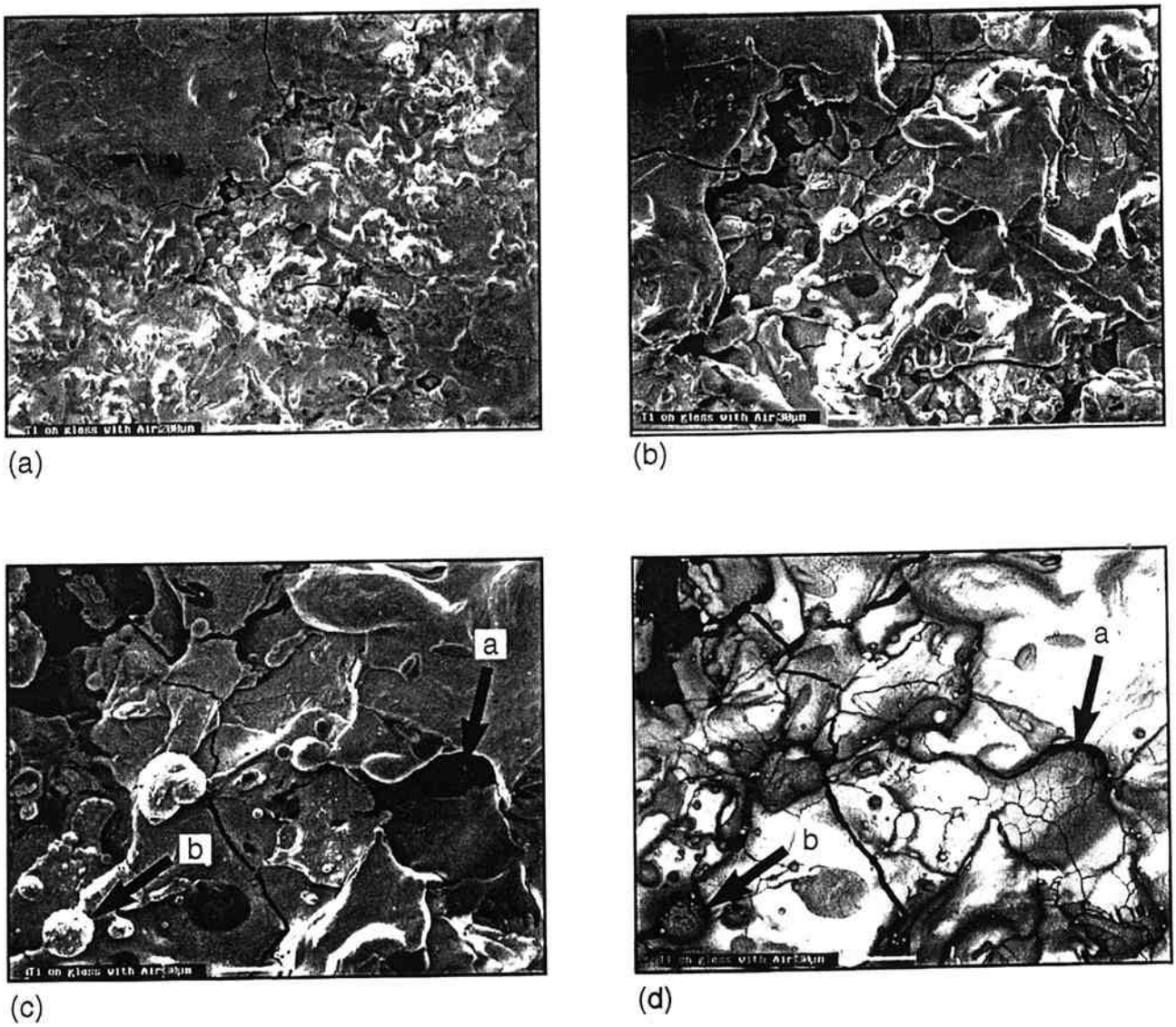

Figure 4.5 SEM photomicrographs of TiPA surface:
(a) SE image, 65X; (b) SE image, 130X; (c) SE image, 300X; (d) BE image, 300X.
Arrows: a) small, highly oxidized, finely cracked splat;
b) small, highly oxidized droplet that froze before impacting the surface.

The surface of TiPA is shown in Figure 4.5. Figure 4.5(a) shows a rough area of splats fused together, and a much smoother area that appears to have been glazed by higher heat input. A

wide range in splat sizes is apparent, representing the distribution of droplet sizes in the initial molten spray. At higher magnification cracks are visible in the surface; larger cracks cross multiple splats. SE and BE images of the same area, Figures 4.5(c) and (d), show a small splat (a) containing a high concentration of non-metallics and is heavily cracked in contrast to the adjacent more a-Ti rich splats. The small droplet (b) solidified before impacting the surface and also contains a high concentration of non-metallics. At earlier stages in the coating formation, such droplets were incorporated within the coating, as will be seen in some of the later photomicrographs (see Figures 4.9, 4.11 and 4.13)

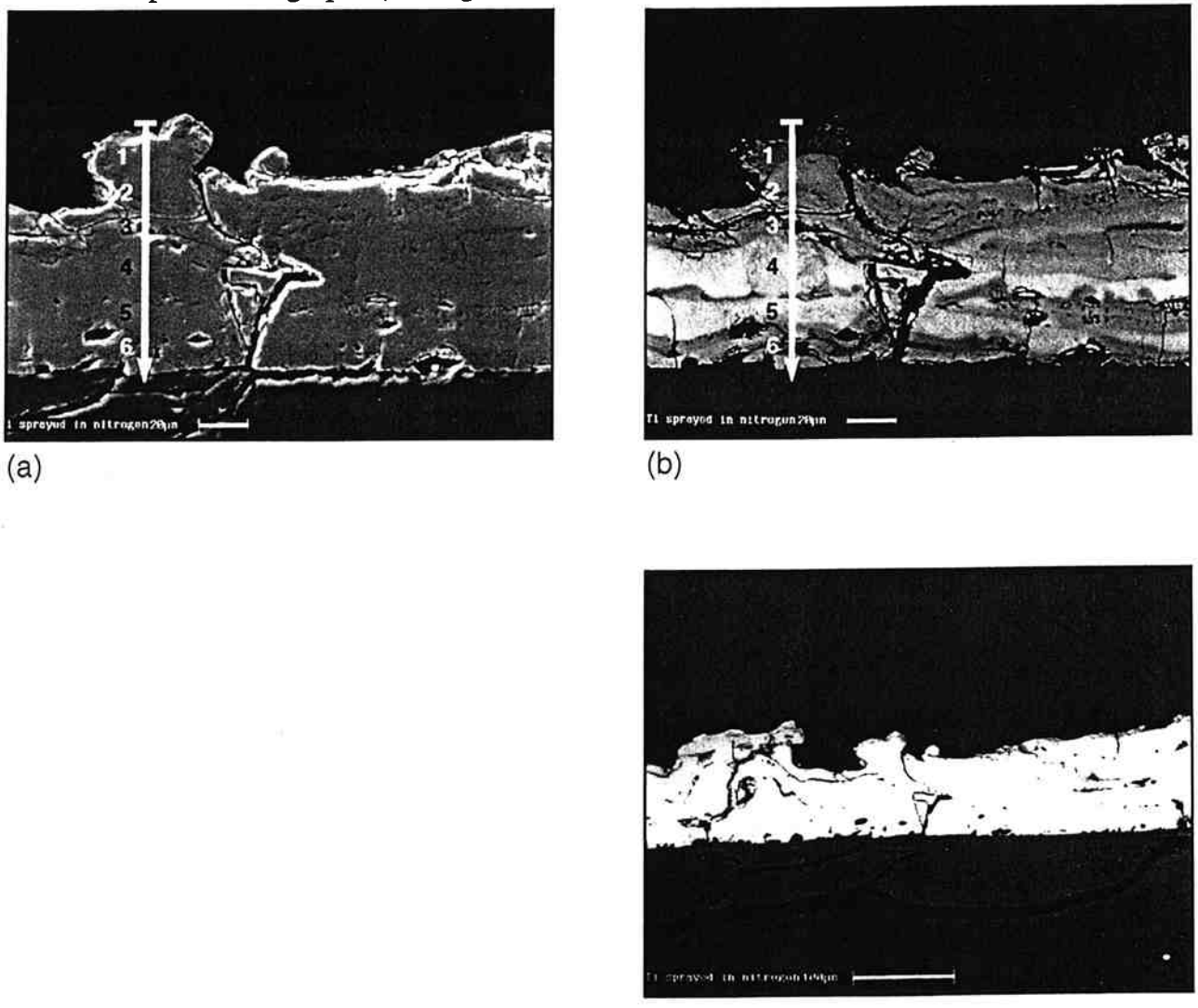

Figure 4.6 SEM photomicrographs of TiPN cross-section:
(a) SE image, 350X; (b) BE image, 350X; (c) BE image, 140X.
Arrow shows path of EMP traverse and the location of six Ti gradient bands in the coating.

Glazing would be produced by small local variations in the heat input to the coating during the coating process. The effect would be two-fold: to weld adjacent splats into a more cohesive structure but also to promote further reaction of the Ti with the atmosphere.

A cross-section of TiPN, typical of coatings applied on glass using nitrogen atomization, is shown in Figure 4.6. The BE image, Figure 4.6(b), shows banding of the coating, indicating gradients in coating composition similar to those observed in Figure 4.3(b) for coatings on glass using air atomization. The depth profile, Figure 4.7, shows the presence of six gradient bands which can be visually observed in the BE image, Figure 4.6(b). The depth profile shows that N levels are typically higher when N atomization is used, around 20 at pct, and O levels are lower, 10 at pct or less.

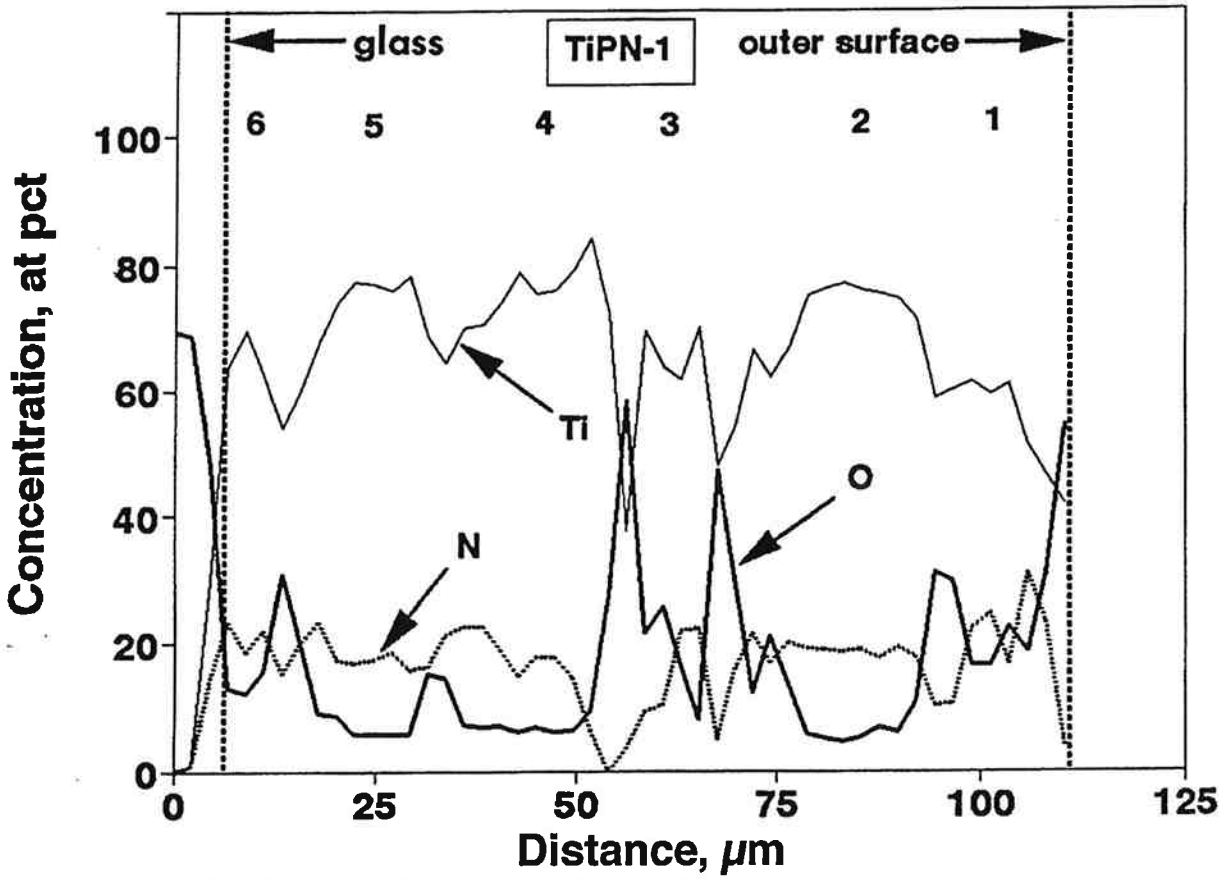

Figure 4.7 EMP composition depth profile for TiPN cross-section shown in Figure 4.6. Glass-coating interface and outer surface of coating are shown with six Ti gradient bands.

Cracks parallel and transverse to the glass/coating interface are visible in Figure 4.6(c) and link with cracks in the glass substrate caused by thermal shock of the glass. The network of parallel and transverse cracks again suggests substantial internal stress within the coating. There was no disbonding of the coating from the glass, indicating a good bond at this interface. Examination of a number of coatings suggests that there is less cracking of the coatings and a more uniform coating chemistry for coatings produced using nitrogen compared to air atomization.

The surface of the coating on TiPN is shown in Figure 4.8. It is similar to that produced using air atomization and has areas roughened by coalesced "splats" and areas smoothed by glazing. The surface is broken by a network of cracks.

(a)

(b)

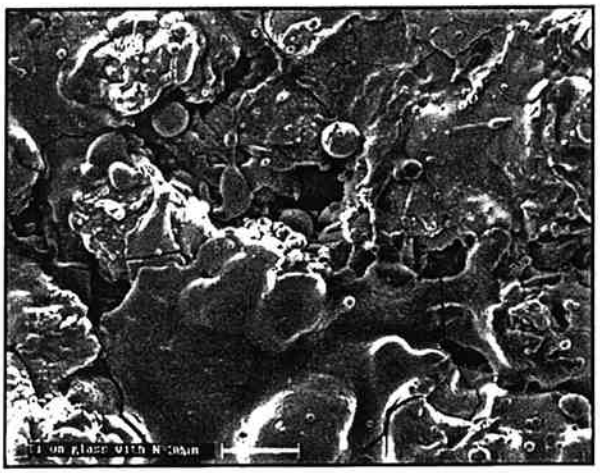

(c)

Figure 4.8 SEM photomicrographs of TiPA surface:
(a) SE image, 65X; (b) SE image, 130X; (c) SE image, 300X.

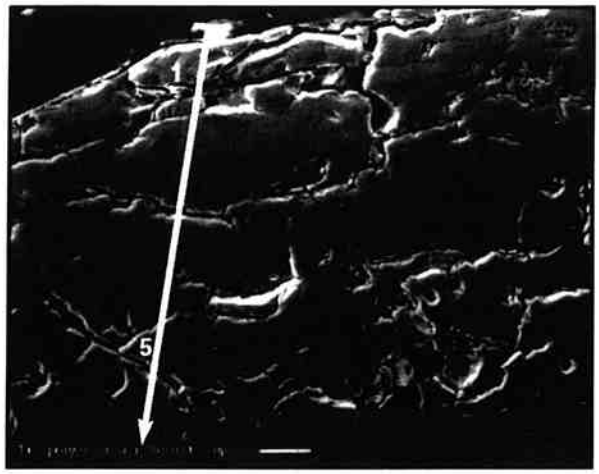

(a)

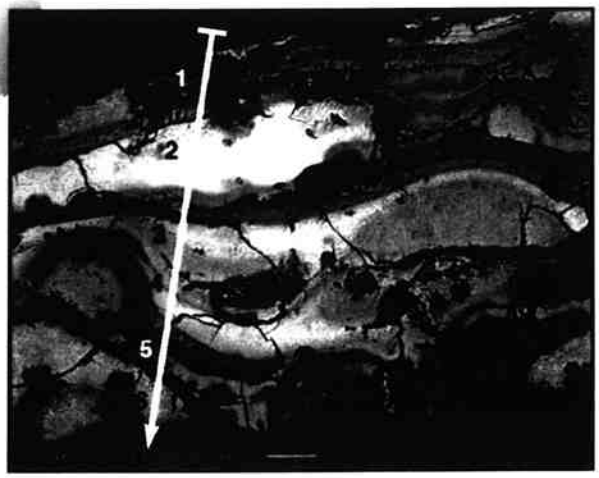

(b)

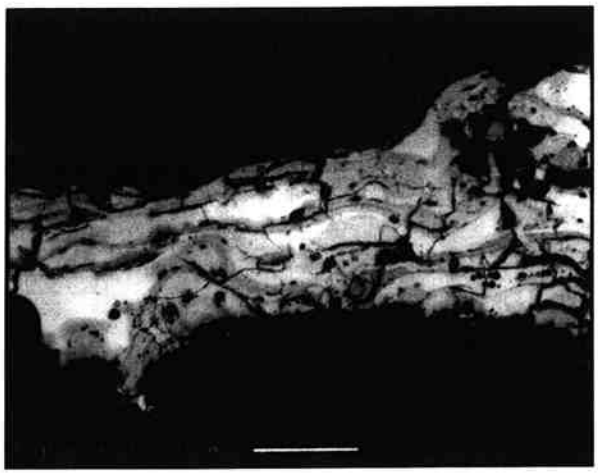

(c)

Figure 4.9 SEM photomicrographs of TiCA cross-section:
(a) SE image, 350X; (b) BE image, 350X; (c) BE image, 140X.
Arrow shows path of EMP traverse and the location of six Ti gradient bands in the coating.

A cross-section of TiCA, typical of coatings applied on concrete using air atomization, is shown in Figure 4.9. Figures 4.9(a) and (b) are SE and BE images of the same area. In general, the coating appears to have formed a good mechanical bond with the concrete substrate, Figure 4.9(c). The coating closely follows the contours of the rough surface. There are some gaps and voids scattered along the coating-concrete interface but the coating fills all but the smallest recesses.

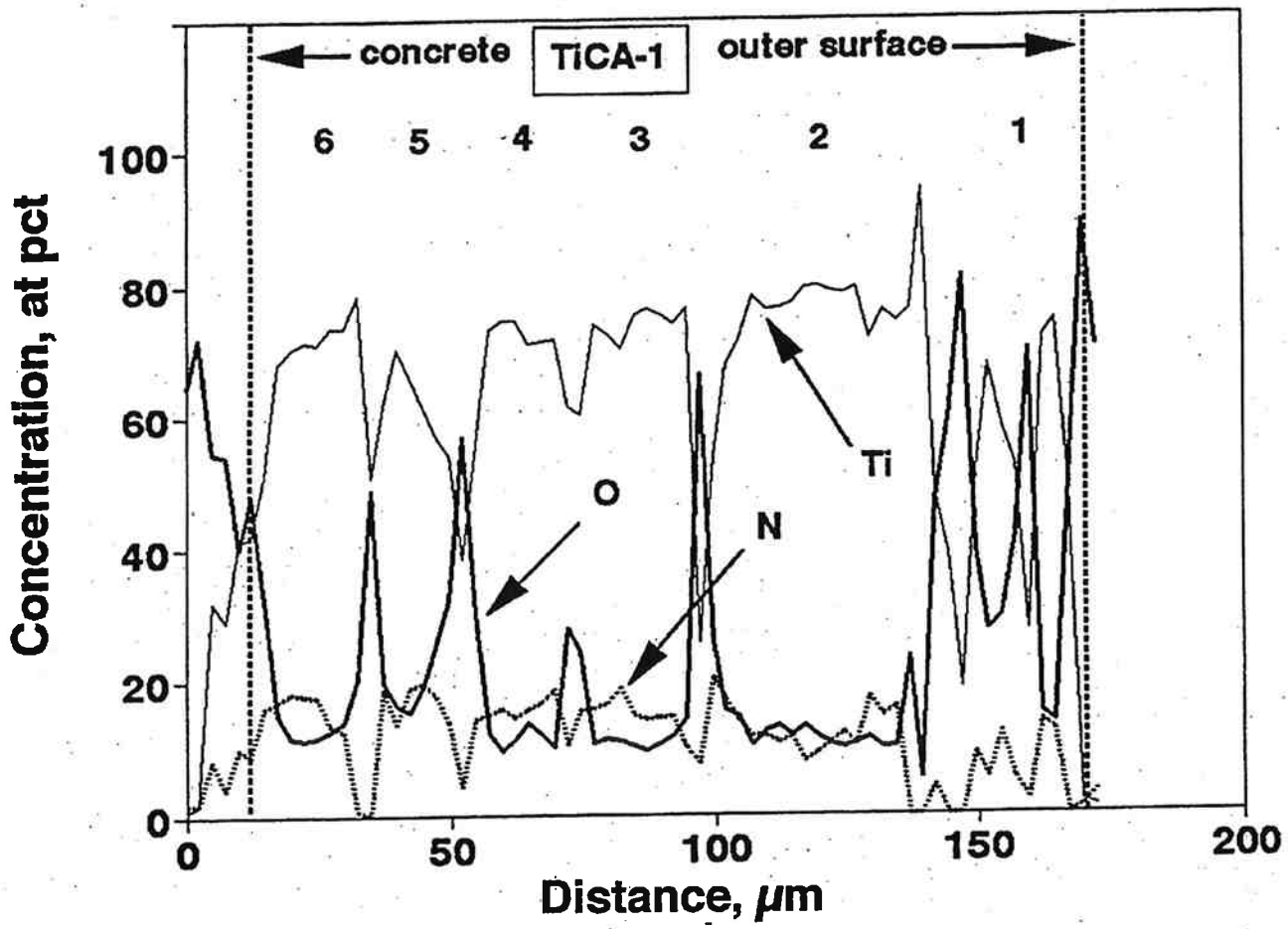

Figure 4.10 EMP composition depth profile for TiCA cross-section shown in Figure 4.9. Concrete-coating interface and outer surface of coating are shown with six Ti gradient bands.

There are very distinct gradient bands and substantial cracking within the coating, Figure 4.9(b). The concentration depth profile, Figure 4.10, shows Ti, N and O concentration levels similar to those obtained from TiPA, Figure 4.4. Six gradient bands are apparent in the depth profile and can be matched visually with gradient bands in the BE image. Parallel cracks tend to be located in the dark portion of the band at the sharp interface. Transverse cracks link the parallel cracks. Some of the transverse cracks cross into the concrete and link with cracks in the cement paste, Figure 4.9(c).

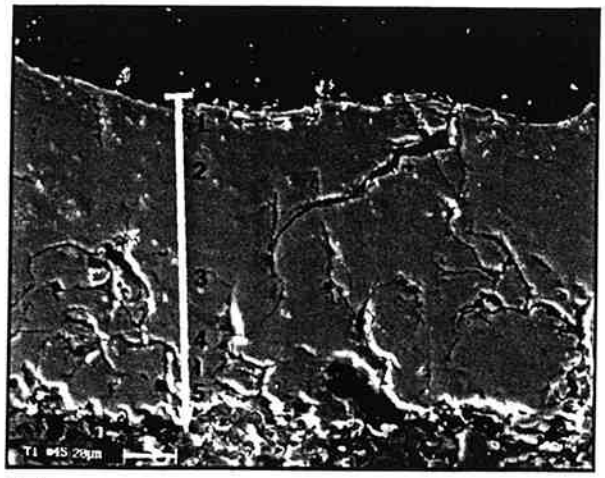

(a)

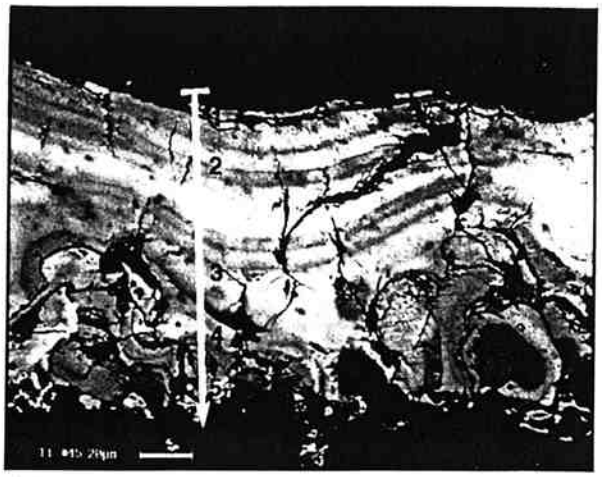

(b)

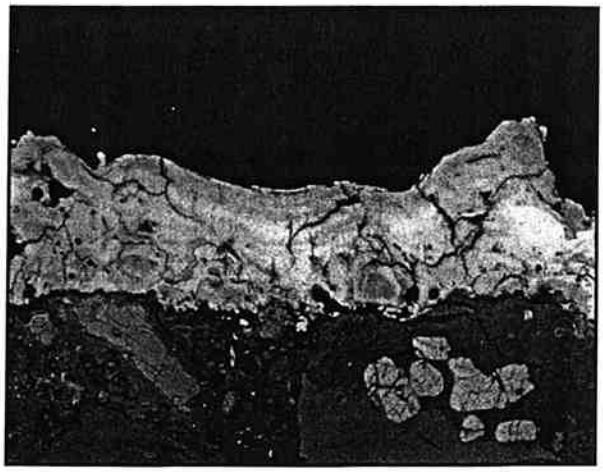

(c)

Figure 4.11 SEM photomicrographs of TiCN cross-section:
(a) SE image, 350X; (b) BE image, 350X; (c) BE image, 140X.
Arrow shows path of EMP traverse and the location of five Ti gradient bands in the coating.

A cross-section of TiCN, typical of coatings applied on concrete using nitrogen atomization, is shown in Figure 4.11. The condition of the coating-concrete interface and the mechanical bond with the concrete appears to be similar to that formed using air atomization. Gradientbands and cracking are apparent, but the composition tends to be more uniform than coatings formed using air atomization and cracking appears to be less. Like TiPN, depth profiles show the nitrogen concentration is typically around 20 atomic percent while the O concentration is about 10 atomic percent, Figure 4.12. Five gradient bands are apparent in the depth profile and can be visually matched with similar features in the BE image, Figure 4.11(b).

Table 4.8: Average Coating Composition, From EMP Line Scans

Coating Sample	Coating Composition, Atomic Percent			(O + N)/Ti Atom Ratio
	O	N	Ti	
TiPA	17.7	14.6	67.5	0.48
TiCA	19.3	13.0	67.5	.048
Average	18.5	13.8	67.5	0.48
TiPN	13.2	17.1	69.6	0.43
TiCN	13.9	16.5	69.5	0.43
Average	13.5	16.8	69.6	0.43

Table 4.9: Minimum and Maximum Element Concentrations in Coatings, from EMP Line Scans

Coating Sample	No. of Ti Gradient Bands	Concentration, Atomic Percent.					
		O		N		Ti	
		min	max	min	max	min	max
TiPA	7	8	39	5	21	63	83
TiCA	6	5	81	0	20	19	94
TiPN	6	5	58	3	31	38	84
TiCN	5	9	56	0	23	43	76

The composition data in the EMP depth profiles, Figures 4.4, 4.7, 4.10, and 4.12, was averaged over the thickness of the coating from the atmosphere-coating interface to the coating-substrate interface. The minimum and maximum elemental concentrations in these data were also tabulated. These results are given in Tables 4.8 and 4.9, respectively. On average, oxygen levels went down and nitrogen levels went up using nitrogen atomization compared to air atomization. Furthermore, oxygen levels were higher than nitrogen levels for air atomization, lower for nitrogen atomization. The (O+N)/Ti ratio was lower for nitrogen atomization, suggesting more of the Ti was available as α-Ti.

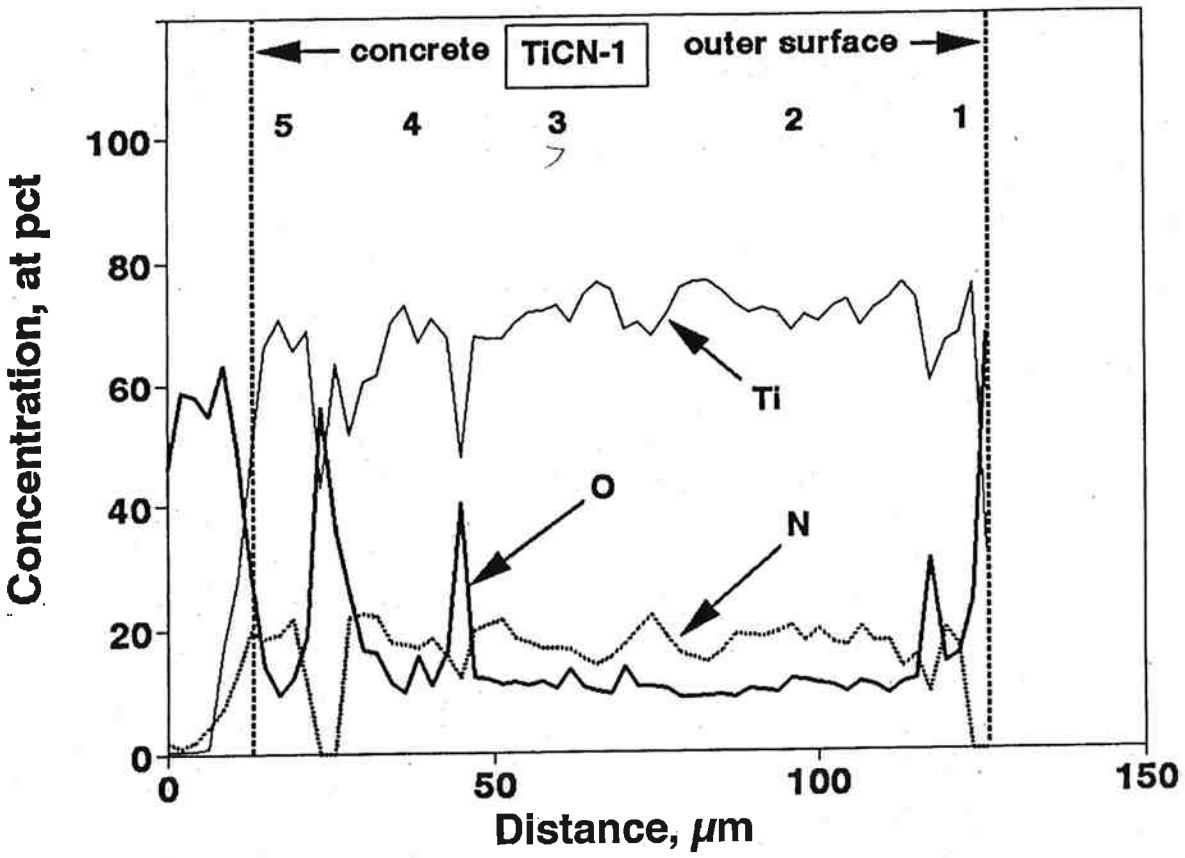

Figure 4.12 EMP composition depth profile for TiCN cross-section shown in Figure 4.11. Concrete-coating interface and outer surface of coating are shown with five Ti gradient bands.

Minimum and maximum element concentrations varied widely for all three elements. Oxygen levels swung far more widely than nitrogen. With one exception, maximum nitrogen levels tended to be under 23 atomic percent. Referring to the Ti-N phase diagram, Figure 4.2, the concentrations in Tables 4-8 and 4-9 put nitrogen largely in the region where α-Ti is the stable phase and nitrogen can be expected to be present as in interstitial in the α-Ti matrix.

Oxygen has a higher solubility than nitrogen in the α-Ti matrix, Figure 4.1. Nevertheless, the wide range in oxygen concentrations suggest that oxygen can be present as an interstitial in the α-Ti matrix and as an oxide of Ti. Since only two significant phases were found in the coating by XRD, the hcp α-Ti and a fcc structure like TiN, choices for the oxide structure are limited. The data in Table 4-3 would indicate only γ-TiO is probable. Solid-state transformations to lower temperature TiO structures and to other Ti oxides are unlikely given the rapid quench rate for the splats, in excess of 10^6 °C/s and the time frame of the measurements (*Krepski, 1993*). No evidence for such changes were found.

Table 4.10: Composition of Phases in Freezing Structures Shown in Figure 4.13, Coating Sample TiCA.

Image area Fig. 4-13	Description of area	Composition, atomic percent			(O + N)/Ti atom ratio
		O	N	Ti	
(b) -- 1	white	9.0	1.5	89.4	0.12
(a) -- 2	light gray	12.4	18.0	69.5	0.43
(c) -- 3a	light phase	28.4	15.7	55.9	0.79
(c) -- 3b	dark phase	42.1	17.3	40.5	1.47
(d) -- 4a	light phase	10.9	0.0	89.1	0.12
(d) -- 4b	dark phase	8.7	9.0	82.3	0.22

Areas 1 through 4 of Figure 4.13(a) were analyzed with the SEM to determine local composition. These areas also represent the freezing structures seen in Figures 4.13(b) through (d). The analytical results are given in Table 4-10. Again referring to the phase diagrams, the compositions for (b) and (d) indicate these regions are α-Ti of varying composition determined by the presence of interstitial nitrogen and oxygen. The light phase in Figure 4.13(c) also appears to be α-Ti surrounded by a matrix of what probably is γ-TiO and perhaps some TiN.

Two types of dendritic freezing structures are observed in Figure 4.13. Their presence is evidence that cooling rates are not so high as to prevent long-range structure and order from developing within the coating. The first structure is shown in Figures 4.13(b) and (d), and forms in α-Ti-rich regions. The second is shown in Figure 4.13 and consists of α-Ti dendrites (the light phase) in a matrix rich in γ-TiO (the dark phase).

As an example of the freezing process and how it leads to the different structures, consider the composition represented by line 1 in Figure 4.1 at 10 atomic percent oxygen, and typical of a coating composition low in oxygen. Starting with the molten splat, α-Ti begins to freeze out at the liquidus curve. At 1720 ^{o}C, freezing is complete, the structure cools through a two-phase region where both α-Ti and β-Ti, with their respective composition differences, are present. On further cooling the β-Ti must transform back to α-Ti since XRD did not reveal the presence of β-Ti. However, the composition associated with the β-Ti is locked into the structure, leading to composition variations such as those seen in the α-Ti-rich region, image areas 4a and 4b in Table 4-10.

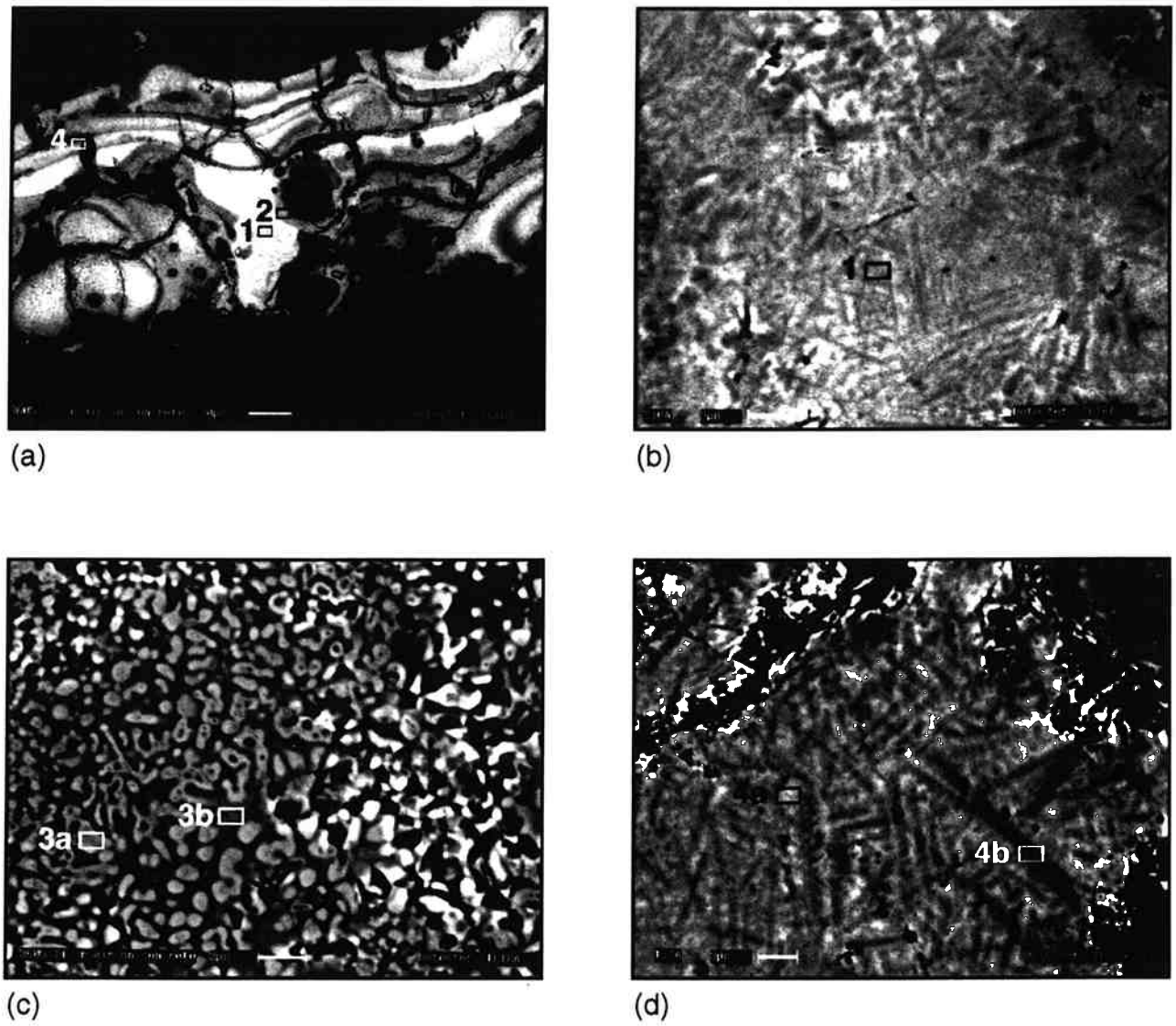

Figure 4.13 Freezing structures in TiCA using BSE:(a) Overall view showing four analysis/image areas, 200X; (b) image area 1 and analysis area 1, 2000X; (c) image area 3 and analysis areas 3a and 3b, 3500X; (d) image area 4 and analysis areas 4a and 4b, 2000X.

Now start with a higher oxygen level, 42 at pct. Again α-Ti is the first to freeze out. At around 1780 °C, freezing is complete, and γ-TiO also has formed, filling the interdendritic region to form the matrix for the α-Ti. Further cooling passes through the two-phase γ-TiO/α-Ti region. There is no XRD evidence that the γ-TiO transforms to other TiO structures or to other Ti oxides, which are typically the stable low-temperature structures.

Consider line 1 in Figure 4.2 for 10 at pct N. Given the compositions in Tables 4-8 through 4-10, this is a typical nitrogen concentration and in almost all cases the nitrogen concentration does not exceed the solubility in α-Ti of 22 at pct N (*"Nitrogen-Titanium, Alloy Phase Diagrams", 1992; Gernitsky, 1995*). The freezing structure produced by line 1 will be similar to that produced by line 1 in the Ti-O system. First, α-Ti will freeze; then a two-phase structure of β-Ti/α-Ti will form. Finally, β-Ti will transform into α-Ti at lower temperatures, leading to composition variations in the α-Ti-rich region.

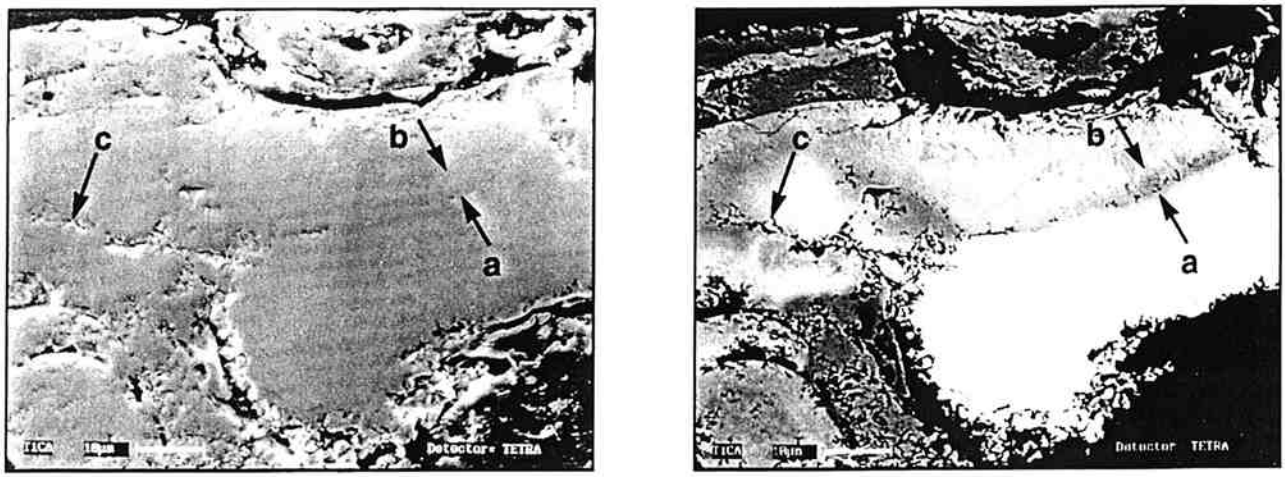

Figure 4.14 Cracks in Ti gradient bands: (a) SE image, 900X;
(b) BE image, 900X. Arrows: a) incipient crack along sharp gradient boundary;
(b) diffuse gradient boundary; c) crack along Ti-poor boundary.

SE and BE images are shown in Figure 4.14 of the location of incipient cracks and their relation to gradient bands. The sharp interface of the oxidized layer is given by arrow "a", the diffuse interface by arrow "b". The locus of voids and microcracks is along the sharp interface and represents a weak boundary in the coating. Arrow "c" points out a similar region where microcracks and voids follow the path of the oxidized layer.

Finally, the structure of the Ti coating revealed by the SE and BE images is substantially different from that observed for thermal-sprayed zinc anodes. (*Covino, et al, 1995; covino, et al,* 1996) and for many other thermal-sprayed .materials (*Bennett, et al, 1995; Leigh, et al, 1995)*. Composition, structure and mechanical properties of the Ti coating are unique, representing a reactive material sprayed in a reactive environment. Individual splats are welded to each other forming a cohesive structure, albeit one incised by many brittle interfaces and vulnerable to damage from internal stresses. However, from another viewpoint the Ti coating is similar to these other materials. Rough measurements from the BE images show the splats to be 10 to 25 μm thick and 100 to 200 μm in width, with a large dispersion in sizes about these median values. These dimensions seem to be typical of thermal-sprayed coatings (*Krepski, 1993*).

4.3.5 X-RAY PHOTOELECTRON SPECTROSCOPY

Survey scans for the substrate side of flakes from sample TiPA showed predominantly Si and O with trace amounts of Ti and nitrogen. Depth profiling yielded relatively constant concentrations of Si and O of 28 and 57 atomic percent, respectively. This agrees with the composition of SiO_2 and corresponds to the glass layer adhering to the substrate side of the flakes removed from Pyrex.

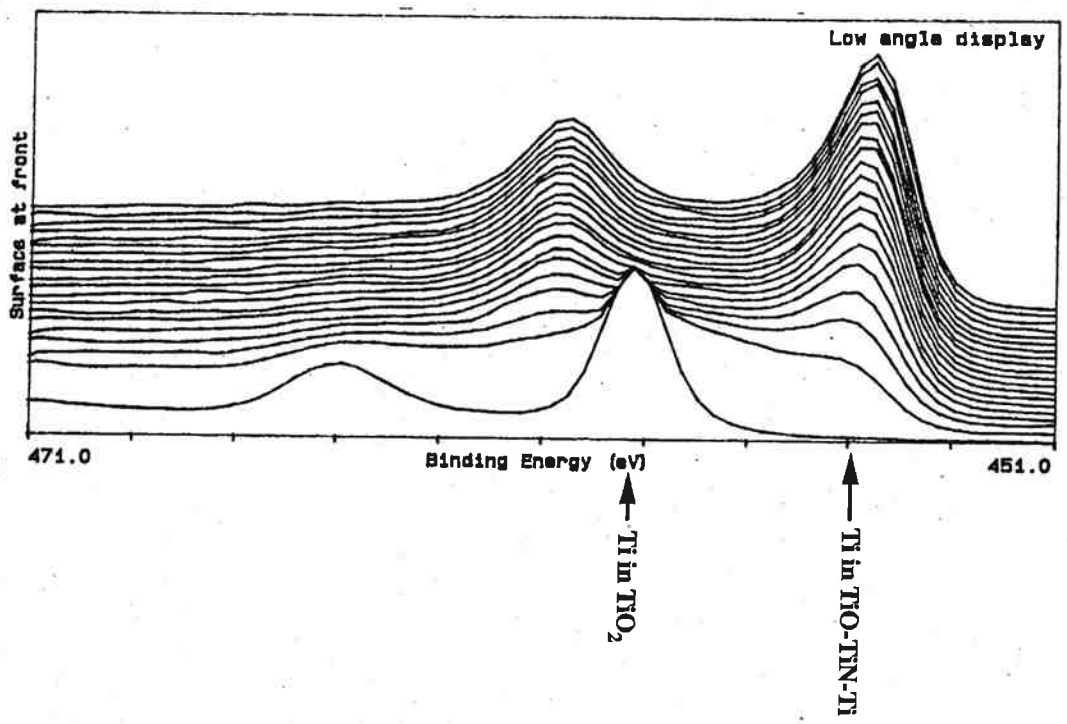

Figure 4.15 $Ti2p_{3/2}$ and $Ti2p_{1/2}$ peaks as a function of sputter etching for sample TiPN.

Survey scans of the *in situ* coating on samples TiPN and TiPA detected only Ti, C, O, and N in significant concentrations. Carbon disappeared within the first three minutes of etching, indicating it was adventitious carbon and not present in significant amounts in the coating.

Sample TiPN was sputter etched for 20 cycles of 120 seconds each for a total depth of 0.15 μm. This represents only the outermost surface of the coating, which is roughly 100 μm thick. The composition of the surface after each cycle is given in Table 4.11. The cumulative sputter depth was estimated from the measured SiO_2 sputter rate of 0.00007 μm per second (0.7 Å per second) assuming that the sputter rate for Ti and its compounds is not greatly different from SiO_2. The ratio (O+N)/Ti is computed as an indicator of the coating stoichiometry. The data show that carbon disappears after sputtering less than 120 seconds. The high oxygen concentration at the outer surface is probably associated with the C.

Oxygen concentrations decreased with depth of sputtering. In contrast, N and Ti concentrations are low at the outer surface but increase with depth of sputtering. The stoichiometric ratio, (O+N)/Ti, ranges from 2 near the outer surface to less than 1 after roughly 0.15 μm has been sputter etched. These values suggest an outer surface that is rich in TiO_2 but quickly transitions into one that is composed of TiO, TiN and/or interstitial O and N.

This is shown by successive X-ray photoelectron spectra for Ti, N, and O in Figures 4.15, 4.16 and 4.17 respectively.

In Figures 4.15, 4.16, and 4.17, the spectra following the first scan cycle referred to in Table 4-11 is oriented in the lowest position on the plot. Successive spectra are then stacked along the y-axis above this spectra. The first spectra represents the composition of the "as received" coating surface and the top spectra represents the composition after sputter etching for 2280 seconds. The binding energy of photoelectrons is given on the x-axis in electron volts. The binding energy of the photoelectrons varies with the type of environment from which the electron is emitted. The area under the peaks of these spectra is proportional to the concentration of the specific element in a particular binding state.

For example, the first spectra in Figure 4.15 contains two peaks typical of Ti. The larger is the $Ti2p_{3/2}$ peak and the smaller is the $Ti2p_{1/2}$ doublet associated with the $Ti2p_{3/2}$ peak. The binding energy of the $Ti2p_{3/2}$ peak in the first scan is around 459.3 eV, close to the binding energy of 458.8 eV characteristic of Ti in a TiO_2 matrix (*Chastain, 1992*). With sputter etching, the peak at 459.3 eV quickly disappears and a new peak emerges at around 455.3, which is characteristic of Ti in a TiO (455.1 eV) or TiN (455.8 eV) matrix (*Chastain, 1992*).

Table 4.11: Depth Profile Table for Sample TiPN

Sputter Cycle	Sputter Time, second	Equivalent Sputter Depth, μm	(O+N)/Ti atom ratio	Concentration, atomic percent			
				C1s	O1s	N1s	$Ti2p_{3/2}$
1	0	.0000	3.13	31.2	51.5	0.7	16.7
2	120	.0084	2.04	2.0	60.0	5.8	32.3
3	240	.0168	1.79	3.0	54.5	7.7	34.8
4	360	.0252	1.54	2.9	49.1	9.9	38.2
5	480	.0336	1.44	2.0	45.9	11.8	40.2
6	600	.0420	1.33	1.9	42.8	13.3	42.1
7	720	.0504	1.27	1.9	39.8	15.0	43.2
8	840	.0588	1.21	1.9	37.6	16.1	44.4
9	960	.0672	1.16	2.3	36.3	16.2	45.2
10	1080	.0756	1.10	3.1	34.7	16.2	46.1
11	1200	.0840	1.09	1.6	34.0	17.4	47.0
12	1320	.0924	1.07	2.5	31.9	18.5	47.1
13	1440	.1008	1.05	2.4	31.6	18.5	47.5
14	1560	.1092	1.00	1.0	30.2	19.3	49.5
15	1680	.1176	0.97	1.8	28.6	19.7	49.8
16	1800	.1260	0.96	2.0	27.9	20.1	50.0
17	1920	.1344	0.93	2.2	27.2	19.9	50.7
18	2040	.1428	0.95	1.7	27.2	20.8	50.4
19	2160	.1512	0.90	2.2	25.6	20.7	51.5
20	2280	.1596	0.90	2.0	26.1	20.4	51.5

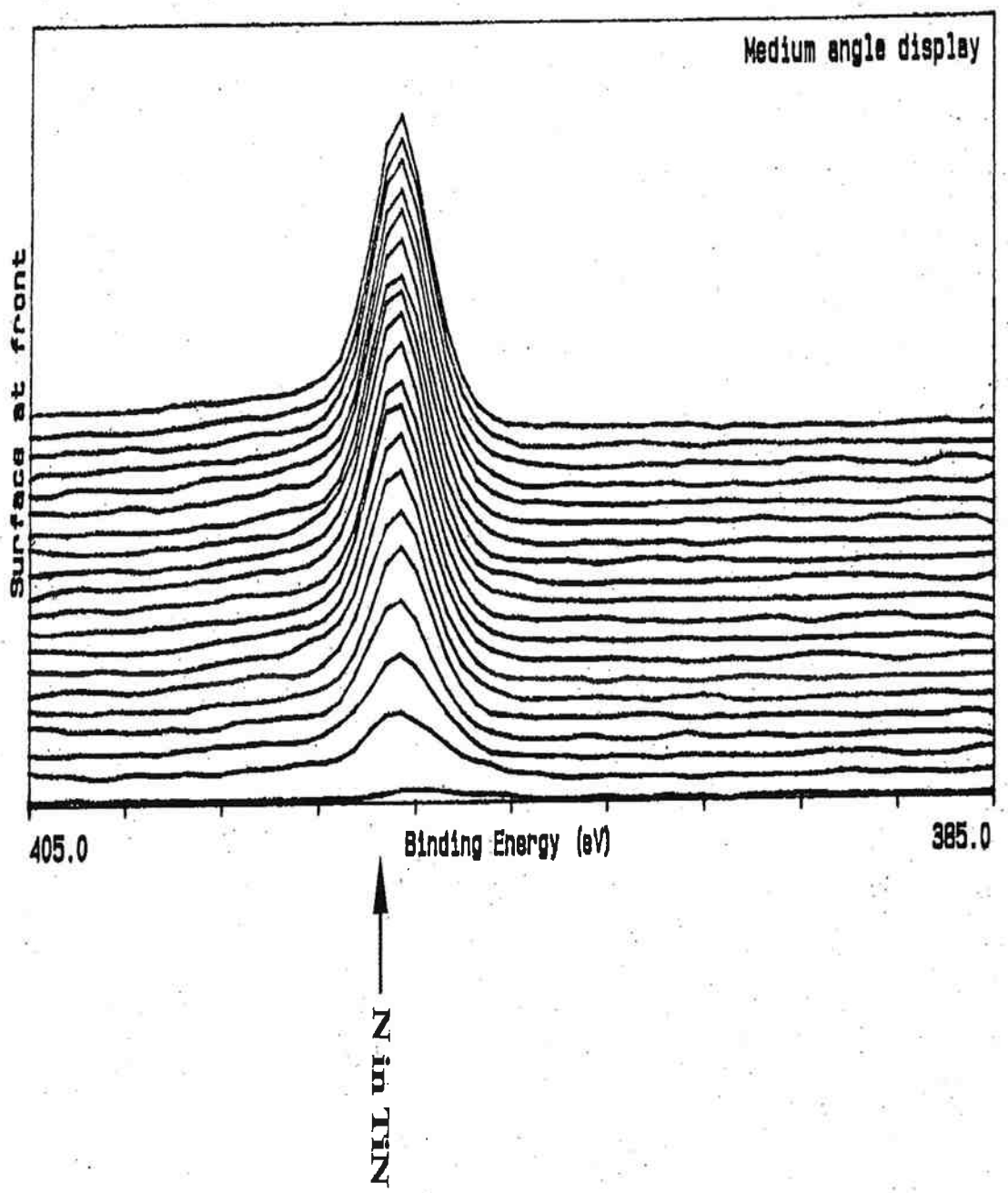

Figure 4.16 N1s peak as a function of sputter etching for sample TiPN.

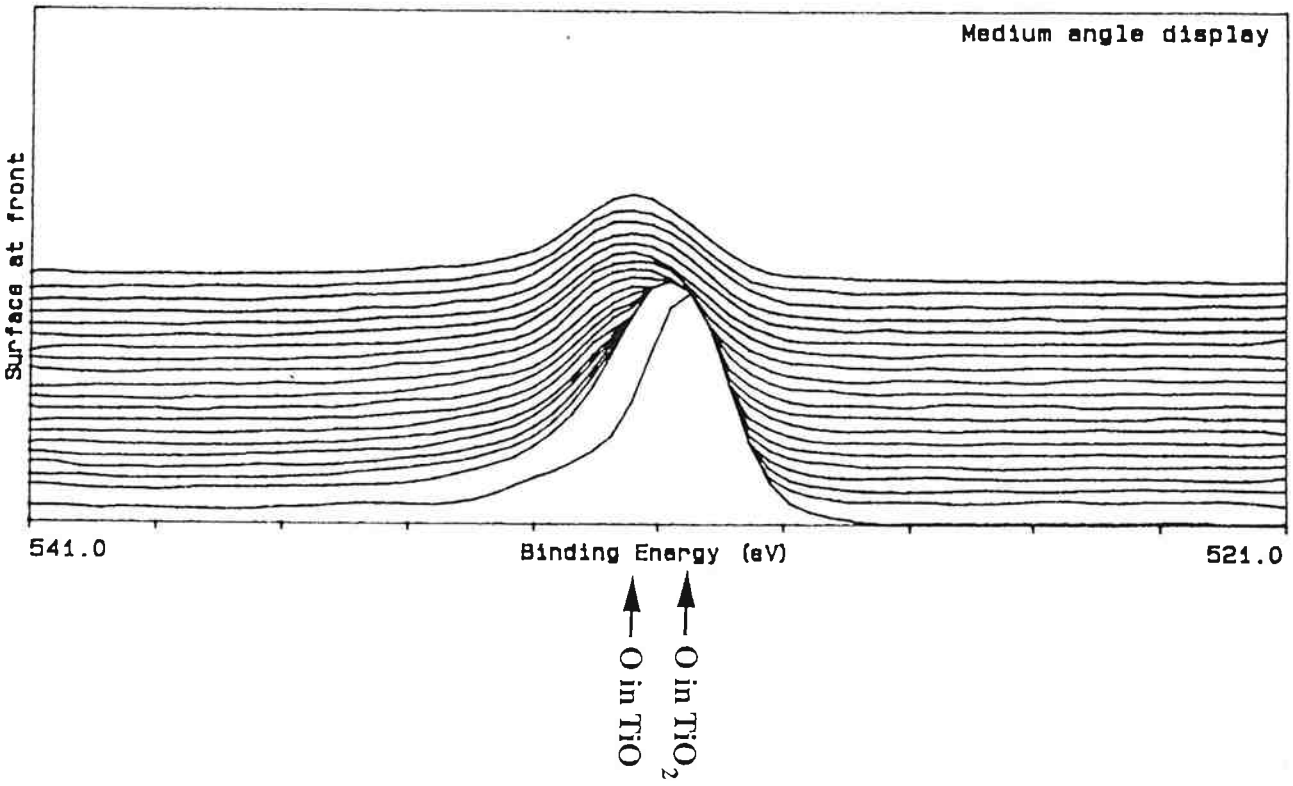

Figure 4.17 O1s peak as a function of sputter etching for sample TiPN.

With further sputtering the $Ti2p_{3/2}$ peak at 455.3 eV continues to grow suggesting an increasing concentration of Ti in a TiO and/or TiN matrix. The binding energy for metallic Ti is 454.1 (*Chastain, 1992*), close enough to 455.3 eV that metallic Ti could also be contributing to the observed peak. In fact, the observed peak shifts towards lower binding energies with increased sputter etching, which indicates an increasing contribution from metallic Ti. Thus, what the spectra indicate is: (1) TiO_2 is present only on the surface of the coating, (2) a mixture of TiO, TiN and metallic Ti underlies the surface, and (3) the metallic Ti concentration increases with depth in the coating, at least for the depth of coating examined by this technique.

Similarly, Figure 4.16 shows spectra for the N1s peak of nitrogen. The peak is located at around 397.4 eV, close to the value of 396.9 eV for nitrogen in a TiN matrix (*Chastain, 1992*). There is little N at the surface, but the concentration quickly builds as more coating is removed by sputter etching. Figure 4.17 shows spectra for the O1s peak of oxygen. In the first spectra, the peak is located at around 530.4 eV, close to the value of 529.9 eV for oxygen in a TiO_2 matrix(*Chastain, 1992*). With sputter etching, this peak quickly shifts to a binding energy value of 531.4 eV. While no data are available in the literature for the binding energy of O in TiO, it must be assumed, given the limited number of O compounds possible in the coating and the results for Ti, that the peak shift to 531.4 eV represents a transition from TiO_2 to TiO.

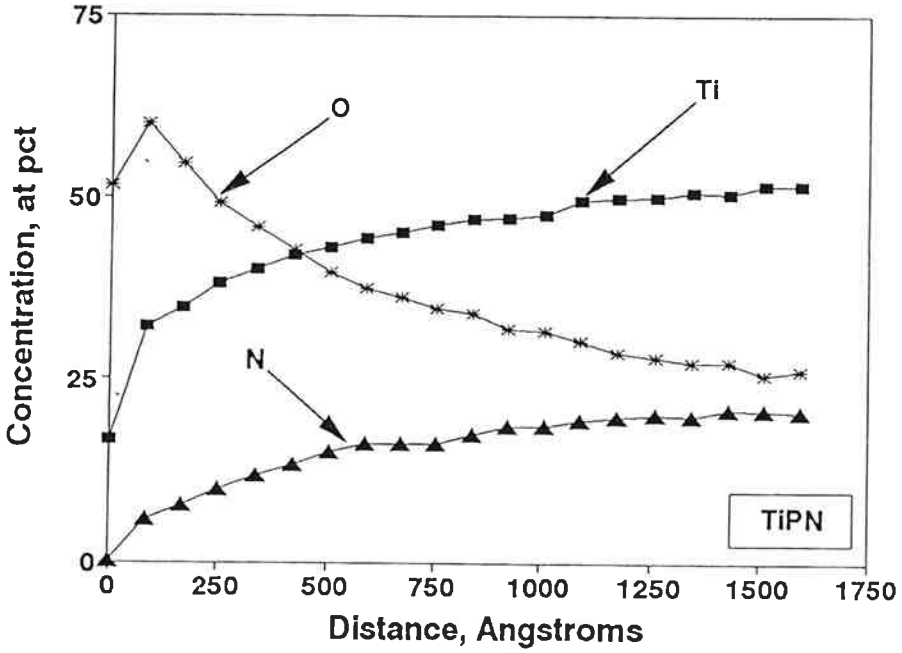

Figure 4.18 Composition depth profiles for sample TiPN.

Referring again to Table 4.11, values of the stoichiometric ratio (O+N)/Ti less than 1 near the end of sputter etching indicate the presence of metallic Ti within less than 0.2 mm of the coating surface. This agrees with the shift in binding energy of the $Ti2p_{3/2}$ peak from 455.3 eV (for TiO/TiN) toward 454.1 eV (for Ti) toward the end of sputter etching. The composition of the coating after each cycle of sputtering is shown by the depth profile in

Figure 4.18 created from the data in Table 4.11. These data show an increase in the N and Ti concentrations and a decrease in the O concentration with increased sputtering. These changes in the concentration profiles are more rapid near the outer surface, initially due to the presence of adventitious carbon but also due to the thin layer of TiO_2 located here.

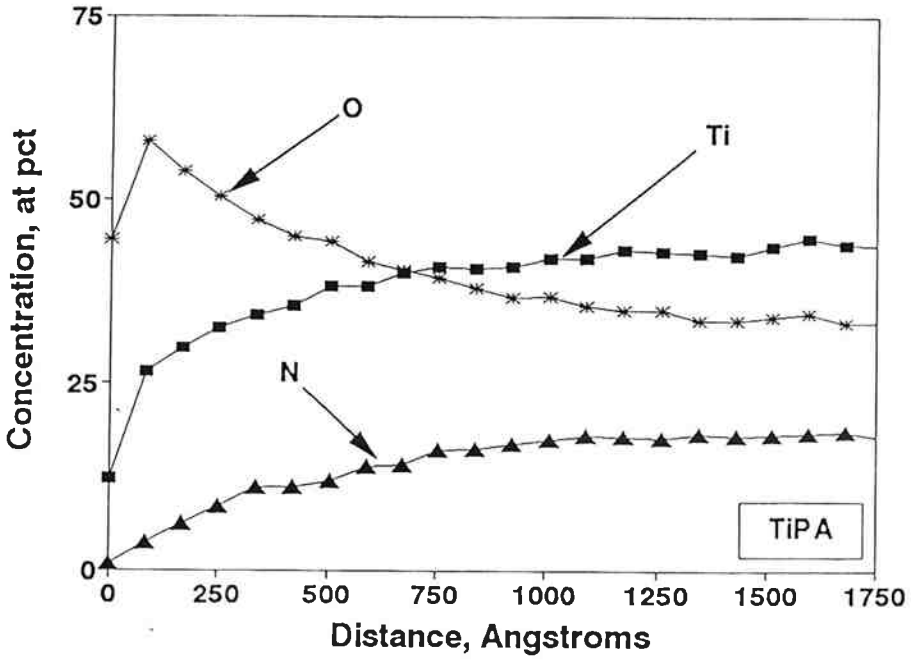

Figure 4.19 Composition depth profiles for sample TiPA.

Sample TiPA was sputter etched for 30 cycles of 120 seconds each. Composition depth profiles are plotted in Figure 4.19, showing data for 21 of the 30 sputter etch cycles. The results are similar to those for sample TiPN. The N curves are practically the same for both N and air atomization. There are significant differences in the Ti and O curves. After sputter etching the equivalent of about 0.05 μm, O values tend to be significantly higher and Ti values lower when air is the atomizing gas. Comparison of Figures 4.18 and 4.19 show these differences increase with sputter depth into the coating surface. They are supported by the fact that the stoichiometric ratio, (O+N)/Ti, for sample TiPA does not fall below 1.0, even after 30 cycles of sputter etching. These results suggest that the TiO concentration is higher deeper into the coating and the fraction of α-Ti remains lower when air atomization is used. It further suggests that shrouding the Ti droplets with nitrogen gas results in some increase in the metallic Ti content of the coating near the coating surface.

4.4 COATING DESCRIPTION

4.4.1 COATING CHEMISTRY

The coatings contained no metallic contaminants or impurities other than those originating in the Ti feed wire. The principal constituents of the coating were Ti, O and N. Coatings formed using air atomization typically contained on average (in at pct): 18 oxygen, 14 nitrogen and 68 Ti (87 weight percent); those formed using nitrogen atomization were 13 oxygen, 17 nitrogen and 70 Ti (88 weight percent). Assuming a portion of the nonmetallic elements reacted with the Ti, these concentrations suggest that a substantial fraction of the Ti, perhaps 50 percent or more, was present as metallic Ti.

However, the coating was not homogeneous but instead contained bands of material representing individual splats with highly variable chemistry. These bands, termed gradient bands, consisted of alternating layers of Ti-rich and nonmetallic-rich material. The nonmetallic-rich material originated in the oxidized layer or skin of the molten droplet formed in flight by reactions with the atmosphere. The Ti-rich material came from the core of the droplet and had little exposure to the atmosphere until the molten droplet hit the substrate surface and the oxidized skin ruptured. Typical ranges of concentration in the coating were (in atomic percent): 5 to 60 oxygen, 0 to 22 nitrogen, 40 to 90 titanium. This range in composition allows for a wide range of chemistries and associated material properties to exist within the coating.

4.4.2 COATING MINERALOGY

The coating contained two distinct phases, the hcp α-Ti and a fcc structure like TiN. No rutile, TiO_2, or β-Ti were detected in macro-samples of the coating. TiO_2 was observed in a very thin layer, less than 0.02 μm thick, on the outer surface of the coatings but was found nowhere else. While some TiN may form, the nitrogen concentrations were sufficiently low (i.e., below 22 atomic percent) that most of the nitrogen was interstitial in the α-Ti matrix. Oxygen concentrations were sufficiently high at some locations that both γ-TiO (the only fcc titanium oxide) and interstitial oxygen in the α-Ti matrix were present.

As two component systems, the α-Ti matrix can contain up to 22 atomic percent nitrogen or up to about 35 atomic percent oxygen. It is not known what exact concentrations of nitrogen and oxygen would be contained in the α-Ti matrix or how nitrogen or oxygen would affect the solubility of the other. But the interstitial solubilities for the two component systems suggest a fairly high solubility for nitrogen and oxygen in the three-component system, in the range of 20 to 30 atomic percent.

Cooling curves suggest that β-Ti formed at low concentrations of the nonmetallic elements. However, even at high cooling rates such as experienced by the coatings (i.e., 10^6 $^{\circ}$C/s), β-Ti transforms to α-Ti at lower temperatures (*Donachie, 1988*). In contrast to this, the γ-TiO is

stable at high temperatures. However, under equilibrium conditions, it could transform into other oxide forms below 1250 °C (*"Oxygen-Titanium Alloy Phase Diagram"*, 1992)This did not happen over the time frame that the coatings were examined and the γ-TiO is an unstable structure at ambient conditions.

4.4.3 COATING STRUCTURE

The coating microstructure consisted of two freezing structures. When the nonmetallic concentrations were sufficiently low (i.e., less than 20 to 30 atomic percent), a fine α-Ti dendritic structure was formed. The composition of the structure was not homogeneous, suggesting, in some cases, that both α-Ti and β-Ti formed and that the β-Ti transformed to α-Ti at lower temperatures, locking in the chemistry uniquely associated with the β-Ti phase. When oxygen levels were sufficiently high (i.e., greater than 30 to 40 atomic percent), α-Ti dendrites also formed, but in this case the interdendritic material was γ-TiO.

While the size of individual splats varied widely, their average size was fairly typical of thermal-sprayed coatings, 10 to 25 μm thick and 100 to 200 μm wide. Most splats appear to have impacted the surface in a molten state and microwelded to preceding splats. A small fraction appeared to have impacted in a partially molten or solid state. These tended to be smaller droplets with less thermal mass and with a large surface-to-volume ratio which aids cooling and reactions with atmospheric gases.

While in flight, the droplets acquired a skin rich in nonmetallic elements from reactions with atmospheric gases. Both nitrogen and oxygen react with titanium by diffusion of the gas into the titanium and internal oxidation (*Hauffe, 1965*). However, oxygen is the more reactive of the gases and, at 850 °C for example, the parabolic rate constant for the Ti-O reaction is almost two orders of magnitude higher than for the Ti-N reaction (*Kubaschewski and Hopkines,* 1992). On impact, the skin ruptures, and skin fragments and the Ti-rich core spread across the surface to form a splat. Typically the oxidized skin fragments cover preceding splats and the Ti-rich core material forms a layer over these fragments. Multiple layers of splats form multiple gradient bands, with highly varying composition across the bands and consisting typically of an oxidized layer and an α-Ti-rich layer.

The coatings were highly cracked, with less cracking present when the droplets were atomized using nitrogen than air. Cracks normal (or transverse) to the substrate surface and parallel to the surface were present within the coating. Parallel cracks tended to form at the interface between splats where remnants of the heavily oxidized droplet skin layer contacted a layer of α-Ti. This is the region with the highest concentration gradient, the greatest mismatch between molecular volumes and mechanical properties of the adjacent materials. Parallel cracks often linked transverse cracks produced by high internal tensile stresses resulting from cooling shrinkage.

The outer coating surface showed evidence of isolated glazing resulting from superheating some of the Ti droplets in the arc. Coatings sprayed on Pyrex formed a bond with the glass consisting of a thin Ti_5Si_3 layer. Sufficient thermal energy in the droplets to form such a bond with glass would suggest that a similar type reaction layer is possible with constituents of the concrete. The coating followed the small scale contours of the concrete surface well and appeared to form a good mechanical bond.

4.4.4 COATING PROPERTIES

Table 4.12: Coating Resistivity Data.

Atomizing Gas	Resistivity, Microhm-cm		Tortuosity
	measured	theoretical	
air	6990	58	120
nitrogen	3430	52	65
ratio of air and nitrogen tortuosity values = 1.8			

The resistivities of the coatings produced by air and nitrogen atomization, measured using the resistance probe described in this report, are given again in Table 4-12. Figure 4.20 compares a series of resistivity values measured with the probe on some standard materials with literature values. It shows that the probe measurements are reasonably accurate. The coating resistivity values are substantially higher than those reported for the component materials, Ti and TiO, reported in Table 4.2.

Assuming continuous filaments of the component materials in the coating, and weighting the resistivity of the component materials by their average volume fraction based on the data in Table 4-8, the theoretical effective resistivity of the coatings would be 58 $\mu\Omega$-cm for air atomization and 52 $\mu\Omega$-cm for nitrogen atomization. These values are well below the measured values and suggest that continuous filaments do not exist in the coating. In fact, the electron path is far more convoluted and constrained than suggested by the nominal dimensions of the coating.

A tortuosity value can be defined which accounts for these differences in resistivity. It is a combination of factors representing the fact that: (1) the coating cross-section is substantially reduced by variations in coating thickness and by the effect of transverse cracks, and (2) the path length is substantially increased by the extensive cracking within the coating. The tortuosity value is computed by taking the ratio of the measured coating resistivity and the theoretical resistivity based on the continuous filament model. The tortuosity value for air atomization was 120 and that for nitrogen atomization was 65. This is in agreement with visual evaluation of the coating cross-sections and surface features and the observation that cracking was less when nitrogen atomization was used. The higher tortuosity value for air atomization suggests an almost two-fold increase in the effect of cracking on the resistance of the coating, an important consideration in using the coating as a conductor for impressed current cathodic protection systems.

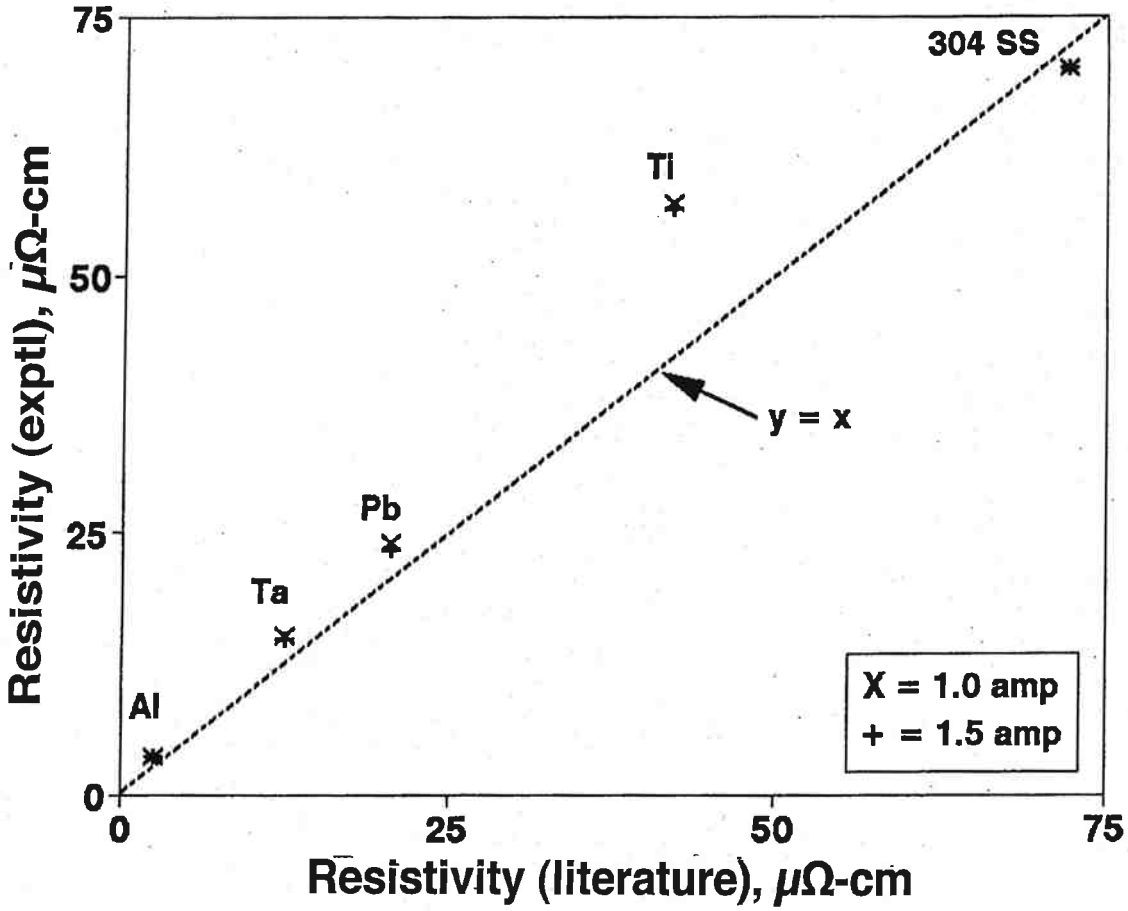

Figure 4.20 Validation curve for resistivity measurements on standard materials made with ODOT resistance probe.

In addition to cracking expected from cooling shrinkage, the non-homogeneous microstructure of the coating will produce local stresses and stress risers that cause extensive cracking. In particular, the presence of TiO in the coating resulting from internal oxidation of the droplets and splats will cause internal stresses to develop because the molecular volume of TiO is 20 percent larger than that of the Ti from which it formed. On the other hand, the molecular volume of TiN is very close to that of Ti and will have a substantially lesser effect. Interstitial nitrogen will distort the α-Ti crystal lattice, as will interstitial oxygen, but the effect on the coating properties will be smaller and more global in nature. The effect of the brittle TiO on cracking can be seen in the tendency of parallel cracks to follow the "sharp interface" where concentration gradients are high between adjacent splats. This is the interface which abuts the nonmetallic-rich layer representing the oxidized skin of the molten droplets against the Ti-rich core from preceding splats.

Local residual stresses could affect the long-term mechanical stability of the coating altering the cohesion of the coating and its adhesion to the concrete. The presence of the unstable γ-TiO in the coating could also have consequences for the long-term operation of the coatings as an anode. These could range from the mechanical stability of the coating to the effectiveness of the coating as a current carrier, i.e., the resistivity of the coating.

While the present measurements did not examine the question of electrochemistry on the coating surface, the locally diverse composition of the coating could have an effect on the electrochemical reactions that make the coating an effective insoluble anode for impressed current cathodic protection. These effects could range from the adsorption and retention of the catalyst on the coating surface to the condensation of moisture on the surface to sustain the anodic reaction.

4.5 COATING CHARACTERIZATION SUMMARY

The presence of γ-TiO in the coating is potentially the most damaging property of the coatings. It produces internal stresses within the coating, creates stress risers for crack nucleation, and brittle zones for crack propagation. It is an unstable structure that may affect the long-term properties and function of the coating in an impressed current cathodic protection system.

Interestingly, the internal oxidation rate of Ti by oxygen is higher in air than pure oxygen because the interstitial nitrogen expands the crystal lattice and facilitates the diffusion of oxygen (*Hauffe, 1965*). Thus, the main concern would be to promote conditions that reduce the concentration of γ-TiO within the coating. Interstitial oxygen and nitrogen are of much less concern, perhaps of no concern except for how they may affect internal stress within the coating.

Without evaluating economic viability, the following recommendations for reducing γ-TiO concentration are made.

1. Nitrogen is an effective atomizing gas with significant benefits in the coating properties. Improve the shrouding of the thermal spray gun and the spray to exclude convective currents of air entering the jet of molten Ti droplets from the gun to the target surface. This might include a mechanical barrier to exclude convective currents or a secondary stream of nitrogen to minimize air intrusion into the jet. These changes could reduce or eliminate γ-TiO in the coating and increase α-Ti.

2. Use argon for the atomizing gas. There would be no Ti-Ar reactions nor interstitial Ar. However, shrouding of the gun and spray would be just as critical as with nitrogen as the atomizing gas. While argon might be three times as expensive as nitrogen, the improved properties of the coating over the coating service life may warrant the additional expense. Carbon dioxide is not an acceptable atomizing gas because it decomposes at the temperatures of the arc and γ-TiO will be formed.

3. Metals with higher valence ions such as tungsten, niobium or tantalum could be incorporated in the Ti at low concentrations. The presence of such ions in the oxidized skin of the droplets in flight and in the freezing splats would, because of the semiconducting properties of titanium oxides, increase the conductivity of the oxide and reduce the oxidation rate of titanium (*Hauffe, 1965; Kubaschewski and Hopkins, 1992*)..

5.0 FIELD INSTALLATION

5.1 DESCRIPTION

The site selected for the field trial was the Depoe Bay Bridge in Depoe Bay, Oregon. The structure, spanning the channel into Depoe Bay on the Oregon Coast Highway, consists of two connected parallel structures. The original McCullough designed structure was constructed in 1926, and it was widened by constructing the adjoining structure in 1939. The resulting structure has a roadway width of 50 feet and a length of 314.7 feet at centerline. Both the original and the 1939 structures consist of one RCDG approach span on the north, a 150 foot concrete arch span, and three RCDG approach spans to the south.

The area of the bridge selected for titanium application was the underdeck and beam areas of the southern-most approach span on the 1939 structure. The 1939 structure is west of the original structure and, therefore, nearer to the ocean. This area on the structure has the advantage of having reasonable access from the ground should future work or testing be required on this experimental section. Since this is a historic structure, the sidewalk overhang and the western face of the architectural curtain wall including the west face of the outer beam were sprayed with zinc, so the appearance of the western face of the bridge is uniform. From the perspective of historic preservation, the color contrast between arc-sprayed zinc and arc-sprayed titanium would have unacceptably altered the appearance of the bridge.

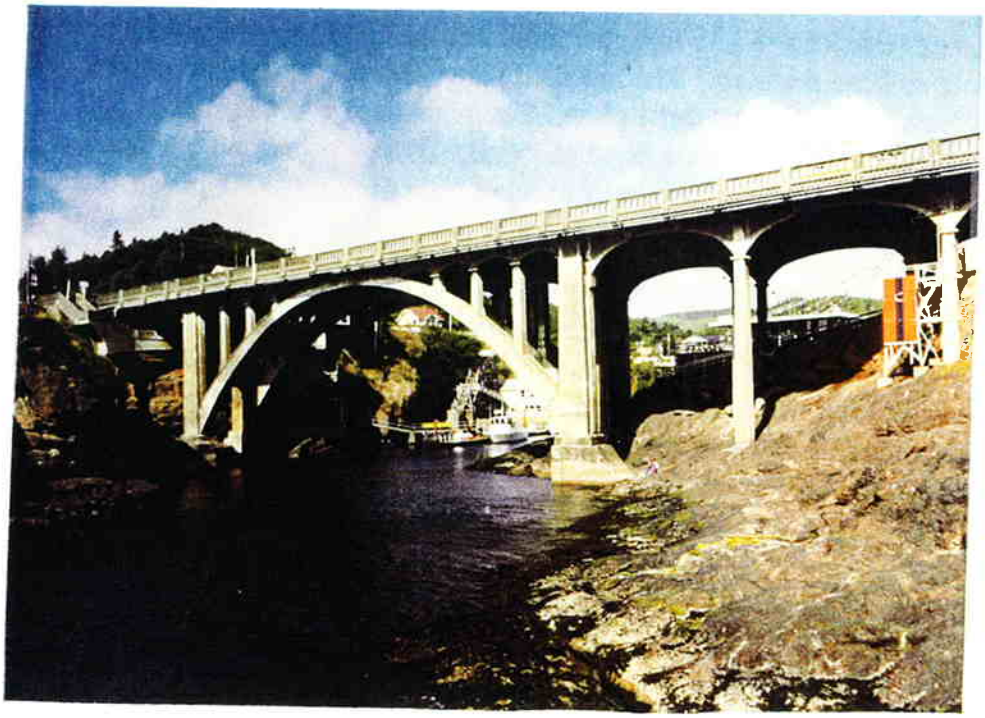

Figure 5.1 Depoe Bay Bridge

5.2 SPECIFICATIONS

The complete specifications used for the field installation are included in Appendix A. Some modifications to these specifications were required, and these modifications are discussed in the text of this report. The field trial work was completed as an experimental feature of an existing contract for rehabilitation and cathodic protection of the Depoe Bay Bridge.

5.3 INSTALLATION

5.3.1 CURRENT CONTACT PLATES

The current contact plates provide the electrical connection between the wires from the zone power supply to the arc-sprayed titanium anode. Typically, CP systems are designed to limit the voltage drop in the anode to 300 mV or less to achieve uniform current distribution in the zone. The spacing of the plates for this project was designed to limit the voltage drop in the anode to 300 mV or less at a current density of 21.5 mA/m^2 (2 mA/ft^2). The contact plates furnished by Eltech Research Corporation were constructed from 1.52 mm (0.060 inch) thick titanium. The dimensions of the plate were 76 mm x 127 mm (3" x 5") with a serrated perimeter (Figure 5.2).

The plates were attached with two titanium screws to the concrete surface after installation of the titanium. The plates were attached to the surface by installing plastic anchors flush with the concrete surface, inserting epoxy into the holes for the anchors, and threading a titanium screw with a washer into the anchor. Electrical connection to the plate was made by attaching a wire with ring connector to a titanium bolt through a tab in the center of the plate.

The serrations were intended to bite into the titanium coating to achieve good electrical contact between the plate and the titanium. The installed plates, however, did not achieve good contact along the entire perimeter of the plate. The plate used was too stiff to pull down tight to the surface when the anchor screws were installed. Even where good contact was achieved along some of the plate perimeter, the resistance between the sprayed titanium and the plate was higher than desired.

In an attempt to decrease distribution-plate-to-sprayed-titanium resistance, the plate design was changed to an embedded-type plate similar to that used on ODOT's sprayed zinc systems. The new 63.5 mm (2.5 in) diameter plate was constructed from a 3.175 mm (0.125 in) sheet of titanium with a titanium bolt welded to the center of the plate for the wire connection. Two countersunk holes were installed in the plate to attach the plate to the concrete with a plastic anchor and titanium screw (Figure 5.3).

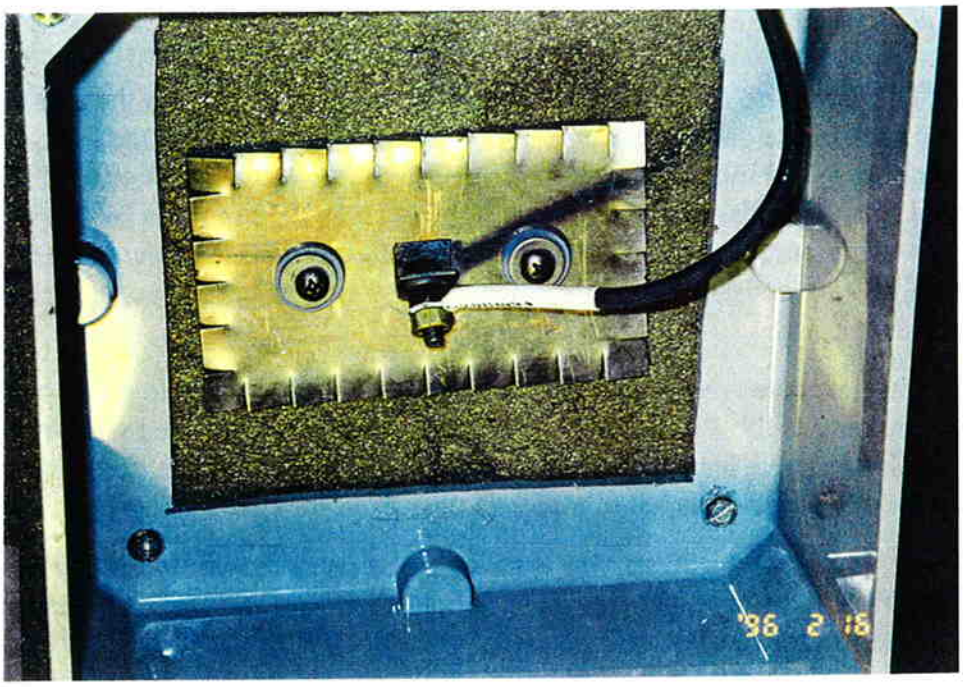

Figure 5.2 Surface Mounted Current Distribution Plate.

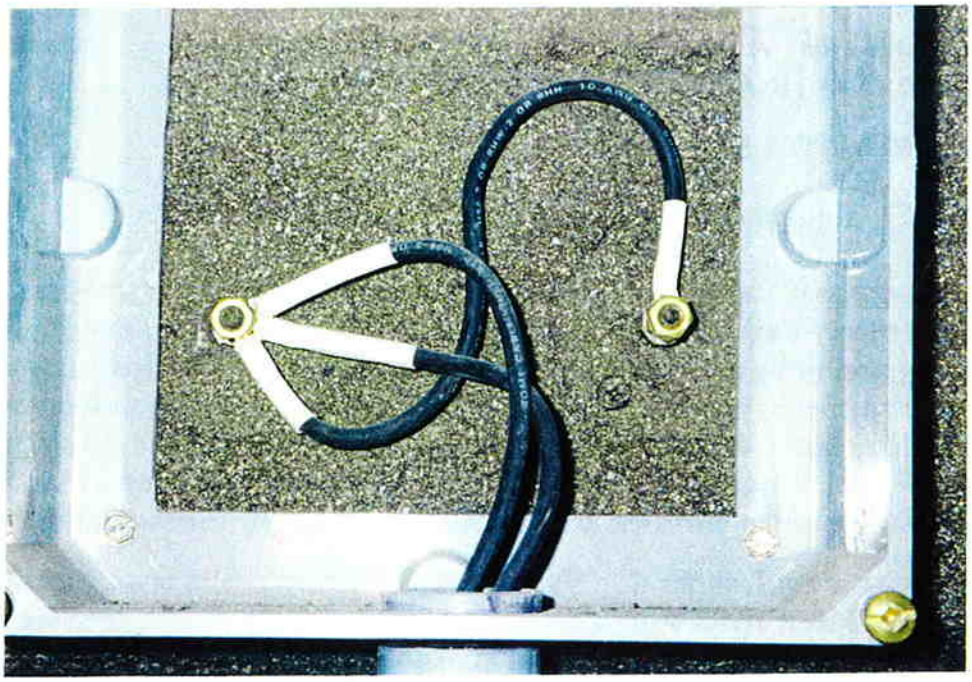

Figure 5.3 Flush-mounted current distribution plates with temporary wiring installed.

The plate was installed by core drilling approximately 4.8 mm (3/16 in) into the concrete and chipping out the center of the core with a chipping gun. Two holes were drilled in the concrete for the anchors, and the excavation was filled with DP-420 epoxy from 3M. The plate was installed flush with the surrounding concrete and was held in place by the anchor screws. After the epoxy cures, any epoxy that has run onto the surface of the concrete or the plate is ground off leaving a clean concrete surface, narrow ring of cured epoxy, and clean top surface of the titanium plate.

When the titanium was sprayed onto the plate, the titanium did not adhere to the epoxy, and since the titanium coating is thin, the titanium did not bridge the epoxy-filled gap between the titanium plate and the concrete leaving the current distribution plate isolated from the surrounding sprayed titanium. This led to a second change in the distribution plate design.

A minimum 13 mm (0.5 inch) deep area was excavated and patched with Rederoc HBA patching material. Plastic anchors were installed to hold the plates in place, and the plates were pressed into the patch material until the plates were flush with the surrounding concrete surface providing a smooth surface for installation of the thermal-sprayed titanium. The resulting installation provided good contact between the current distribution plate and the arc-sprayed titanium. Measurements with a Fluke 87 digital multimeter indicated a resistance of zero ohms between the titanium bolt at the center of the plate and the arc-sprayed titanium adjacent to the perimeter of the plate.

The size of the plate affects the amount of anode area that can be served by a single plate and limit the voltage drop to 300 mV. Two round plates were installed adjacent to each other as shown in Figure 4.2 to approximate the perimeter of the 5"x3" plates. For the installation at Depoe Bay, one current distribution plate (or set of round plates) was installed for each 500 square feet of surface area. A calculation of the maximum amount of area per current distribution plate is shown in Appendix B.

5.3.2 TITANIUM INSTALLATION

5.3.2.1 Equipment

The equipment used for the field trial was a Thermion Bridgemaster arc-spray system. The power supply used initially was a PowCon 630SM inverter-type supply. This is the same system being used for applying zinc to the Depoe Bay Bridge using 4.76 mm (3/16 inch) zinc wire; however, several modifications were required to spray titanium. The feed rolls, liners, and contact tips were changed to accommodate the smaller 3.175 mm (0.125 inch) diameter titanium wire. Hardened feed rolls are required to spray titanium because of the increased wear associated with the harder titanium wire.

Titanium wire is much stiffer than zinc wire, and the wire retains some curvature as it comes off the spool. Wire straighteners were installed to try to straighten the wire as it entered the wire feed unit. As discussed in section 2.2.2, an arc-shorting system was installed, and a short circuit detection system was connected to the gun control circuit.

5.3.2.2 Titanium Wire

The wire specified for use on this project was 3.175 mm (0.125 inch) annealed, grade 1 or 2 titanium wire. Grade 1 and grade 2 are high-purity commercial grades of titanium that differ in oxygen and iron content (grade 1 Fe-0.2%, O-0.18%; grade 2 Fe-0.3%, O-0.25%) (*Boyer, et al, 1994*). The increase in oxygen and iron content increases the strength of grade 2 but also decreases its ductility. The wire actually supplied for installing the arc-sprayed titanium on the bridge was 3.175 mm (0.125 inch) wire meeting the AWS A5.16-90 ERTI 1 specification. This specification is for a weld filler metal wire that fits within the grade 1 specification, but it has lower iron and oxygen content (Fe-0.1%, O-0.1%). The wire was annealed at 704 °C (1300 °F) for one hour. The Brinell hardness of annealed grade 1 titanium is 120 (67.5 HRB) compared to a value of 200 HB (93 HRB) for annealed grade 2(*Bauccio, 1993*).

5.3.2.3 Application

Several problems were encountered during the field spraying of the titanium. The operator of the spray equipment experienced great difficulty achieving a smooth arc. The arc-shorting control system was apparently too slow to stop the wires from shorting, so the wires tended to fuse frequently causing an extensive amount of down time for the spray equipment. When the feed wires fuse at the tip of the gun, the operator must stop, remove his air hood, clip the wires off at the tip, and put his air hood back on. Since this procedure is inconvenient and time consuming, the operators had the tendency to hold the trigger down to try to melt the fused wires. The problem with this technique is that, if the wires are solidly fused, the wires will heat back into the spray tip and fuse to the tip. When this happens, a very time consuming tip replacement process must take place.

When the fused wires do melt without fusing to the spray tip, they are propelled away from the gun as a large piece of molten wire. This flying piece of molten wire does not cool as quickly as the small spray particles, so the wire created a burn hazard for the operator and a fire hazard for the plywood work deck.

Smooth arc operation seemed to be at least partially related to movement of the gun head. Quick changes in the bending radius of the gun leads tended to interrupt the arc. This relationship was thought to be caused by the stiffness of the titanium wire. The wire retained some curvature even after passing through the wire straighteners. When the leads are moved, the stiffness and the curvature of the wire cause movement of wire within the spray tips and, therefore, a changing arc gap. Wear of the spray tips seemed to cause this problem to become worse since greater wire misalignment is possible with increasing internal diameter of the spray tips.

Spray tip wear was a significant problem encountered during spraying. The copper alloy used for the spray tips has a Rockwell B hardness value of 45 and an electrical conductivity of 95% IACS. As discussed in section 4.3.2.2 above, the hardness for annealed grade 1 titanium is 120 HB (67.5 HRB). Charge is transferred to the wires

via sliding contact with the spray tips. The large difference between the hardness of the titanium wire and the spray tips caused rapid wear of the spray tips. The tips were wearing out at the rate of approximately two sets of tips per 11.4 kg (25 pound) spool of wire.

Because of these problems that were experienced, spraying on the project was suspended until possible solutions to the problems could be considered. Approximately one-quarter of the area had been sprayed in 102 hours at the time spraying was stopped. The production rate for this initial phase was 0.7 m^2 (7.35 ft^2) per hour.

Investigation of what could be done to make the wire less stiff revealed that, although annealed wire was specified, unannealed wire was delivered to the job. Not only is the unannealed wire more stiff, but the hardness difference between the wire and the spray tip was greater than that discussed above. Fully annealed wire was ordered for spraying the remaining area. Interestingly, the annealed wire was sold for the same price as the unannealed wire. The annealed wire was expected to improve the alignment problem by reducing wear and by being less resistant to lead movement.

Also to further combat the wear problem, the U.S. Bureau of Mines (now U.S> Dept. of Energy, Albany Research Center) constructed a set of spray tips from an age hardened M25 beryllium copper alloy. This alloy has a Rockwell B hardness of 114, but its conductivity is only 22% IACS. Although this material is hard enough to greatly reduce the wear problem, it was not conductive enough to effectively transfer charge to the wire. When these tips were tried on the spray gun, an arc could not be established between the wires. A different beryllium copper alloy (alloy 3) with a Rockwell B hardness range of 95 to 102 and a conductivity of 48 to 60% IACS was also tried with similar results.

For the second phase of spraying, a Miller model FC-6 constant potential DC welding power supply was substituted for the PowCon 630 SMP supply. This change produced substantial improvement to the arc operation. Arc-spraying with the Miller power supply produced smooth arc operation and a stable arc voltage. To understand this difference in operation between the two supplies, the characteristics of each supply was investigated.

The PowCon supply is rated at 630 amps and 44 volts. These specifications are derated at 100% duty cycle to 450 amps and 38 volts. The Miller supply is rated 600 amps and 40 volts at 100% duty cycle. The PowCon supply is a switchmode supply which uses a feedback circuit to maintain constant output power. The Miller supply is a rectifier and transformer-type supply with no feedback.

The PowCon supply depends on the feedback and electronic control to maintain the desired output power. During spraying the output voltage of the supply fluctuated continuously. The operating characteristics of the titanium arc-spray process are probably much different from the operating characteristics of wire feed welding for which the power supply was designed. It is possible that the operating variations for

arc-spraying titanium exceed the compensating ability of the feedback circuit. An unstable control circuit could explain the observed fluctuation of the output voltage.

Since the PowCon supply was being operated toward the upper end of its output range, the difficulty sustaining an arc may also be related to protective, power-limiting circuitry in the PowCon supply and the constant power operating characteristic. When a wire begins to fuse, the PowCon supply may not be capable of supplying the instantaneous current peaks required to prevent the wires from shorting.

The Miller supply, however, is designed to maintain a constant voltage output. Since this voltage is dependent on arc gap, the Miller supply operates to maintain a constant arc gap. There is no feedback control circuit, but as conditions change at the spray tips, the amount of current increases or decreases to maintain the constant voltage. The large inductance which is typical in the output circuit for this type of supply enables the supply to provide short-term current output exceeding the rating of the power supply when it is required to maintain the desired voltage.

The change in power supplies provided a major improvement to the spray quality and improvement to the production rate. Approximately 190 hours were required to complete approximately 209 m^2 (2250 ft^2) remaining in the experimental zone. In this time, there were only 27.55 hours put on the spray machine hour meter. This computes to a machine production rate of approximately 7.6 m^2 (81.7 ft^2) per hour, but an actual production rate of only approximately 1.1 m^2 (11.8 ft^2) per hour.

The annealed wire reduced the wear rate on the spray tips; a set of spray tips lasted for approximately one set of (25 lb.) spools. Although the annealed wire increased spray tip life, much of the down time during the spraying was still attributed to adjustment and replacement of spray tips. Significant production rate improvement could be obtained with more wear-resistant spray tips.

An additional influence on the production rate for the titanium spraying was the heat experienced by the operator. The heat from the titanium spraying creates a difficult working environment for the operator. To combat the operator fatigue resulting from the high temperatures, the operators took more break time than is typical for zinc spraying.

The total titanium usage for the project, including waste, was 342.3 kg (753 lb.). This is significantly more than was expected. The expected maximum titanium usage rate was 0.807 kg/m^2 (0.165 lb/ft^2). The actual titanium usage rate was 1.22 kg/m^2 (0.25 lb/ft^2) — a 50% increase over the maximum expected usage rate.

There are several possible explanations for this higher-than-expected usage rate. The usage rate was clearly affected by the difficulty experienced during the initial spraying. During the first phase of spraying, when a stable arc could not be established, the operator pointed the gun at the ground until the arc stabilized. Since frequent difficulty was experienced during this initial phase, there was probably a significant portion of wire used trying to adjust the equipment for consistent arc performance.

As a result of the heat and the shower of sparks associated with arc-spraying titanium, the operators had difficulty maintaining the specified spray distance. The operators had a tendency to increase the spray distance which decreases deposit efficiency. Also, there are some areas in the zone which have a much lower coating resistance than was specified. In these areas, titanium usage would have been higher than expected.

The average coating resistance, however, was investigated and found to be 0.233 $\pm$ 0.044 ohms/square (95% confidence interval). Data from the shop spray portion of this study was used to develop a relationship between sample weight gain and coating resistance for the spray parameters used during field spraying. The equation developed was

$$\mathbf{R = -1.426Ln(w) + 3.2} \qquad \textbf{(5-1)}$$

where: $\mathbf{R}$ = coating resistance (ohms/square)
$\mathbf{w}$ = weight gain of sample

The fit of the equation to the experimental data provided an R^2 of 95.5%. The equation was used to investigate the impact of variation from the specified coating resistance on titanium usage. If an average deposit efficiency of 80% is assumed and the 95% confidence interval limits for the mean coating resistance are plugged into the regression equation, the titanium usage at the confidence interval limits can be calculated to vary from a 5.5% increase to a 2.5% decrease versus the titanium usage required to achieve the specified coating resistance. Variation in coating resistance, therefore, cannot explain a very significant portion of the increase in titanium usage experienced.

During this second phase of spraying, a set of spools of 3/32" wire was sprayed. This size wire seemed to spray more smoothly, and the wire was sprayed at 390 A and 37 V compared to 300 A and 40 V for the 1/8" wire. Since current is a measure of feed rate, the smaller wire actually can be sprayed with a feed rate 30% greater than the feed rate for the 1/8" wire. Although the smaller wire has a cross-sectional area of only 56% of the larger wire, the net effect is just a 25% reduction in the calculated production rate. However, if the 3/32" wire can be sprayed with less down time, it may offer the opportunity for an increase in the actual production rate.

5.3.3 CATALYST

According to the developers of the catalyst for the arc-sprayed titanium coating, Eltech Research Corporation, application of the catalyst must take place with an impressed current system operating, and the system must remain in operation for a minimum of 72 hours after catalyst application. For this installation, the power supply was set to deliver 5.4 mA/m^2 (0.5 mA/ft^2). The amount of Eltech-supplied catalyst specified to be applied to the titanium was 355 ml/m^2 (0.035 quarts/ ft^2) minimum; however, the application rate must allow the catalyst to absorb without dripping or running from the surface.

The catalyst was delivered from Eltech premixed in a drum. The quantity of catalyst to be applied was 110 liters (29 gallons). This quantity equates to 392 ml/m^2 (0.038 quarts/ ft^2) which allows for 10% waste during application of the catalyst.

Figure 5.4 Catalyst Application

The original plan was to apply the catalyst in two coats. The first coat would require slightly more than half of the catalyst from the drum. The remaining catalyst would then be diluted with water to equal the volume of catalyst used in the first coat. After allowing for drying time between coats (30 minutes minimum), the remaining catalyst would be applied at the same rate as the first coat.

The catalyst installation was applied by two workers each using a 7.6 liter (2 gallon) pressurized spray tank. After completing the first coat of the catalyst, approximately 50 liters (13.3 gallons) of the catalyst had been used. The second coat used approximately 31 liters (8.3 gallons) leaving approximately 28 liters (7.4 gallons) in the drum. Water was added to the drum to dilute the remaining catalyst to approximately 37.9 liters (10 gallons) prior to the third and final coat. The fact that three coats were required instead of two probably provided more uniform coverage of the catalyst. As specified, a minimum of 30 minutes of drying time was allowed between coats. The entire process took two workers four hours to complete including set up and clean up. After completion of catalyst application, the power supply was operated at 10.8 mA/m^2 (1mA/ft^2) for one week before returning to 2.15 mA/m^2 (0.2 mA/ft^2).

After the catalyst has dried, it is not possible to visually detect a difference between catalyzed and uncatalyzed titanium. If it is desired to verify complete catalyst coverage, project

specifications should specify that application of the catalyst take place in the presence of the inspector. An additional factor that should be considered when specifying catalyst application is the amount of waste resulting from using the spray process for vertical and overhead surfaces. At the completion of the catalyst application the plywood decking below the sprayed surface was very damp from the catalyst overspray. The application efficiency, however, was not measured.

5.4 FINAL TESTING

5.4.1 VISUAL INSPECTION

Approximately one month after completion of the titanium and catalyst installation, a visual inspection was performed. Three rust stains were located indicating the presence of tie wires at the surface of the concrete. These tie wires were not detected by the short circuit detection system and did not show up in the voltage drop measurements discussed below. Apparently, the wires were either not making good electrical contact with the titanium or are not connected to the rebar. Although the presence of the wires does not seem to be affecting system performance, the wires were removed to prevent future problems.

The visual inspection also revealed some small areas where the coating has disbonded. The areas are typically of irregular shape as shown in Figure 5.5. The disbonded areas are typically 50 mm in diameter or less, although, there are some larger areas. Further investigation into the areas that had disbonded revealed two distinct characteristics. All areas that delaminated were either areas where the coating was much thicker than specified or patches which had not received proper surface preparation prior to installation of the coating.

Coating resistance measurements made near the disbonded areas revealed that in all cases, except near the unprepared patch areas, the coating resistance was 0.10 ohms/square or less. This is significantly less than the specified coating resistance of 0.25 ohms/square and indicates a coating much thicker than specified. The unprepared patch areas were surface metal patch areas that were patched after the surface preparation for the zone had been performed. The patches tended to have a smooth, weak concrete slurry on the surface of the cured patch.

The reduction in bond strength with coating thickness is well documented for many different thermal-sprayed coatings, as discussed in section 3.2. The mechanism that causes this observed phenomena has not, at this point, been clearly demonstrated. Gudge, et al., determined through experimental work and numerical modeling that a plasma-sprayed tungsten coating contains increasing residual stress with increasing coating thickness (*Gudge, 1990*). The postulate is that residual stresses are formed during three separate phases. First, the coating is applied in layers which heat to an average temperature which, for a metal on a concrete substrate, is greater than the temperature of the substrate. Next, the coating cools to

the average temperature of the substrate, and the bonding of the coating to the substrate constrains contraction of the coating. Finally, the coating and substrate cool to ambient temperature and differences in thermal expansion coefficients betweenthe coating and substrate create further stresses.

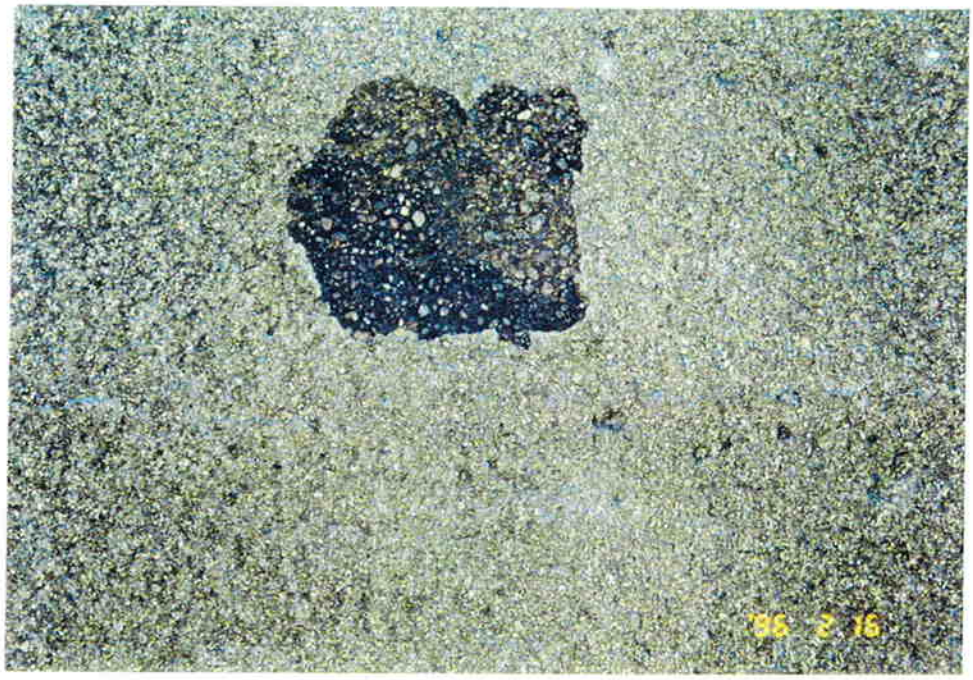

Figure 5.5 Typical Disbonded Area

Decreasing bond strength with coating thickness is explained by the higher temperature differences that occur between the coating and the substrate during the process of depositing a thicker coating. This theory applies well to coatings that are applied in one continuous process. The bond-strength samples for this study, however, were coated in discrete one pass layers. The samples were weighed between each pass allowing time for cooling of each coating layer, and causing the coating to go through multiple heating and cooling cycles.

The statistical analysis of these samples showed no significant correlation between number of spray passes and bond strength, but the correlation between bond strength and coating resistance (inversely proportional to coating thickness) was clearly demonstrated. Greving, et al., described a mechanism which may explain the results observed in this study (*Krepski,*

1993). Their work with a 95% nickel, 5% aluminum coating on a steel substrate showed no increase in residual stresses with coating thickness. However, they did observe a substantial decrease in coating bond strength with increased coating thickness.

The theory used to explain these observations is called the free-edge effect and is drawn from experience with the disbonding within laminated composites. This theory analyzes what happens to the planar residual stresses at the edge of a coating. A coating edge occurs at a coating defect as well as at the boundary of the sample. In a steady state, the forces within a coating must be balanced, so at a coating edge, the planar tensile stresses within the coating, having no balancing planar forces outside the coating at the free edge, create a moment that tends to lift the coating at the free edge. As the coating thickness increases, this moment increases.

There are additional properties of arc-sprayed titanium that increase its susceptibility to damage from residual stresses within the coating. Titanium is an allotropic element meaning it can exist with two different lattice structures. At temperatures below $882 \pm 2^{\circ}C$ ($1620^{\circ}F$), titanium has a hexagonal close packed lattice structure referred to as the α phase. Above this temperature, pure titanium has a body centered cubic structure referred to as the β phase. The lattice parameters for the β phase are larger than the lattice parameters for the α phase. The melting temperature for titanium is $1670 \pm 5^{\circ}C$ (*Boyer, et al,* 1994). During the arc-spraying process, the α phase, grade 1 titanium wire melts and on a cooling portion converts to the β phase. As the titanium cools further, the β-Ti returns to the smaller α phase providing an additional source of residual stresses in the deposited coating.

Coupled with these sources of residual stresses, there are factors that make the coating more brittle. At elevated temperatures, oxygen and nitrogen are highly soluble in the titanium. In addition, the oxidation rate of the titanium increases with increasing temperature (*Donachie, 1988*). The presence of these interstitial elements and of titanium compounds (particularly γ-TiO) causes the titanium to become more brittle and, therefore, more susceptible to fracture.

The observed coating disbondment is probably the result of a combination of the material properties of arc-sprayed titanium and the residual stresses resulting from the spray process. Further work is needed to define, for specification purposes, the minimum coating resistance (i.e., maximum coating thickness) for which acceptable bond can be achieved. This maximum value, however, is also dependent on substrate variables. For example, the weak concrete slurry surface of the unprepared patch areas allowed coating failure at normal coating thickness.

To date, the disbonded areas have not grown in size, and additional disbonded areas have not appeared. With manual application of the coating to the bridge, it may be difficult to completely avoid areas of excess thickness. However, if the size and quantity of disbonded areas remain small, these areas will not affect the effectiveness of the cathodic protection system.

5.4.2 ANODE VOLTAGE DROP

After installation of the titanium anode and catalyst, the DC voltage drop in the anode was investigated. The system was designed to have a maximum of 300 mV of voltage drop in the anode at 21.5 mA/m^2 (2 mA/ft^2). To perform this test, the system was connected to a constant current power supply operating at 3 amps (10.7 mA/m^2 or 1 mA/ ft^2). The positive lead of a Fluke 87 digital multimeter was connected to a current distribution plate, and the negative lead was used to take voltage measurements in a grid pattern over the entire surface area of the anode.

Since the power supply was set at half the design current, the maximum expected voltage drop was 150 mV. The measurements showed reasonable agreement with the theoretical values for most of the anode area. The measurements were made with the positive lead connected to a single distribution plate, so the voltage drop measurements also included the voltage drop in the conductors between the plates and between the plate and the titanium. The voltage drop between the positive lead connection point and the other plates was in the range of 42 to 54 mV.

After compensating for the voltage drop in the wires, the maximum voltage drop in the anode appears to be around 180 mV. The testing revealed one surface-mounted current distribution plate with poor contact to the titanium. The voltage drop between the connection point and that plate measured 195 mV. Measurements in the southeast corner of the zone where this plate is located are higher than expected with measurements as high as 548 mV. There are also areas in the northeast corner of the zone which have high voltage drop measurements around 300 mV.

The anode seems to perform reasonably close to the theoretical calculations except where installation problems have occurred. The faulty surface-mounted plate will be corrected, and the reason for the high voltage drop in the northeast corner will be investigated further. When these corrections are made and the contractor completes the permanent wiring installation, this test will be repeated.

This test has proven to be useful for final inspection of the arc-sprayed titanium anode. It is difficult to visually detect all coating areas that are too thin. In one area of this zone, a 25 mm (1 inch) wide, 45-degree beveled edge along the bottom of a beam had been missed during spraying. This created an area of anode that was isolated from the current distribution plate. This area was not detected during visual inspection, but it was readily apparent through voltage drop measurements (during a preliminary voltage drop test) that exceeded 1 volt. The test provides a quick verification that the anode will successfully distribute current throughout the zone. The entire test for this zone took two people approximately 1.5 hours to complete.

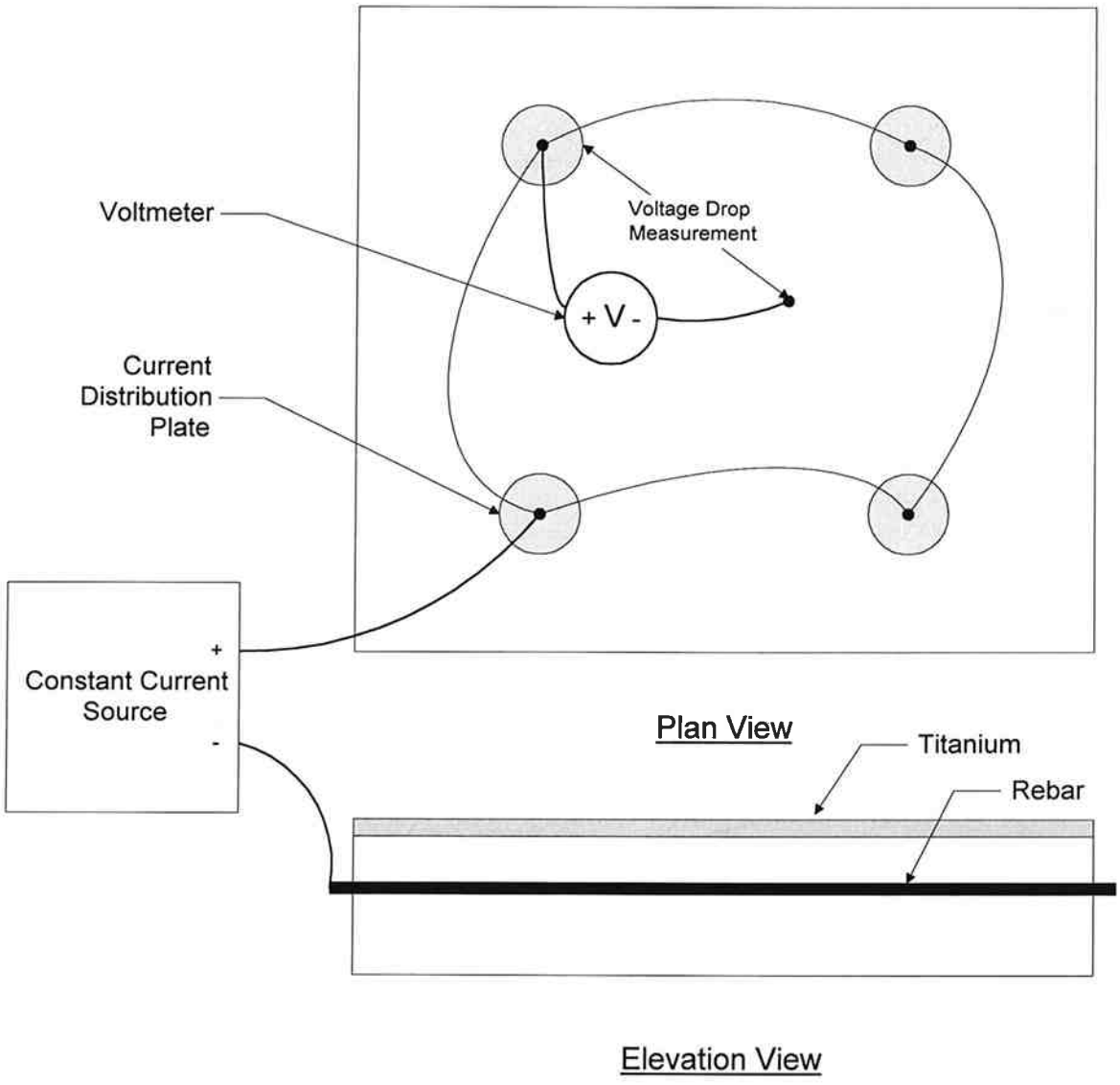

Figure 5.6 Connections for Anode Voltage Drop Testing

5.4.3 CURRENT-POTENTIAL RELATIONSHIP

About one hour after completion of catalyst application, the current supplied on the zone (i.e. 280 m^2/3015 ft^2) by the power supply was varied and the output voltage and the potential of the titanium anode versus a saturated calomel electrode (SCE) were recorded. The results are shown in Table 5.1. The stability of the anode potential versus the SCE verifies that the catalyst is working.

Table 5.1: Variation in Voltage and Potential with Changes in Applied Current

Current (amps)	Voltage (volts)	Potential vs. SCE (volts)
0.5	0.97	0.347
1.0	1.15	0.349
1.5	1.32	0.351
2.0	1.48	0.354
2.5	1.63	0.357
3.0	1.81	0.359
3.5	1.97	0.362
4.0	2.16	0.367
4.5	2.33	0.371
5.0	2.50	0.375
5.5	2.66	0.380
6.0	2.85	0.383

5.5 COST ANALYSIS

The costs for the project are summarized in Table 5.2. The bid price for installation of zinc on Depoe Bay Bridge was 88.80/m^2 (8.25/ft^2), so the cost for installing the titanium exceeded the bid cost of zinc by just 18%. Considering the difficulties experienced in this first titanium project, this result is encouraging.

Additional equipment development to reduce wear of the spray tips could substantially reduce the amount of labor shown in Table 5.2. The fact that titanium usage was 50% over the maximum expected usage indicates that an improvement in the amount of titanium used can also be achieved.

Even at the costs achieved on this project, the titanium appears to be a good solution from the life cycle cost perspective. Assuming the titanium system can achieve a 40-year life, the 40-year life cycle cost to complete the 280 m^2 (3015 ft^2) of bridge area for this project was $29,366. Assuming the zinc system will last 20 years, inflation will be 4% and the proper discount rate is 7%, the 40-year life cycle cost for applying zinc to this same bridge area would be $38,958. If only application costs are compared, the titanium system appears to offer a $10,000 savings over zinc. At 20 years, the zinc system would also incur costs for surface preparation, mobilization, constructing access to the bridge, and re-installing electrical wiring. These additional zinc system costs increase the life cycle cost advantage provided by the titanium system.

Table 5.2: Cost Summary

Item	Quant.	Unit Price	Total	$/m^2$	$/ft^2$
Titanium Wire	342.3 kg	$41.8/kg	$ 14,308	51.13	4.75
Catalyst	110 liter	$16.45/liter	$ 1,810	6.46	0.60
Labor	292 hrs	$42.90/hr	$ 12,527	44.67	4.15
Freight/Misc.	—	—	$ 723	2.58	0.24
		Total Cost	$29,368	$104.84	$9.74

6.0 CONCLUSIONS AND RECOMMENDATIONS

Although some difficulties were experienced during the field installation, the coating shows promise as a cathodic protection anode. Further work is warranted, however, prior to full-scale application of this anode material. The following conclusions and recommendations are presented to summarize the results of this project:

6.1 CONCLUSIONS

- Measurement of the coating resistance of a thermal-sprayed titanium coating provides a non-destructive technique for determining the suitability of the coating for distributing current. At a coating resistance value of 0.5 ohms/square, a 100 mm (4") diameter current distribution plate is required for each 46.5 m^2 (500 ft^2) of anode area. When measuring coating resistance on a large sheet of anode material, additional current paths at the edge of the resistance measuring probe cause the measured resistance value to be less than the actual value. The amount of reduction in the resistance value was determined empirically to be 50% (e.g., if an actual resistance value of 0.5 ohms/square is desired, the measured resistance on a large sheet of anode should be 0.25 ohms/square).

- The apparent deposit efficiency for arc-sprayed titanium is low initially, but it increases rapidly to between 80% and 90% by the third and fourth spray passes for the spray parameters investigated in this study. Several problems were identified with deposit efficiency measurements of arc-sprayed titanium, so deposit efficiency does not appear to be a good single measure for optimizing spray parameters primarily due to the effect of the spray parameters on the conductivity of the coating.

- The best measure for evaluating the effectiveness of the coating for distributing current is the product of coating resistance and sample weight gain which produces a quantity correlated to coating resistivity. A multiple regression equation was constructed to determine the spray parameters that would yield the best combination of low resistance and low titanium usage. The equation revealed that, for the data collected in this study, gun travel speed and the pressure of the propellant are insignificant variables. Decreasing spray distance increases the effectiveness of the coating for distributing cathodic protection current. Increasing the current at which the titanium is sprayed increases the effectiveness of the coating, although, this effect is more pronounced at higher spray distance. Using nitrogen as the propellant produces a more effective coating, by reducing coating resistivity. Spray parameters used for field application were 150 mm (6") spray distance and 300 A. Compressed air was used as the atomizing gas instead of nitrogen because the cost savings from reduced titanium usage was offset by the cost of providing nitrogen for this project. However, possible coating long term performance benefits resulting from nitrogen usage need further study.

- This study provided an initial examination of the bond strength of the titanium coating. Bond strength appears to be good for the variety of conditions tested. However, a relationship between coating resistance and bond strength was noted. As the coating resistance decreases the bond strength decreases. This effect is probably related to residual stresses in the coating.

- Arc-sprayed titanium bridges cracks poorly. The maximum crack width bridged during this study was 0.127 mm (0.005"). This did not appear to present problems during the field spraying trial. Resistance measurements across cracks showed satisfactory coating resistance values.

- Catalyzed operational samples have been operated satisfactorily at accelerated constant current levels for over 300 days at a stable voltage. This indicates suitable operation of the catalyst including a sample that was catalyzed to simulate an overhead surface. Unexpectedly, the uncatalyzed sample has not experienced large increases to the operating voltage. The uncatalyzed sample, however, appears much more sensitive to changes in humidity. This will be investigated and the results reported in the final report.

- An arc-sprayed titanium coating is a non-homogeneous due to reactions with atmospheric gases (O_2 and N_2). It contains, on average, about 88 weight percent titanium using air or nitrogen atomization. The principal constituents of the coating are α-Ti containing interstitial nitrogen, interstitial oxygen, and γ-TiO with the possibility of some TiN. Alternating layers of α-Ti rich and γ-TiO rich material comprise the coating.

- Nitrogen atomization produces a coating with less cracking and more uniform chemistry than air atomization. This results in substantially lower coating resistivity than produced by air atomization. Coating cracking substantial increases the tortuousity of the electrical conduction path over the nominal dimensions on the coating.

- The presence of γ-TiO in the coating causes some undesirable coating properties. It is an unstable structure that produces internal stresses within the coating, creates stress risers for crack nucleation and brittle zones for crack propagation.

- Current distribution plates embedded flush in a concrete patch material provide the best means for providing a low resistance attachment of a power supply to the anode.

- A constant power, switchmode welding power supply does not provide stable arc operation for arc-spraying titanium. The older technology constant voltage transformer and rectifier type welding power supply is more suitable for arc-spraying titanium.

- Annealed wire should be used for improved ductility and reduction in equipment wear. One spool set of 3/32" wire was tried during the field trial while the remainder of the project was sprayed using 1/8" wire. The smaller diameter wire seemed to spray more smoothly, with less equipment down time, and at a higher feed rate than the 3.175 mm (1/8") wire. The approximately 25% reduction in application rate attributed to the smaller diameter of wire would probably be more than offset by a reduction in down time.

- Anode voltage drop measurements provide an excellent final inspection tool for identifying performance problems in the coating.
- Although difficulty was experienced during the field spraying portion of this study, the costs for performing this work exceeded the bid costs for installing zinc by just 18%. Considering life cycle costs, the titanium system offers a cost advantage over the zinc system even at the costs experienced on this project. Provided the performance of the catalyzed titanium system is proven, this system is promising since there is much room for improvement in installation costs.

6.2 RECOMMENDATIONS

- Techniques to reduce the γ-TiO content of the coating should be investigated since this would improve the durability and conductivity of the coating. Several suggested areas for investigation are: improved shrouding of the spray jet; the use of an alternate atomizing gas; and the use of titanium alloyed with tungsten, niobium or tantalum to produce a coating with greater resistance to oxidation.
- The highly varied chemistry of the coating suggests future work on how the electrochemistry at the coating surface is effected and how internal stresses leading to coating cracking can be reduced.
- The short circuit detection system developed for use during the field trial provided results that were difficult to interpret. More work is needed to develop a system that can more reliably detect short circuits between the titanium anode and the rebar.
- Since low coating resistance appears to be linked to low bond strength and coating bond failure, further work is needed to determine the minimum allowable coating resistance for specification purposes. Perhaps more importantly, a better understanding of the bond failure mechanism may suggest techniques to eliminate or reduce residual stresses in the completed coating.
- Even with annealed wire, contact tip wear is a problem. Further work is needed to develop tips that are wear resistant and conductive enough to effectively transfer charge to the wire.
- Although 1/8" wire was used for the majority of work on this project, the better sprayability of 3/32" wire suggests that future work should, at least initially, focus on the use of 3/32" wire.

7.0 REFERENCES

J.P. Bars, D. David, E. Etchessahar, and J. Debuigne, "Titanium α-Nitrogen Solid Solution Formed by High Temperature Nitriding: Diffusion of Nitrogen, Hardness, and Crystallographic Parameters, *Metallurgical Tranactions A*, Vol. 14A, pp. 1537-1543, August 1983.

Michael Bauccio, ed., *ASM Metals Reference Book*, 3rd edition, ASM International, 1993.

J.E. Bennett, T.J. Schue, and G. McGill, "Protecting Reinforced Concrete Using Thermally Sprayed Titanium Anodes, *Materials Performance*, Vol. 34, No. 11, pp. 23-26, November 1995.

J.E. Bennett, T.J. Schue, and G. McGill, "A Thermal Sprayed Titanium Anode for Cathodic Protection of Reinforced Concrete Structures", NACE International Corrosion 95, paper No. 504, Orlando FL, March 26-31, 1995.

C.C. Berndt, S. Reddy, and M.L. Allen, "Optimization of Thermal Spray Parameters for Cathodic Protection of Reinforcement in Concrete", NACE International Corrosion 95, paper No. 12, Orlando, FL, March 26-31, 1995.

J.M. Blocher, Jr., "Nitrides", *High Temperature Materials and Technology*, i.e. Campbell and E.M Sherwood, eds., Wiley and Sons, New York NY, P. 391, 1967.

Rodney Boyer, Gerhard Welsch, and E.W. Collings, eds., *Materials Properties Handbook: Titanium Alloys*, ASM International, 1994.

I.E. Campbell, and E.M. Sherwood, eds., "Ceramic Oxides", *High-Temperature Materials and Technology*, Wiley and Sons, New York NY, p. 271, 1967.

R.A. Carello, D.M. Parks and J.A. Apostolos, "Development, Testing and Field Application of Metallized Cathodic Protection Coatings on Reinforced Concrete Substructures", California Department of Transportation, FHWA/CA/TL-89/04, May 1989.

J. Chastain, ed., *Handbook of X-ray Photoelectron Spectroscopy*, Perkin-Elmer Corporations, Physical Electronics Division, Eden Prairie, MN, 261 pp., 1992.

B.S. Covino, Jr., S.J. Bullard, G.R. Holcomb, S.D. Cramer, G.E. McGill, and C.B. Cryer, "Bond Strength of Electrochemically-Aged Arc-Sprayed Zinc Coatings on Concrete", Corrosion/96, Preprint 308, NACE International, 17 pp., March 1996.

B.X. Covino, Jr., S.J. Bullard, G.R. Holcomb, S.D. Cramer, G.E. McGill, and C.B. Cryer, "Factors Affecting the Bonding of Arc-Sprayed Zinc to Concrete", *Balancing Economics and compliance for Maintaining Protective Coatings*, SSPC 95-09, Steel Structures Painting Council, Pittsburgh PA, pp. 115-128, November 1995.

Matthew J. Donachie, Jr., *Titanium: A Technical Guide*, ASM International, Metals Park OH, 1988.

Engineering Property Data on Selected Ceramics, Nitrides, MCIC-HB-07-Vol. 1, Metals and Ceramics Information Center Battelle, Columbus OH, pp. 5.3.4-1 through 5.4.8-9, July 1981.

Engineering Property Data on Selected Ceramics - Single Oxides, MCIC-HB-07-Vol. 3, Metals and Ceramics Information Center, Battelle, Columbus OH, pp. 5.4.8-1 through 5.4.8-9, July 1981.

W.A. Gernitsky, Test Certificate 941474 Titanium wire Corporation, P.O.B. 8177, Frackville, PA 17931, January 12, 1995.

H. Gruber, and E. Krautz, "Electrical Conductivity, Thermopower, Hall Coefficient and Magnetoresistance of Titanium Oxides with different Oxygen Content", *Z. Metallkunde*, Vol. 77, No. 4, pp. 203-206, April 1986.

M. Gudge, D.S. Rickerby, R. Kingswell, and K.T. Scott, "Residual Stress in Plasma Metallic and Ceramic Coatings", *Thermal Spray Research and Applications, Proceedings of the Third National Thermal Spray conference*, Long Beach CA, pp. 331-337, May 20-25, 1990.

K. Hauffe, *Oxidation of Metals*, Plenum Press, New York NY, pp. 209-228, 1965.

R.P. Krepski, *Thermal Spray Coating Applications in the Chemical Process Industries*, Materials Technology Institue Pub. 42, NACE International, Houston TX, p. 16, 252, 1993.

O. Kubaschewski, and B.E. Hopkins, *Oxidation of Metals and Alloys*, Butterworths, Longon, pp. 5-14, 24, 213-217, 1992.

W.J. Lackey, D.P. Stinton, G.A. Cerny, A.C. Schaffhauser, and L.L. Fehrenbacher, "Ceramic coatings for Advanced Heat Engines -A Review and Projection", *Advance Ceramic Material*, Vol. 2, No. 1, pp. 24-30, 1987.

S.H. Leigh, S. Sampath, H. Herman, C.C. Berndt, G. Montavon, and C. Coddet, "Quantitative Analysis of Thermal Spray Deposits Using Stereology", *Proceedings 8th National Thermal Spray conference*, ASM International, pp. 273-278, September 1995.

Martin S. McGovern, "CP OK with ODOT", *Concrete Repair Digest*, pp. 291-295, October/November 1994.

A. Munster, and K. Sagel, "Some Electrical Properties of Titanium Nitride and Titanium Carbide", Z. *Physik*, Vol. 144, pp. 139-51, 1956 (Also: A. Goldsmith, T.E. Waterman, and H.J. Hirschhorn, *Handbook of Thermophysical Properties of Solid Materials*, Vol 4, MacMillan, New York NY, p. 303.

"Nitrogen-Titanium Alloy Phase Diagrams", *ASM Handbook*, Vol. 3. ASM International, Materials Park OH, P. 2-324, 1992.

"Oxygen-Titanium Alloy Phase Diagrams", *ASM Handbook*, vol. 3, ASM International, Materials Park OH, p. 2-324, 1992.

R.F. Stratfull, "Experimental Cathodic Protection of a Bridge Deck", Transportation Research Record No.500, pp. 1-15, Federal Highway Administration Report No. FHWA-RD-74-31, January 1974.

Wayne J. Swiat, and Joseph W. Rog, "Further Improvements in Cathodic Protection", Report FHWA/R87/062, pp. 7-8, June 1987.

Herbert H. Uhlig, and R. Winston Revie, *Corrosion and Corrosion Control*, 3rd edition, John Wiley and Sons, pp. 28, 375-382, 1985.

R.C. Weast, ed., "Electrical Resistivity and Temperature Coefficients of the Elements", *Handbook of Chemistry and Physics*, 60th edition, CRC Press, Boca Raton FL, p. F-172, 1980.

R.C. Weast, ed. "Refractory Materials", *Handbook of Chemistry and Physics*, 60th edition, CRC Press, Boca Raton FL, P. D-51 through D-60, 1980.

R.C. Weast ed., "Thermal Conductivity of the Elements", *Handbook of Chemistry and Physics*, 60th Edition CRC Press, Boca Raton FL, p. E-12 through E-17, 1980.

R.C. Weast, ed., "Thermal Properties of Pure Metals, *Handbook of Chemistry and Physics*, 60th edition, CRC Press, Boca Raton FL, p. E-12 through E-17, 1980.

APPENDIX A

SPECIFICATIONS FOR FIELD APPLICATION OF ARC-SPRAYED TITANIUM

SECTION - 01251 INSTALL CURRENT DISTRIBUTION PLATES

01251.00 Scope - The Contractor shall install the current distribution plates at the locations indicated on the plans and approved by the Engineer. Current distribution plates provide the connection between the conductors from the DC power distribution system positive wires and the arc-sprayed titanium anode in zone 14.

Additional current distribution plates shall be installed where necessary to bridge cracks in the bridge. Connection to the plates is included in Section 01265, Install DC Power Distribution System.

01251.02 Timing - Current distribution plates shall be installed after installation of the titanium anode (Section 01261).

01251.11 Materials Requirements - The titanium current distribution plates and mounting screws and washers will be furnished by the State. The Contractor shall furnish the plastic anchor, the bolt and nuts required for attaching the ring connector and the epoxy required for mounting the plates. The epoxy shall be Concresive 1419 as manufactured by Adhesive Engineering Co., DP-420 as manufactured by 3M, or an Engineer-approved equal.

01251.31 Installation Requirements - The current distribution plate shall be installed and located as shown on the plans. At least one current distribution plate per each 600 square feet of anode area is required. Install each plate centered in the 600 square foot area it supplies. Where the coating is unable to bridge a crack, one distribution plate shall be installed centered over the crack to provide a conductive path across the crack. The top of the plastic anchor shall be installed flush with or slightly below the concrete surface. Control the amount of epoxy used to prevent flow of the epoxy between the titanium and the plate.

01251.71 Acceptance Criteria - The work performed under this section will be accepted if it is in accordance with all requirements of the plans, specifications, the Engineer-approved working drawings, material submittals, and work procedures.

01251.80 Measurement - Installation of the current distribution plates will be measured for payment on a unit basis per each by actual count of items in place, completed, and accepted.

01251.90 Payment - The current distribution plates will be paid for at a unit price per each for the bid item "Install Current Distribution Plates". Payment as above specified will be full and complete compensation for furnishing all labor, tools, equipment, and materials and doing all work called for by the plans and specifications.

SECTION - 01261 INSTALL TITANIUM ANODE

01261.00 Scope - The titanium anode consists of thermally sprayed titanium wire applied to the concrete surface for distribution of DC electrical charge over the concrete surface in zone 14. The Contractor shall furnish labor, materials and equipment for installation of the anode and masking to separate the zones.

01261.02 Timing - The titanium shall be applied within 24 hours after completion of the work required under Section 01255, Prepare Secondary Anode Surfaces.

Surfaces shall be scrubbed with a bristle brush and then thoroughly vacuumed or blown clean within 15 minutes before titanium spraying of the area is started. Any oil, grease, soil, water, or other foreign matter which deposits on the surface after the surface preparation has been completed shall be removed as described in 01255.31 before the titanium is applied.

The Contractor shall perform no work on this item until written approval is received from the Engineer, all supervisors and technicians have been certified for this work, and certifications have been approved by the Engineer.

01261.05 Installation Conditions - Coating application shall only be performed when the concrete surface is clean and dry and the relative humidity is less than 60% adjacent to and/or surrounding the entire current work surface.

01261.11 Equipment and Material Requirements -

(a) Masking - The masking material shall be non-conductive and shall be four inches wide between zones. Masking shall be installed to provide two inches between the titanium and any exposed metal object. Duct tape to which sprayed titanium does not adhere and which is heat resistant is an acceptable material. Multiple layers of tape may be required for adequate masking performance. The masking shall not disbond the titanium coating on adjacent surfaces when it is removed.

(b) Titanium Application Equipment - Application equipment shall be electric-arc type. The spray equipment manufacturer shall be:

Thermion, Inc.
P O Box 2136
Silverdale, WA 98383 - 2136
(206) 698 - 1539

or equivalent.

The Contractor is responsible for making the necessary modifications to the arc-spray system required to spray the titanium wire.

Spraying equipment from other manufacturers must be qualified as an equivalent by a demonstration test (planned, prepared, and conducted by the Contractor), and approved by the Engineer. This test must demonstrate equivalency under the full range of conditions which are likely to be encountered during this project. Evaluation of the demonstration will be based on 01261.71 below.

The Contractor shall be responsible for surface preparation, environmental control, conducting the test, and cleanup of the test area. This test shall be accomplished at the Contractor's expense.

The Contractor shall submit the manufacturer's equipment specifications, recommended operational procedures, and the Contractor's test plan including test facilities and procedures, for the Engineer's approval.

(c) Titanium - The coating material shall be 0.125 inch, annealed, grade 1 or 2, titanium wire. The Contractor shall submit the chemical analysis of the wire to certify the purity of titanium wire to be used on this project. The Contractor shall obtain and submit a certification to the Engineer for each lot of titanium used.

(d) Catalyst - A catalyst must be applied to the titanium anode after the titanium is applied to the concrete surface. The catalyst is available from Eltech Research Corporation, 625 East Street, Fairport Harbor, OH.

(e) Short Circuit Detection Equipment - This equipment shall consist of a constant current source that applies a constant current between the titanium and the steel, and a voltage detection system that monitors the voltage between the steel rebar and the titanium coating and causes shutdown of spraying equipment when a short circuit occurs. The detection system shall consist of a Newport digital voltmeter, number Q2005AVR2-SPC, or approved equivalent, installed in a NEMA 4 enclosure for use at the work area. The State will furnish the constant current supply. The Contractor is responsible for providing the voltage detection equipment and labor required for operation of the short circuit monitoring system.

01261.12 Technician Certification Requirement - Technician certification will take place prior to commencement of titanium spraying on the bridge. To be certified, the technician must have verifiable previous experience applying arc-sprayed zinc to a minimum of 5000 square feet of concrete surface area. The certification test shall begin by having each candidate perform titanium spraying, as specified, on prepared concrete specimens.

Concrete test specimens or approved test locations on the bridge shall be fully cured and abrasive-blasted as required under Section 01255, Prepare Secondary Anode Surfaces. The concrete test areas shall be 2 ft. x 2 ft. minimum.

One test specimen shall be provided by the Contractor for the testing of each candidate. The specimen shall be sprayed in one multi-pass operation.

The following inspection and testing will be performed on the specimens by the Engineer, who will make the final decision on certification.

(a) Visual Examination - Test specimens will be visually inspected using a lens with a magnification of 10x. To be acceptable, the coating shall have uniform appearance and follow the form of the concrete surface. The coating shall not contain any lumps, blisters, coarse texture, or loosely adhering particles, nor shall it contain any cracks, pinholes, or chips which expose the concrete substrate.

(b) Adhesion Test - Three aluminum or steel test discs will be cemented to the test area. After curing, the test discs shall be pulled from the test area with a calibrated Proceq, Model DYNA Z 5, or equal. To be acceptable, the minimum adhesion strength shall be 150 psi or greater.

(c) Resistance Test - To be acceptable the resistance of the coating shall be less than 0.25 ohms per square.

Technicians whose specimens satisfy these three requirements shall be certified as qualified Titanium Thermal Spray Technicians for this project.

An operator failing the initial certification tests may be permitted to perform one complete retest. If the operator fails the retest, he shall not be certified until completion of additional training and certification testing.

Re-testing and re-certification will be required whenever a technician's work falls below the acceptable criteria given in 01261.71.

Records of technician certification shall be maintained by the Contractor for a period of 6 months after completion of the contract work. Copies of the records shall be made available to the Engineer upon request.

01261.31 Anode Installation Requirements - During application the thermal spray nozzle shall be maintained at a travel speed and a distance from the work surface such that titanium deposit efficiency and bond strength are maximized. Travel speed should be 18 to 24 inches per second. The distance from the arc to the surface should be 4 to 7 inches.

Begin the titanium anode installation by spraying the area in which the current distribution plate will be installed. Install the current distribution plate and connect the short circuit detection system before spraying additional area. The titanium shall be installed in a continuous coating to facilitate short circuit detection. The coating shall be applied in multiple passes and shall overlap on each pass in a crosshatch pattern to ensure complete coverage. Uniform gun movement shall be used to ensure uniform thickness. Sufficient material shall be sprayed to achieve a maximum coating resistance of 0.25 ohms/square over the entire surface.

Compressed air used for spraying shall be clean, oil-free and dry, per ASTM D 4285. Air line filters and moisture separators shall be installed upstream from the spraying equipment. These shall be inspected daily for cleanliness and correct operation. Any indication of malfunctioning equipment, indicated by oil or water in the filter or traps, shall be corrected immediately.

Bend tests shall be performed by the Contractor to verify the proper operation of the equipment prior to starting work on each shift. The bend test shall consist of spraying two 2"x 4"x 0.05" carbon steel coupons with a 6 - 8 mil coating. The bend coupons shall be bent 180 degrees around a ½ inch diameter rod. The coating shall be on the tensile side of the bend test specimen. The bend test passes if there is no or only minor cracking of the coating as visually observed. The bend test fails if the titanium cracks and can be picked off with a knife blade. The titanium shall be applied to the bend coupons in the same manner and with the equipment adjusted for spraying the concrete.

01261.32 Short Circuit Detection - The short circuit detection system uses a constant current source to create a voltage between the rebar and the titanium. The detection scheme consists of monitoring this voltage and opening an alarm contact which controls the arc-spray equipment if the voltage drops below a preset level. A sharp drop in voltage is a definite indication of a short circuit. A short circuit or near short circuit will reduce the measured voltage to less than 100 millivolts.

Operation of the monitor requires one conductor from the positive input terminal of the detection equipment to be attached to the current distribution plate nearest the area in which work is being performed. A second conductor is required to connect the negative input terminal of the detection equipment to the rebar in the zone.

The Contractor may change the DC voltage at which the alarm is actuated with written approval from the Engineer.

The Contractor shall be responsible for furnishing all materials, equipment (except constant current supply) and labor to set up and operate the short circuit detection system.

The short circuit monitoring system shall be used during any work which may cause a short circuit between the titanium anode and the rebar. The system shall be used for titanium installation and for any conduit installation over titanium-coated surfaces. During the conduit installation the alarm contact shall operate a visual or audio alarm to indicate when a short is detected. When this alarm is actuated, all monitored installation work shall stop until the short circuit has been eliminated. The Contractor shall perform a functional test of the short circuit monitoring system prior to beginning the monitored work.

Elimination of detected short circuits shall be performed and paid for according to Section 01215, Locate and Remove Surface Metal.

01261.33 Catalyst Installation Requirements - The catalyst may be sprayed, brushed, or roller-coated onto the surface of titanium after the titanium is applied to the concrete surfaces. Before applying the catalyst, connect a constant current supply between the titanium and the rebar with the positive terminal of the supply connected to the titanium. Use jumpers to connect all of the distribution plates to the current supply. Set the current source to supply one milliamp per square foot of anode surface area.

Apply the catalyst at the minimum rate of 30 milliliters per square foot (0.32 quarts/sq. ft. or 323 milliliters/sq. meter). Multiple coats may be required to prevent the catalyst from dripping or running. Allow the current supply to run continuously for a period of 72 hours after completion of catalyst installation.

01261.41 Environmental Control Requirements - No discharge of noxious or hazardous waste material will be allowed onto the ground or into the air or water outside the platform/enclosure. Discharge of particulate from the enclosure shall not exceed 2 grains/1,000 cubic feet of air, (4.6 milligrams/cubic meter), in addition to complying with all applicable Oregon Department of Environmental Quality requirements. Waste containment and disposal requirements is covered under Section 01210, Prepare Waste Handling Plan.

01261.71 Acceptance Criteria - Do not perform catalysis before inspection and testing of the arc-sprayed titanium anode is complete. The work performed under this section will be accepted if it is in accordance with all requirements of the plans and specifications and the Engineer-approved working drawings, materials submittals and work procedures, and the titanium anode passes the inspections and tests described below. Anode surfaces shall be visually inspected using a lens with a magnification of 10x. To be acceptable the coating shall have uniform appearance and follow the form of the concrete surface. The coating shall not contain any lumps, blisters, coarse texture, or loosely adhering particles, nor shall it contain any cracks, pinholes, or chips which expose the concrete substrate. Unacceptable areas shall be repaired or replaced by the Contractor at no additional cost to the State. Anode repair shall be by a procedure proposed by the Contractor and approved by the Engineer. Repair work shall not be started until the Contractor receives the written approval of the Engineer.

Adhesion strength will be measured by the Engineer with a Proceq, Model DYNA Z 5, or equal. A minimum of five adhesion tests will be performed in zone 14. The target adhesion strength of the titanium coating shall be greater than 150 psi. Areas with adhesion strengths below 50 psi shall have the titanium removed and shall be recoated with titanium in accordance with these specifications.

Coating resistance will be measured by the Engineer at a minimum of 20 locations per 1000 square feet. All measurements shall be less than 0.25 ohms. Where the measurements indicate that the anode has excessive resistance, additional titanium shall be applied by thermal spraying after the surface is completely dry and any visible contamination has been removed.

Adhesion test areas (each approximately 2 inches in diameter) shall be recoated with titanium after scraping any loose or delaminated titanium caused by the adhesion test. Use care to avoid excessive coating thickness (greater than 10 mils) on the adjacent titanium surface.

01261.80 Measurement - There will be no separate measurement for individual items of work done under this Section. The estimated area to which the titanium shall be installed is 3,015 square feet.

01261.90 Payment - Payment for installing the titanium anode will be made at the lump sum amount for the item "Install Titanium Anode". Payment of the lump sum amount will be complete compensation for all labor, materials, equipment and incidentals required to perform the work specified in this section.

APPENDIX B

Calculation of Area Per Current Distribution Plate

CALCULATION OF MAXIMUM AREA PER CURRENT DISTRIBUTION PLATE

ASSUMPTIONS:

Current is distributed uniformly across surface area
R' = coating resistance per square = 0.50 ohms/square
Maximum current delivery = 0.002 A/ft^2
Cylindrical coating geometry as shown in figure B.1
Maximum desired coating voltage drop = 300 mV

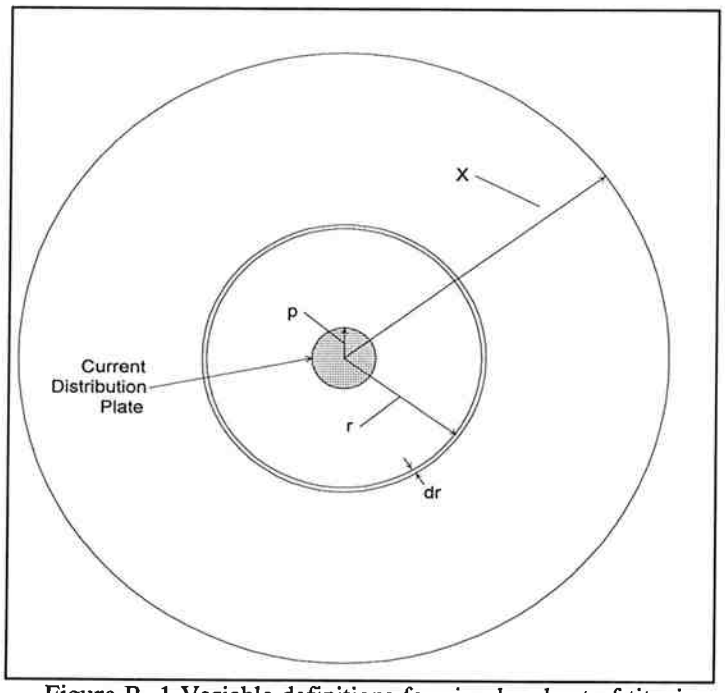

Figure B. 1 Variable definitions for circular sheet of titanium

SOLUTION:

The resistance of a thin ring of coating is defined by the following equation:

$$dR = \frac{\rho \cdot L}{A} = \frac{\rho \cdot dr}{t \cdot 2\pi \cdot r} = R' \frac{dr}{2\pi \cdot r} \qquad \text{(B-1)}$$

where:
ρ = resistivity of coating
L = length of coating section
A = cross-sectional area of coating
t = coating thickness
r = radius of coating ring
R' = coating resistance in ohms/square
dR = differential resistance in ohms

For uniform current distribution of 0.002 amps/ft^2, the current flowing through any cross-section of the coating, dr, is given by:

$$I = 0.002\pi\left(X^2 - r^2\right) \qquad \text{(B-2)}$$

Therefore, the voltage drop in the coating is given by the following integral:

$$V = \int I \cdot dR = \int_p^X 0.002\pi\left(X^2 - r^2\right) \cdot 0.5 \frac{dr}{2\pi \cdot r} = 5 \times 10^{-4} \int \left(\frac{X^2}{r} - r\right) dr \qquad \text{(B-3)}$$

Given that a maximum of 300 mV voltage drop is desired, the equation can be integrated and solved for X to determine the maximum area per distribution plate for a given plate radius:

$$\begin{aligned} 0.300 &= 5 \times 10^{-4}\left(X^2 \ln(r) - \frac{r^2}{2}\right]_p^X \\ &= 5 \times 10^{-4}\left[X^2\left(\ln(X) - \ln(p)\right) - \frac{1}{2}\left(X^2 + p^2\right)\right] \end{aligned} \qquad \text{(B-3)}$$

Roots to this equation for various values for p were solved for using numerical techniques in Mathcad 4.0. A graph showing the values for p versus the maximum allowable anode area is shown below:

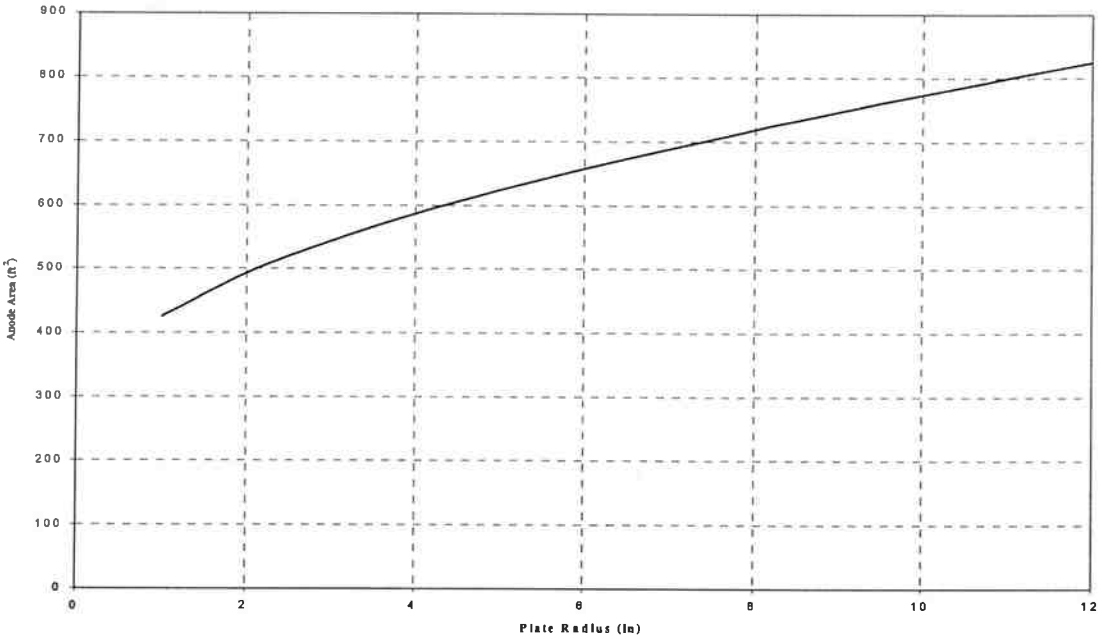

Figure B. 2 Allowable Titanium Surface Area vs. Plate Size

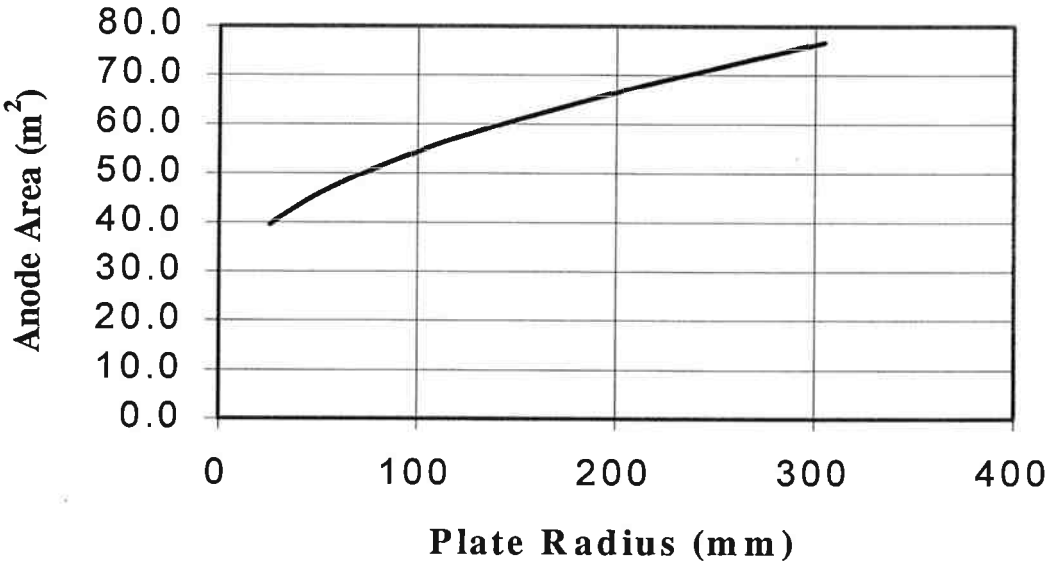

Figure B. 3 Allowable Titanium Area vs. Plate Size (metric)